New perspectives for surface EMG in clinical neurophysiology

From biophysics to applications

Blok, Johanna Helena
New perspectives for surface EMG in clinical neurophysiology. From biophysics to applications

ISBN: 90-8559-125-2

The work presented in this thesis is part of the research program of the Institute for Fundamental and Clinical Human Movement Sciences (IFKB), and was carried out at the Department of Clinical Neurophysiology, Institute of Neurology, Radboud University Nijmegen Medical Centre. It was financially supported by the Technology Foundation (STW)

Cover: The sculpture “Beweging” (Motion) by Marinel Vieleers over a background picture of the spatiotemporal profile of a motor unit action potential
Printer: Optima Grafische Communicatie, Rotterdam, The Netherlands

New perspectives for surface EMG in clinical neurophysiology

From biophysics to applications

een wetenschappelijke proeve
op het gebied van de Medische Wetenschappen

Proefschrift

ter verkrijging van de graad van doctor
aan de Radboud Universiteit Nijmegen,
op gezag van de Rector Magnificus,
prof. dr. C.W.P.M. Blom,
volgens besluit van het College van Decanen
in het openbaar te verdedigen
op dinsdag 31 januari 2006,
des namiddags om 3.30 uur precies

door

Johanna Helena Blok
geboren op 22 januari 1972
te Veldhoven

Promotores:	Prof. dr. ir. D.F. Stegeman Prof. dr. M.J. Zwarts
Manuscriptcommissie:	Prof. dr. B.G.M. van Engelen (voorzitter) Prof. dr. J.G. van Dijk, Leiden Prof. dr. R. Merletti, Turijn (Italië)

Nothing tends so much to the advancement of knowledge as the application of a new instrument - Sir Humphry Davy, 1778-1829

CONTENTS

Part I

Introduction

1

MUSCLES, MOTOR UNITS, AND ELECTROMYOGRAPHY

1.1 Introduction

Disorders of the human neuromuscular system are quite common. Depending on the precise definition of this category of diseases, estimates range from 150.000 to 500.000 patients in the Netherlands alone. "Neuromuscular disorder" is, in fact, a very general term. It is applicable to any disease that affects the peripheral nervous system, which begins in the anterior horn cells in the spinal cord and further comprises the motor and sensory nerves, the transition from the motor nerves to the muscle (the neuromuscular junctions) and the muscles themselves. The varied nature and the extent of the peripheral nervous system imply that it can malfunction in a great number of ways and at a great number of sites. This may be illustrated by the fact that such widely different diseases as amyotrophic lateral sclerosis (ALS, which affects the anterior horn cells and nerve fibers in the spinal cord), polyneuropathies such as the Guillain Barré syndrome (in which the nerve fibers fail), myasthenia gravis (in which the transmission from nerve to muscle is disturbed), and the purely muscular disorders such as Duchenne muscular dystrophy all belong to the category of neuromuscular diseases.

The percentage of all these disorders that causes lasting handicaps or inability to work is large. Some conditions are lethal. For these reasons, the initial stage of a neuromuscular disorder is often very threatening to patients. To be able to inform them as well as possible with respect to their prognosis, reliable and fast diagnostic tests are required. Moreover, if treatment is available, it should often be commenced as soon as possible, again requiring early diagnostic testing possibilities. These possibilities may also be utilised in follow-up studies to monitor the course of the disease and/or the effects of treatment, preferably quantitatively.

Clinical neurophysiology is a medical specialty serving diagnostics, especially within the area of clinical neurology. Its main efforts are directed toward the functional evaluation of brain, nerve, and muscle. In the case of suspected nerve or muscle disorders, the clinical neurophysiologist uses electromyographical (or EMG) techniques to record and interpret the electrical signals coming from a muscle or a nerve. As can be deduced from the number of annual EMG registrations (2500 patients per year in the University Medical Center Nijmegen, or approximately 150.000 in the Netherlands[145]), electromyography is a widely used technique, which yields an important contribution to the diagnostic process.

1.2 Electrophysiology

To enable the use of our muscles, information has to be transferred over fairly long distances in the human body – from the brain to the muscle in question and back. Theoretically, this can be realized in a number of ways, but in practice the body uses propagating electrical signals for this purpose. Electrical signal transfer is sufficiently fast. Furthermore, the electrical message to move can be transferred over long distances in the body without significant signal decay. This is primarily due to the special properties of the membrane that surrounds nerve and muscle cells. A pumping mechanism actively maintains concentration differences of ions between the inner and the outer side of this membrane. Because the majority of ions on the outside of the membrane have a positive electrical charge, while those on the inside are predominantly negatively charged, an electric potential difference over the membrane results. This physically unstable situation allows for a rapid reaction of the membrane to disturbances (incoming information).

Ions may cross the membrane through so-called ion channels, the most important of which in the present context are sodium (Na) and potassium (K) channels, with a secondary role for chloride (Cl). Each sodium channel has an activation gate and an inactivation gate, while potassium channels have only one gate. In the resting condition, the sodium activation gates are closed, sodium inactivation gates are open, and potassium gates are closed, together prohibiting ionic current from nullifying the transmembrane potential difference. However, if for an arbitrary reason the transmembrane potential difference is reduced sufficiently, the activation gates of the sodium channels open, allowing sodium ions to enter the cell. This causes a sudden depolarization of the membrane. (In fact, excess sodium ions enter the cell, causing the potential to become even positive on the inside of the cell membrane.) The local increase in potential elevates the potential at adjacent segments of the nerve fiber that are still at rest. Soon, this increased potential at the new locations ignites the opening of sodium channels there. In the mean time, at the original site the sodium inactivation gates close and potassium gates open. This causes sodium ions to stop entering the cell and K^+ ions to leave the cell. A little later, the sodium activation and potassium gates close, and the sodium-potassium pump begins to re-establish the resting membrane potential. The continuing nature of this process, in which neighboring segments of the nerve or muscle fiber are subsequently activated, allows transport of the stimulus or action potential over long distances, with sufficient velocity, and without loss of signal strength.

In a sense, this physiological process may be compared to the toppling over of a chain of domino stones. It requires some time and energy to put them all in upright position (the workings of the active ion pump), and the result is an unstable balance (resting transmembrane potential difference) compared to the stable position of fallen stones (membrane with channels open). A small disturbance of the system – it is not necessary to push a stone all the way to the ground, just a little flick (change in potential) suffices – may topple one stone over, with a chain reaction in adjacent stones as a consequence. When a particular stone has toppled over sufficiently far (if enough sodium current has flown to lift the potential in neighbouring membrane segments sufficiently) it will "ignite" the falling of the next stone (activation of the adjacent segment). This process is robust and does not depend on the exact position of a stone within the chain, but only on a sufficient proximity of the previous stone (how large the potential change induced by the previous segment is).

The ionic currents that cross the membranes upon depolarization and subsequent repolarization of a fiber also flow throughout the rest of the tissue volume. Due to this "volume conduction", transient potential changes are set up in the whole surrounding volume, including potential changes at its surface. It is these changes that can be measured by electrodes distant from the fiber and that are recorded in the EMG examination.

1.3 Anatomy and physiology

Depending on their characteristics, muscles can be divided into different categories: cross-striated muscles, non-striated (or smooth) muscles, or cardiac muscle. Each of these three categories shows a different structure when viewed with a microscope. As most of the muscles that are investigated in clinical neurophysiology are of the striated type, only these will be considered further. Cross-striated muscle fibers are innervated by (receive electrical information from) an α-motoneuron from the spinal cord. The connection between this nerve fiber and the muscle is made at the so-called motor endplate or neuromuscular junction. A group of muscle fibers innervated by the same motoneuron, together with that neuron, is called a motor unit.[128] See the left part of Figure 1.1A. Motor units may contain 20 to 500 muscle fibers,[19] or even up to 2000 in larger limb muscles.[50]

In voluntary contractions, each motor unit has its own pattern of activation, with firing moments that are only weakly related to those of other motor units. This pattern is determined in the brain and spinal cord, and depends on the desired output force of the muscle. With increasing central drive, and, hence, force, either the firing rate of already active motor units may increase or new, thus far inactive motor units can be recruited. Because in most conditions many motor units are simultaneously (albeit intermittently) active, their unrelated firing results in a so-called EMG interference pattern (Fig. 1.1A, right).

It is important to note that a motor unit does not occupy a physical area in the muscle which is clearly separate from that of other motor units. Rather, it is spread over an area that is shared between multiple units. Hence, within such a

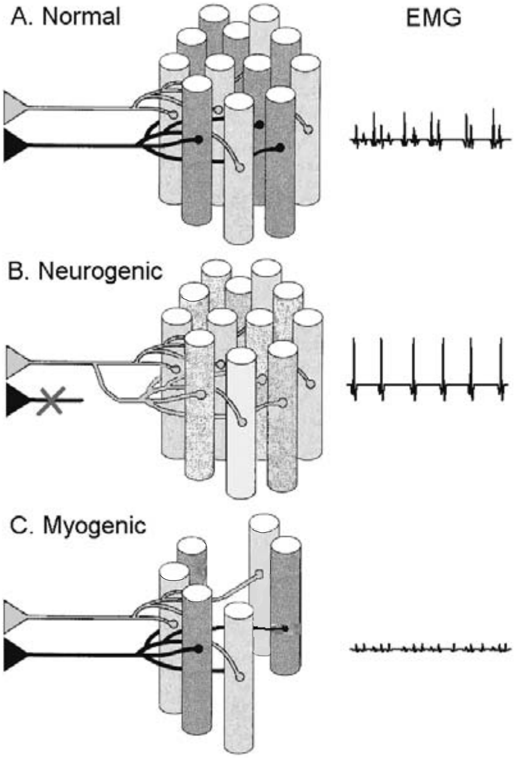

Figure 1.1: (A) Structure of normal motor units (MUs), each consisting of a single motor nerve fiber together with the muscle fibers it innervates. The innervation area or motor endplate is located approximately halfway along the muscle fibers. From there, action potentials propagate in two directions towards the tendons. In a muscle, the anatomical areas of multiple motor units overlap. (B) Characteristic pathological changes in neurogenic disorders: reduced number of MUs and increased MU size. (C) Characteristic pathological changes in myogenic disorders: normal number of MUs with reduced MU size. Adapted from Ref. [144]. The signals on the right schematically depict approximately half a second of the EMG that might be recorded from a normal or affected muscle, respectively.

motor unit territory, fibers of more than one motor unit are present. Such motor unit territories typically have a cross-sectional diameter between 3 and 10 mm. The fibers are homogeneously distributed over the territory.[20] The motor endplate zone consisting of the neuromuscular junctions of the fibers are found in a small region of less than a centimeter, which often lies about halfway both ends of the muscle fibers.

A particularly relevant consequence of the fibers of a motor unit being innervated by one single motoneuron, is that they all are excited more or less simultaneously. In that sense, they form a functionally recognizable, rather than a simply traceable anatomical unit. The electrical signal generated by a motor unit (motor unit action potential or MUAP) basically is the sum of all action potentials from the constituent fibers. For that reason, it shows some similarity with the signal coming from a single fiber (single fiber action potential or SFAP).

Considering the motor unit in a pathological context, a basic distinction can be made between two types of neuromuscular disorders: the neurogenic disorders that primarily affect the nerve fibers or the cell bodies in the spinal cord, and the myogenic diseases with a major impact on the muscle fibers. In the neurogenic disorders (Fig. 1.1B), the process of nerve fiber loss (denervation) leads to a reduced number of functioning motor units, and, thus, an "emptier" EMG signal. Subsequent reinnervation by newly formed sprouts from other, still intact nerve fibers results in an increased motor unit size (expressed as the number of muscle fibers per motor unit) and an increased EMG potential amplitude. As a general rule, myogenic disorders do not significantly affect the number of motor units. They result in a loss of muscle fibers, and, thus, in smaller units (Fig. 1.1C). For the EMG, this means smaller potentials at a normal or increased number of peaks (motor unit firings) in the signal.

1.4 Needle EMG and surface EMG

A central aspect of the electromyographic examination is gathering information with respect to the functioning and structure of motor units. The most often used method to identify motor units is the needle EMG investigation. As the name suggests, a needle electrode is inserted into the investigated muscle. The electrical potential set up by the ionic currents from the active muscle fibers is picked up by the metal needle tip, and then amplified and analyzed.

Because the distance between the active muscle fibers and the needle electrode is relatively small, the action potentials recorded with needle electrodes have high amplitudes and can be recorded fairly easily. They offer the clinical neurophysiologist a lot of information with respect to both the muscle itself and the nerve connecting it to the command centers in the brain. In fact, needle EMG is widely regarded the technique of choice for the diagnostic evaluation of the functioning of muscles and motor units.

Over the past 40 years, many methods have been developed that allow interpretation of the needle EMG signals in terms of the most important characteristics of the contributing motor units.[133] But however important needle EMG may be, its usefulness and reproducibility are limited by the fact that the amplitude and morphology of the needle EMG signal are largely determined by only a few muscle fibers that are close to the needle tip. Because not all of these fibers are equally affected by a pathological process, this implies that coincidence may become a factor of importance during the recording, and that multiple sites within a muscle should be sampled. It also means that needle EMG signals tend to have poor reproducibility. Furthermore, needle electrodes cause pain and stress to patients. Especially in children, they may limit the use of EMG more than can be justified on the basis of the clinical questions asked. Needle electrodes also hinder the (near-)maximal contractions required to assess a muscle's pattern of voluntary motor unit recruitment. Thus, much could be won if the present invasive EMG techniques were (as far as possible) replaced by a non-invasive alternative, yielding similar diagnostic information.

It has been known for a long time that muscle activity can be recorded not only in the immediate neighborhood of the EMG needle in the muscle, but also at larger distances from fibers. As said, through the phenomenon of volume conduction, the electrical activity of superficial muscles can even be recorded at the skin surface. In fact, clinical neurophysiologists routinely use recordings of the EMG at the skin surface (surface EMG) in nerve conduction studies. These studies assess action potential propagation over motor nerves from the amplitude and latency of the compound muscle action potential (CMAP), which is obtained through transcutaneous electrical stimulation of the afferent nerve. Furthermore, surface EMG (sEMG) of active muscles is used in many areas of muscle research, also outside of the clinical neurophysiology laboratory (e.g., in rehabilitation sciences, sports sciences and ergonomics). Yet, the single bipolar signal (derived from two electrodes attached to the skin above the muscle) that is commonly used in these fields, is of limited value for diagnostic purposes because it contains little information about the essential level of single motor units. Indeed, with the exception of the abovementioned nerve conduction studies, the value of conventional, single-lead sEMG recordings is often considered negligible for the clinical diagnosis and management of neuromuscular disorders.[58, 116] Before sEMG can be applied for diagnostic purposes, it therefore requires extension of its scope and possibilities.

1.5 Aim and survey of this thesis

The work presented in this thesis aims to expand the clinical possibilities of surface EMG by means of a biophysical and engineering approach. Amongst several other possibilities offered by these disciplines, such an approach may take one of the following three routes:

1. Development of a theoretical framework to provide new insights. Such a theoretical framework often takes the form of a mathematical description of the problem at hand. It can be especially useful if implemented on a computer to allow simulation studies. This route was followed in Part II of this thesis. The first chapter in this part, Chapter 2, shows how a different mathematical perspective on an already existing sEMG application, the statistical method of motor unit number estimation (MUNE), can solve a number of methodological problems that thus far limited its usefulness and accuracy. The most convincing evidence supporting the new method comes from a simulation study, although experiments in healthy subjects were also performed. The advantage of a simulation study is that it allows to get variables under control which cannot easily be controlled in reality. Whereas the number of motor units present in a muscle is never known exactly, a computer model allows this number to be set by the experimenter. Hence, it provides a true gold standard with which the results of the new and existing MUNE methods can be compared.

In general, extracting relevant information from sEMG signals requires insight in the factors that influence these signals as well as in the interactions between these factors. More specifically, the volume conduction behavior of a medium needs to be known qualitatively and quantitatively to determine exactly the physiological basis of the extracellular phenomena that are of clinical interest. The work presented in Chapter 3 aims to provide a better understanding of sEMG signal characteristics, again by means of a computer model. Chapter 3 describes the mathematics that underly this model and provides some examples of applications. It focuses on the volume conductor properties of muscle, subcutaneous fat, and skin layer tissue because of their large influence on sEMG signals, certainly when compared to needle EMG signals.

2. Design and development of new instrumentation. As mentioned before, present single-channel surface EMG recording techniques are of limited use for diagnostic purposes. The information obtained through single-channel recordings is necessarily restricted to the time-varying aspect of the EMG signal. Information with respect to spatial motor unit characteristics (such as its position and extent, the position of the motor endplate, and action potential propagation), some of which are essential for the force-generating capacity of the motor unit, can only marginally be obtained with this type of recording. Furthermore, motor unit changes in disease tend to be of a primarily spatial nature.[154] For these reasons, it may be expected that the diagnostic possibilities of sEMG can be increased by adapting the technique so that it is able to provide spatiotemporal rather than merely temporal information. In principle, this might be achieved by increasing the number of recording electrodes, covering a larger part of the muscle. As is known from electroencephalography and electrocardiography (the recording of the electrical signals of the brain and heart, respectively), increasing the number of electrodes can add spatial (topographical) information that is largely independent from the temporal information that can be provided by a single electrode.

The main goal of the developments laid down in Part III of this thesis was the design of a system that would allow exploration of the clinical and scientific possibilities of topographical surface electromyography (sEMG). To enable the comparison of this new technique with conventional needle EMG, the design focus was on its possibilities in motor unit analysis. At the same time, the aim was to make maximum use of the additional information that multichannel sEMG may yield on the whole muscle. Chapter 4 provides an overview of the data-acquisition system realized, a multichannel surface EMG recording system with a high electrode density.

The mere recording of multichannel sEMG data generally will not yield quantitative information regarding single motor units. Indeed, in the sEMG interference pattern that results from voluntary contractions, the contributions of individual motor units cannot be recognized as easily as from needle EMG recordings. In

Chapter 5, the second necessary step toward single motor unit information is taken. This chapter shows that, at least for low contraction levels, the firing moments of individual motor units can be accurately determined from high-density multichannel sEMG recordings. Using the topographical differences between the motor units that contribute to the sEMG, a peak-detection and -classification algorithm can decompose the sEMG interference pattern. First, this offers the possibility to investigate central components of the motor system by means of the resulting motor unit firing pattern. Second, averaging the sEMG over the detected firing instances for all electrodes yields a low-noise template ("fingerprint") of the motor unit's spatiotemporal potential profile, which allows for extensive motor unit characterization.

3. Development and validation of applications. A third type of contribution from biophysics to improvements in surface EMG lies in the translation of recorded data to clinically meaningful information. More specifically, with the availability of a new, multichannel data-acquisition system, new tools should be devised and validated that can perform the abovementioned extraction of relevant information from the (multichannel) sEMG signals.

These tools can be based only partially on existing needle EMG analysis techniques. One of the major questions that needle EMG aims to answer is whether there are signs of denervation/reinnervation in a particular muscle. In needle EMG, usually the combination of several assessments (of so-called insertional activity and spontaneous activity, MUAP size and morphology, recruitment pattern – especially at maximum voluntary effort, etc.) results in a conclusion about the presence and degree of motor nerve fiber loss. That is, about the number and sizes of the remaining functioning motor units. In surface EMG, insertional activity is eliminated because of the absence of needle insertions. Spontaneous activity occurs at the single fiber level and is too small to allow registration at the skin surface. Other variables are more difficult to assess or contain less information than in needle EMG, either because the larger number of contributing MUs complicate the sEMG interference pattern, or because sEMG parameters are more severely affected by the filtering properties of the volume conductor. Obtaining information regarding number and sizes of motor units from multichannel surface EMG should, therefore, not follow the approach taken in needle EMG. Instead, it should rely on its own strengths: the possibility to incorporate not only temporal but also spatial information in the evaluation, and the availability of data on many MUs or even the entire muscle from a single registration. Part IV presents, therefore, alternative data-analysis techniques that are based on multichannel sEMG recordings. First, Chapter 6 addresses motor unit number. In this chapter, a different MUNE method was used than in Chapter 2, because it allowed a clearer demonstration of the advantages of multichannel recordings. Finally, Chapter 7 shows how a reliable estimate of the distribution of MU sizes can be obtained using high-density sEMG.

Part II

Mathematics and simulations

2

STATISTICAL MOTOR UNIT NUMBER ESTIMATION ASSUMING A BINOMIAL DISTRIBUTION

The statistical method of motor unit number estimation (MUNE) uses the natural stochastic variation in a muscle's compound response to electrical stimulation to obtain an estimate of the number of recruitable motor units. The current method assumes that this variation follows a Poisson distribution. We present an alternative that instead assumes a binomial distribution. Results of computer simulations and of a pilot study on 19 healthy subjects showed that the binomial MUNE values are considerably higher than those of the Poisson method, and in better agreement with the results of other MUNE techniques. In addition, simulation results predict that the performance in patients with severe motor unit loss will be better for the binomial than Poisson method. The adapted method remains closer to physiology, because it can accommodate the increase in activation probability that results from rising stimulus intensity. It does not need recording windows as used with the Poisson method, and is therefore less user-dependent and more objective and quicker in its operation. For these reasons, we believe that the proposed modifications may lead to significant improvements in the statistical MUNE technique.

JH Blok, GH Visser, S de Graaf, MJ Zwarts, and DF Stegeman
Muscle & Nerve 31: 182-191, 2005

2.1 Introduction

Many neurogenic disorders are characterized by a reduction in the number of recruitable motor units (MUs) in affected muscles. A reliable count or estimate of this number is then of obvious importance, both for diagnostic purposes and for following disease progression or therapeutic effects. Comprehensive overviews of the available electrophysiological motor unit number estimation (MUNE) techniques, their underlying assumptions, and advantages and disadvantages have been provided elsewhere.[35, 127] All of these MUNE methods start by trying to find a mean MU action potential (MUAP) that is representative of the muscle as a whole. The MUNE is subsequently determined by dividing this representative MUAP into the maximal compound muscle action potential (CMAP), which is generated by the muscle after supramaximal electrical stimulation of its motor nerve.

The various methods differ primarily in their means of obtaining a representative sample of MUAPs, as well as in how they deal with the probabilistic activation of motor units: when stimulus intensity is increased, starting from the recruitment threshold of an individual MU, the firing probability of this MU changes gradually from 0 (never activated) to 1 (always activated). When the recruitment ranges (range of stimulus intensities over which the firing probability increases from 0 to 1) of a number of MUs overlap, any combination of these units can be activated upon successive stimuli with equal strength, a phenomenon known as alternation. The statistical method of MUNE uses the stochastical properties of the resulting variation in the recorded CMAP amplitude to obtain an estimate of the mean electrical size of the MUs.[23, 81]

The statistical method is implemented as proprietary software on one of the commercially available EMG systems (Viking product line; Nicolet Biomedical, Madison, WI). It is easy to perform in clinical practice, fairly sensitive to changes in motor unit number, and yields reproducible results.[60, 79–81, 101, 111, 129] For these reasons, it has become one of the most commonly used MUNE techniques. The statistical technique has some limitations, however. As discussed recently by Lomen-Hoerth and Slawnych,[81] its validity depends on the degree by which several assumptions are met. The most important of these is the assumption that the variation in CMAP size follows a Poisson distribution. In turn, this Poisson distribution assumption requires that all MUs undergoing probabilistic activation at a particular stimulus intensity respond independently to each stimulus pulse, have MUAPs of the same size, and have the same probability (p) of activation. Moreover, and this defines the distribution as Poisson rather than more generally binomial, p should be small (i.e., much closer to 0 than to 1).

In this chapter, we argue that the latter assumption is not met in statistical MUNE recordings. In a vast majority of cases, p is larger than 0.05 (a value that may be taken as maximum for a Poisson distribution to be a valid description). In fact, in many cases, p approaches 0.5. The resulting distribution then is binomial rather than Poisson. We show how the assumption of a binomial distribution alters the existing statistical MUNE technique, both in theory and in its practical application. We first present a mathematical description of the Poisson method and the binomial method. This theoretical section is followed by an analysis of the performance of the two methods, using computer simulations and the results of a study of normal subjects.

2.2 Theoretical background

2.2.1 The Poisson method

The mathematical basis of the Poisson distribution technique has recently been described by Lomen-Hoerth and Slawnych.[81] To allow a comparison with the binomial distribution, we present it in a slightly different form.

Basically, the Poisson statistical MUNE method distinguishes MUs into 3 groups: MUs that are always active ($p = p_s = 1$), MUs that are probabilistically activated (with identical, supposedly small p_s value; $p_s \approx 0$), and MUs that are never activated ($p_s = 0$) at a particular stimulus intensity (s). Only the observed CMAP amplitudes or areas of the second group of MUs ($0 < p_s < 1$) are analyzed. The method assumes that the MU potential sizes of these MUs are identical, implying that the CMAP size $A_s(i)$ varies in integer multiples $I_s(i)$ of the (unknown) single motor unit size ΔA with stimulus number (i). The distribution of these multiples, i.e., of the values $I_s(i) = [A_s(i) - \min(A_s)]/\Delta A$, is assumed to be Poisson. In this expression for I_s, $\min(A_s)$ is the smallest observed CMAP size at the particular stimulus intensity, s. It is assumed to be the total response of the first group of always active MUs (with $p_s = 1$) and represents a baseline shift in the response sizes used for the analysis.

Characteristic for a Poisson distribution is the equality of its mean and variance: $\text{mean}(I_s) = \text{var}(I_s)$. From the above expression for I_s it follows that:

$$\text{mean}(I_s) = [\text{mean}(A_s) - \min(A_s)]/\Delta A \tag{2.1a}$$

$$\text{var}(I_s) = \text{var}(A_s)/(\Delta A)^2 \tag{2.1b}$$

Hence, the mean MUAP size ΔA can be estimated from:

$$\Delta A = \frac{\text{var}(A_s)}{[\text{mean}(A_s) - \min(A_s)]} \tag{2.2}$$

with $\text{var}(A_s)$ the variance of the observed CMAP sizes. The Poisson MUNE N_p easily follows as:

$$N_p = \text{CMAP}_{\max}/\Delta A \tag{2.3}$$

or:

$$N_p = \text{CMAP}_{\max} \times \frac{[\text{mean}(A_s) - \min(A_s)]}{\text{var}(A_s)} \tag{2.4}$$

with $\text{CMAP}_{\max}$ the response of the muscle to supramaximal stimulation.

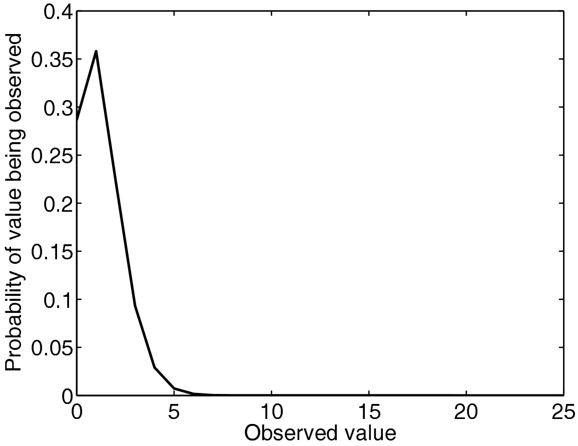

Figure 2.1: Probability density function for a Poisson distribution of CMAP sizes, generated by an assumed population of 25 MUs of equal size. Each of these MUs is activated with the same probability $p = 0.05$, so the mean of the corresponding distribution is 1.25.

2.2.2 Problem statement

The Poisson method of MUNE assumes that the group of probabilistically active MUs is fairly small. The minimum of the observed CMAP sizes recorded in response to a series of constant-intensity, submaximal pulses is taken to represent the case where all MUs in this group with $0 < p_s < 1$ are not recruited. This assumption is questionable, as demonstrated in Appendix 2A at the end of this chapter, but it will be adopted here.

For healthy subjects, the observed range of CMAP sizes is of the order of 10% of the maximum CMAP.[60,101] The variably active group of MUs may therefore be assumed to constitute about 10% of the total population; for instance, $n_s = 25$ MUs out of population of $N = 250$. For the sake of simplicity, we will assume them to be of unitary size. This implies that from this population 26 different values can be observed: from 0 when no MU is active to 25 when they all are. The probability with which each of these observable values occurs is determined by the combined probabilities of activation of the 25 MUs. To obtain a Poisson distribution, this probability has to be equal for all MUs and small (e.g., 0.05). The resulting probability density function is shown in Figure 2.1. It has a low mean, $m_s = n_s p_s = 25 \times 0.05 = 1.25$ and is strongly skewed to the right. At this point, a paradox arises, as the range of amplitudes in this example is closer to 0 - 5 than to the 0 - 25 that was the premise of the example. This paradox points to $p_s > 0.05$ or to a number of MUs in the probabilistically active group of more than 25.

Figure 2.2 shows representative results of four series of CMAP recordings at different stimulus intensities in a healthy subject (for a description of the method of acquisition, see Section 2.3). The histograms on the right show the distribution

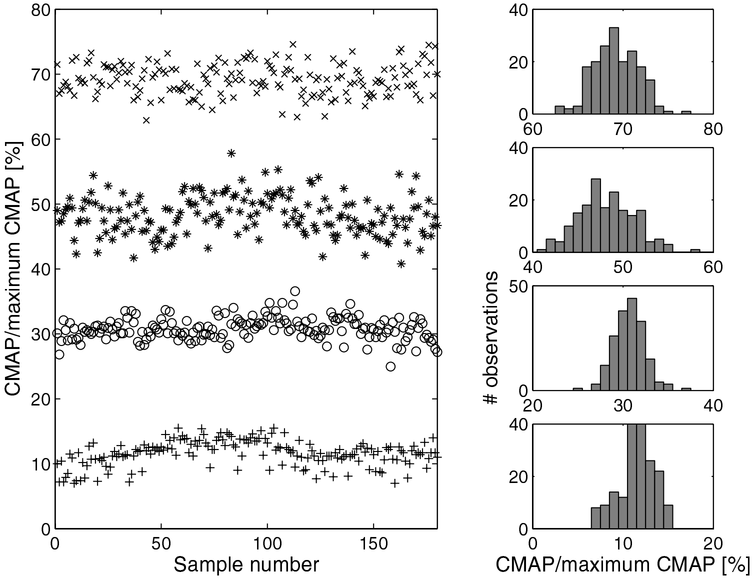

Figure 2.2: Left: representative results from a healthy subject, showing CMAP sizes as percentage of the maximum CMAP in response to series of 180 stimuli at 4 different stimulus intensities (different symbols). Right: histograms illustrating the distribution of CMAP sizes for each of the 4 intensities.

of the observed values. The symmetry of the histograms is apparent. There is no skew of significance, implying that the mean of the distribution is close to the center of the range of observable values. Because this mean is determined fully by the two parameters n and p, the disparity between the means in Figures 2.1 and 2.2 (relative to the minimum and maximum value of the distributions) again indicates that either the group of variably active MUs is larger, or the Poisson distribution (small-p) assumption is not met, or both.

It is shown in Appendix 2A that assuming a larger group of probabilistically active MUs cannot solve the inconsistency between Figures 2.1 and 2.2. By contrast, abandoning the assumption that the probability of activation, p_s, of the n_s MUs is small and allowing it to vary between 0 and 1 implies that the distribution mean can take any value between 0 and n_s for n_s MUs of unitary size. However, the Poisson distribution is no more or less than the small-p member of the wider class of binomial distributions (with arbitrary p). Lifting the small-p assumption is, therefore, identical to assuming a binomial instead of a Poisson distribution. In other words, when a group of n_s probabilistically active MUs with equal-sized MUAPs generates a distribution with a high mean (that is, a mean that is larger than a few percent of the range of potentially occurring values), then the observed distribution is binomial rather than Poisson.

The Poisson MUNE technique usually employs so-called windows to limit the range of response sizes included in the analysis.[60,80,101] These windows are placed relative to the distribution mean. Most often, the stimulation intensity is adjusted until the distribution mean falls at either the lower quarter of the window (at 25% of the window width) or at its center (50% of the window width). In terms of the activation probability p, these positions must imply p-values of 0.25 and 0.5, respectively. Therefore, in our opinion, the Poisson MUNE method uses Poisson calculation algorithms for a distribution that by all descriptions is binomial and not Poisson. Of course, treating it mathematically as if it were Poisson is possible (mainly a matter of calculating mean and variance of the distribution), but is bound to generate erroneous MUNE values.

2.2.3 The binomial method

As for the Poisson distribution, the binomial method that we propose also requires the assumption that all MUs that are variably active have the same size. In contrast to the Poisson method, however, the binomial method does not distinguish MUs into three groups, but assumes that they all have the same activation probability. (This choice may seem surprising given the physiological reality in which the groups exist. It was motivated by our hypothesis that at most stimulus intensities the second, probabilistically activated group of MUs is, in fact, large compared to the other groups. This issue is discussed extensively in the Appendix to this chapter.) Let the electrical size of the MUs again be ΔA and their probability of firing at a given stimulus intensity s be p_s. If there are N motor units, then the expected number of responding MUs is $m_s = Np_s$ and the expected CMAP size equals $m_s \Delta A$. This expected CMAP size can be estimated by the mean of the observed values of the CMAPs: $\text{mean}(A_s) \simeq m_s \Delta A$. When it is noted that the observed distribution mean can also be expressed as:

$$\text{mean}(A_s) \simeq m_s \Delta A = (Np_s)\Delta A = p_s(N\Delta A) = p_s \text{CMAP}_{\text{max}} \tag{2.5}$$

it is clear that p_s, the activation probability of the MUs at a particular stimulus intensity, s, can be obtained easily from the data as:

$$p_s \simeq \frac{\text{mean}(A_s)}{\text{CMAP}_{\text{max}}} \tag{2.6}$$

From first principles, if the distribution I_s of the multiples of the MUAP size ΔA (i.e., the underlying process) is binomial, then its variance is given by:

$$\text{var}(I_s) = \sigma(I_s)^2 = \sigma_s^2 = Np_s[1 - p_s] \tag{2.7}$$

with σ denoting standard deviation. In that case, the variance, $\text{var}(A_s)$, of the observed CMAP size distribution is $\sigma_s^2 \Delta A^2$, which can also be estimated from the data. As can be verified by substitution of $\text{mean}(A_s) \simeq Np_s \Delta A$ and $\text{var}(A_s) \simeq Np_s[1 - p_s]\Delta A^2$, it follows that the binomial MUNE N_b of the true MU number N can be deduced from:

$$\frac{\text{var}(A_s)}{\text{mean}(A_s)^2} \simeq \frac{(1 - p_s)}{Np_s} \tag{2.8}$$

or:

$$N_b = \left[\frac{(1-p_s)}{p_s}\right] \times \frac{\text{mean}(A_s)^2}{\text{var}(A_s)} \tag{2.9}$$

Finally, inserting Equation (2.6) into the above expression for N_b yields:

$$N_b = [\text{CMAP}_{\text{max}} - \text{mean}(A_s)] \times \frac{\text{mean}(A_s)}{\text{var}(A_s)} \tag{2.10}$$

This method is different from all existing MUNE methods in that it does not need a representative MUAP to be divided into the maximum CMAP. The motor unit size, ΔA, is estimated simultaneously with the motor unit number, N_b, from the distribution characteristics. When desired, ΔA can be obtained by dividing the maximum CMAP by the MUNE.

A concluding remark concerns the relation between the Poisson and binomial distributions. From Equation (2.7) for binomial variance, it can be seen that, when p_s is small compared to 1 (so that $1 - p_s$ remains close to 1), then:

$$\sigma_s^2 = Np_s[1-p_s] \simeq Np_s = m_s \tag{2.11}$$

This equality of mean and variance is characteristic for the Poisson distribution and illustrates that the Poisson distribution is the small-p limiting case of the binomial distribution. Equation (2.11) also shows that the factor of $(1 - p_s)$ functions as a moderator, allowing adaptation of the distribution shape to an increase in activation probability (Fig. 2.3).

Thus, from the responses to a series of submaximal stimuli, the average CMAP size is measured together with its variability, expressed as variance. Together with the recorded maximal CMAP, these two variables suffice to estimate the size of the underlying population (the number of motor units). The proposed method differs from the existing Poisson method in the distribution that is chosen to explain the observed variance (binomial rather than Poisson). This choice appears to be critical and largely determines the outcome, as shown in what follows.

2.3 Methods

2.3.1 Simulation study

To simulate alternation, a computer model was constructed and implemented in Matlab (The MathWorks, Natick, MA). For this purpose, we started from the observation that the CMAP size as a function of stimulus strength (the scan in the statistical MUNE technique) usually has a sigmoid shape. Previous work by Doherty and Brown suggests that MU activation depends more on relative proximity of the nerve fibers to the stimulus electrodes than on fiber diameter or MU size.[36] This implies that the steep increase in CMAP size in the center of the scan is not caused by an increase in the size of the newly recruited MUs, but

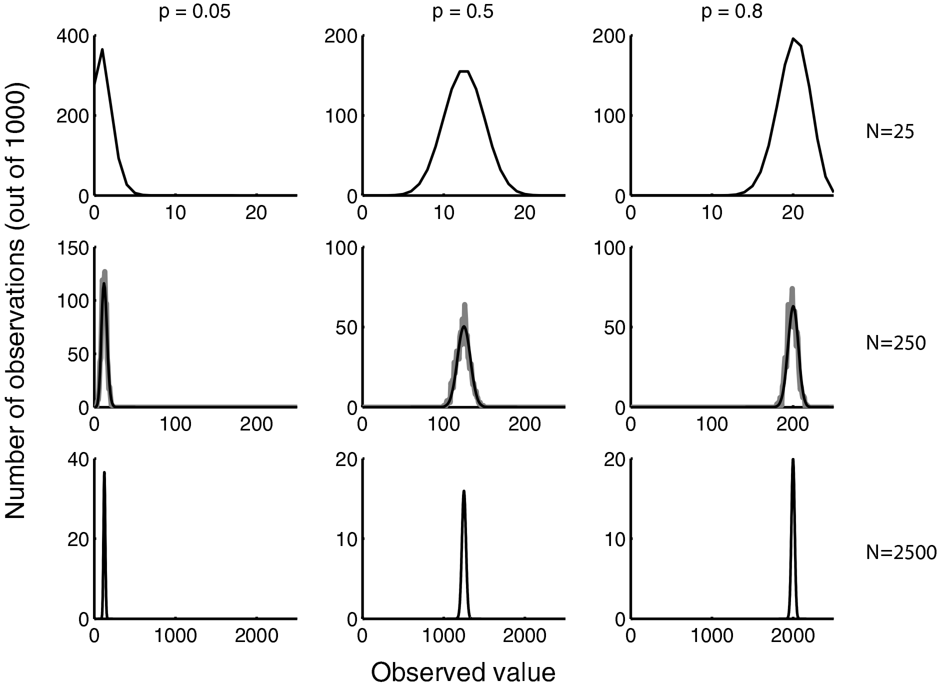

Figure 2.3: Examples of binomial distributions, for varying probability of activation (columns) and generated by a varying population size (top row: 25 MUs, middle row: 250 MUs, bottom row: 2500 MUs). The binomial distribution is widest when p=0.5, becoming thinner at higher or lower activation probabilities (compare columns). Furthermore, its relative width (width expressed as percentage of the maximal observable value or maximum CMAP) decreases with an increase in the size of the contributing population (compare rows). Note the similarity between the top left figure and Figure 2.1, illustrating that the Poisson distribution shown in Figure 2.1 is the small-p member of the family of binomial distributions. The gray curves in the middle row show distributions obtained with the computer model of alternation (see Fig. 2.4 and text). The correspondence between the black and gray curves indicates that the CMAP size distributions generated by the model can be considered binomial in nature.

rather by an increase in the number of MUs with similar recruitment thresholds. For a pool of 250 motor units, recruitment thresholds were therefore drawn at random from a normal distribution (see histogram in Fig. 2.4A). For this purpose, recruitment threshold was defined as the stimulus intensity at which the MU was active in 50% of the cases. The mean of the normal distribution corresponds to the stimulus intensity (SI) at which the scan shows the steepest increase in CMAP size.

The firing probability of a particular MU was assumed to increase linearly from 0 to 1 with SI, over a range that was centered around the recruitment threshold of that MU (Fig. 2.4A; solid line for a MU with recruitment threshold at 27). This range, which runs from a stimulus intensity (SI) of 12 to 41 for the MU shown, will henceforth be referred to as the recruitment range. The rate of increase in

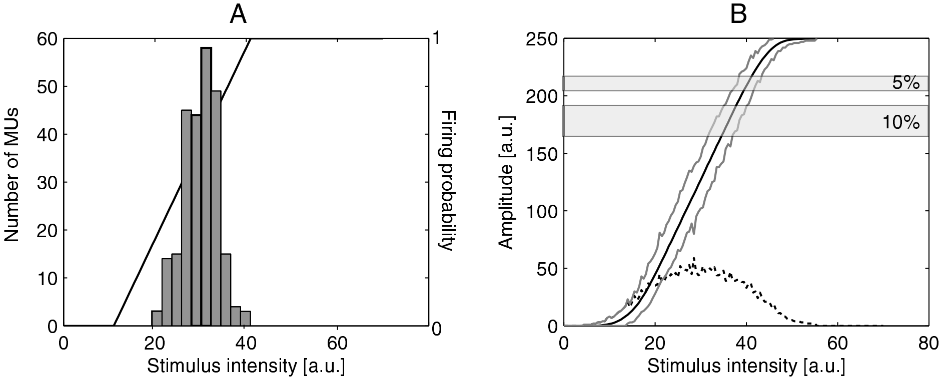

Figure 2.4: (A) Model input. The histogram shows the (normal) distribution of the recruitment thresholds of 250 MUs. Recruitment threshold was defined as the stimulus intensity at which the MU was active in 50% of the cases. Stimulus intensity is in arbitrary units (a.u.). The line shows the recruitment range for one of the MUs (from 12 to 41 a.u., with threshold at 27). (B) Summary of model output, showing mean (black, solid line), maximum, and minimum (gray solid lines) of the resulting CMAP size distribution as a function of stimulus intensity. The width of the distribution (dashed line) is the difference between the maximum and minimum.

firing probability (i.e., the slope of the linear increase and, hence, the width of the recruitment range) was assumed to be the same for all MUs, and all MUs had the same (unitary) size. This implies that in the model, MUs differed only by their recruitment threshold, as represented by the histogram in Figure 2.4A. However crude this approximation may seem, it results in a CMAP curve (or scan; see Fig. 2.4B) that is similar to physiological scans. As will be discussed in Appendix 2A, we believe that this model follows the physiology of MU recruitment more reliably than the assumptions behind either the Poisson or the binomial estimation approach. In that sense, it is a powerful tool for comparing both MUNE methods, showing an additional advantage over experimental studies in that the true number of MUs is known (i.e., a gold standard is available).

For the pool of 250 motor units, the CMAP size distribution was simulated for a range of SI, from 0 to supramaximal. At each intensity, 1000 stimuli were applied. Depending on the firing probability of a particular MU at that SI, it was determined by chance whether it was or was not activated in response to a particular stimulus. If activated, it added a response size 1 to the CMAP size. Hence, at supramaximal stimulus intensities, CMAP size is 250. A summary of the model output (CMAP size) is shown in Figure 2.4B. The binomial MUNE and Poisson MUNE were calculated for this simulated CMAP size distribution using the mathematical approach in the previous section. To assess the influence of recording windows, calculations were performed for three situations: 5% and 10% centered windows, and a 10% window with the distribution mean in its lower quarter instead of center. In these cases, the window width is expressed as percentage of the maximum CMAP and its position is expressed relative to the distribution mean at a specific stimulus intensity. The horizontal gray bars in

Figure 2.4B illustrate the use of a 5% and 10% window.

To assess the effect of motor unit loss on the MUNE, simulations were repeated for a model input number of MUs ranging from 10 to 350. In each case, results for four stimulus intensities were simulated. The lowest yielded a mean CMAP size of 15% of the maximum CMAP, followed by 30%, 45% and 60% means, in accord with the recommendations of Lomen-Hoerth and Olney.[80] In this study, 10% centered windows were used for the Poisson calculations.

2.3.2 Experimental study

The motor unit number was estimated in the thenar muscle group of 19 healthy subjects (8 male, 11 female) without neuromuscular complaints. Their mean age was 42.7 years (range, 22-63 years). The experimental protocol was approved by the medical ethics committee of the Erasmus Medical Center. All subjects gave informed consent.

The statistical MUNE technique was performed using the MUNE500 program[60] implemented on a Viking Select EMG machine (Nicolet Biomedical, Madison, WI). To record the potential at the skin surface, we used 2.5-cm × 3.5-cm disposable, self-adhesive electrodes. The active electrode was placed over the belly of the abductor pollicis brevis muscle, and the passive electrode in the middle of the proximal phalanx of the thumb. The ground electrode was placed at the base of digits 3 and 4. The median nerve was stimulated transcutaneously at the wrist, 8 cm from the active electrode. After determining the optimal position for the stimulating electrodes, these were taped securely to the wrist. Subjects were asked to recline and relax without speaking, with the hand in a pronated position at their side. As observed by Miller et al.,[101] this approach to reducing baseline fluctuations and artifacts proved superior to restraining the hand or arm.

Recordings were started with the recording of the maximal CMAP, and a scan of the muscle's response to increasing stimulus intensity was made. Subsequently, four runs of tests were performed at stimulus intensities that evoked responses around 10%, 30%, 50% and 70% of the maximum CMAP (slightly different intensities were used in the experiments compared to the simulations to ascertain a wide range of tested MUs). Each run consisted of 180 stimuli; stimulus frequency was 2 Hz.

For each subject, both the Poisson MUNE and the binomial MUNE were obtained from the recorded data. In both cases, the areas of the recorded CMAPs were used for analysis. The Poisson MUNE was calculated using only the data within a 10% centered window. Data were first assessed visually for the presence of motion artifacts, drifts of more than a few percent of the maximum CMAP, or spread.[60] If any of these were present in a run, this run was excluded from further analysis. Next, as in the conventional Poisson method, data were subdivided into series of 30 consecutive responses for which binomial and Poisson MUNE values were determined. The MUNE of a particular run was taken to be the median of the

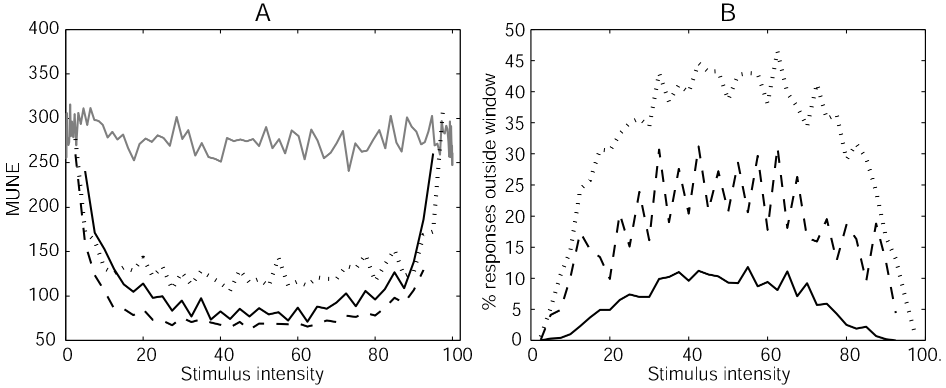

Figure 2.5: (A) Results of the Poisson (black) and binomial (gray) MUNE calculations for the simulated data. For the Poisson calculations, three types of recording window were used: 10% centered (solid), 10% low quarter (dashed) and 5% centered (dotted). In the first and third case, the window was centered around the distribution mean at a particular stimulus intensity (SI). In the second, the window was placed such that the distribution mean fell at 25% of the window width. The x-axis shows the distribution mean as percentage of the maximal CMAP, and may be taken to represent stimulus intensity: 0 implies an SI that is just below the activation threshold of the lowest threshold motor unit, whereas 100 corresponds to a supramaximal SI and 50 to an SI that on average activates 50% of the MUs. (B) Percentage of responses that fell outside of the recording windows.

resulting six MUNE values. This procedure reduces the effect of a slight drift in the recorded CMAP sizes compared to analyzing all 180 responses together. We present MUNE results as median values rather than means because the results were not normally distributed. For the same reason, the median of MUNEs that were obtained for the four runs was taken to obtain an overall estimate. An overall MUNE was determined only if at least three runs in a particular subject were artifact-free.

2.4 Results

Figure 2.5 shows the results of the simulation study. Figure 2.5A demonstrates that the binomial estimate is nearly independent of SI, with a mean of 276 ± 3, and 5th and 95th percentiles of 254 ± 1 and 299 ± 1, respectively (errors represent standard error of the mean, evaluated over 10 simulation runs). This implies that for the simulated data, the binomial method overestimates the correct outcome of 250 by approximately 10%. The Poisson estimate, by contrast, strongly depends on SI. For low intensities (SI<5), the Poisson values are nearly as high as the binomial MUNEs, whereas in the middle range they decrease to below 100. At high stimulus intensities (SI>95), the Poisson MUNE returns to the initial values. The use of windows only slightly modulates this behavior, as may be deduced from the three examples in Figure 2.5A. For all three window settings used (10% centered, 10% low quarter and 5% centered), reasonably accurate results compared

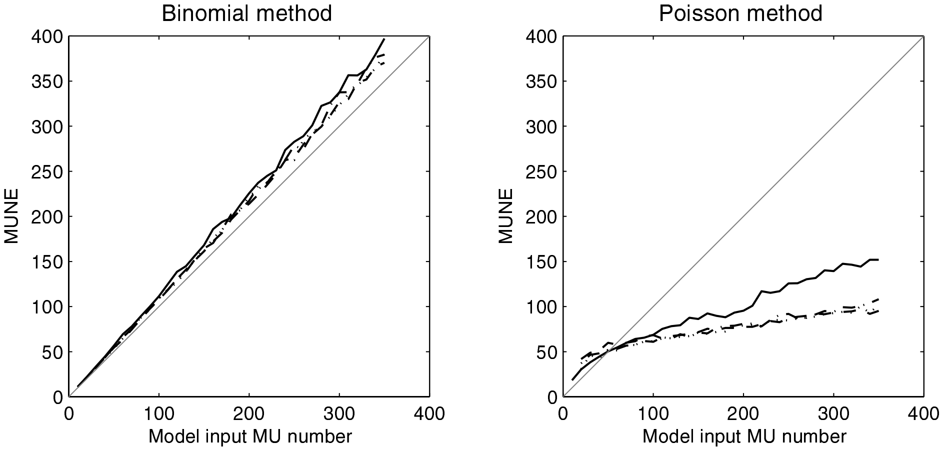

Figure 2.6: Model results for a range of motor unit numbers (model input). The gray line marks the ideal situation, in which the MUNE method would be able to determine the number of MUs perfectly. Results are shown for 4 stimulus intensities, resulting in distribution means at 15% (solid), 30% (dashed), 45% (dotted), and 60% (dash-dot) of the maximum CMAP size.

to the known model input of 250 MUs are obtained only for very low or very high stimulus intensities.

Figure 2.6 indicates that the binomial MUNE decreases proportionally with a decrease in number of MUs present, overestimating the true MUNE by approximately 10%. This factor appears to be independent of the number of motor units present. By contrast, the Poisson method decreases also linearly, but not proportionally, with a decreasing MU number over most of the tested range. This results in a more gradual decline in MUNE. Consequently, the Poisson MUNE at first is lower than the true MU number, but with increasing MU loss may eventually be higher (for numbers of MUs below approximately 50; left of Fig. 2.6B). The extent of over- or underestimation in the Poisson method is, therefore, highly variable.

The experimental MUNE results confirm the higher binomial values. For the Poisson method, a median MUNE value of 88 was obtained (range, 65 to 137); for the binomial method, median MUNE was 303 (range, 160 to 479). Both the binomial and the Poisson result agree well with the results of the simulation study. The experimental results are based on the data of 12 of the 19 subjects and a total of 37 runs. In the other 7 subjects, 11 runs yielded valid data but in only 1 or 2 runs per subject. Data from 28 runs were excluded for various reasons: severe drift in 9 subjects (12 runs), spread in 4 subjects (4 runs), motion artifacts in 2 subjects (2 runs), and steps in 4 subjects (4 runs). In a few cases, extremely high binomial MUNE values (>1000) could be observed. In these cases, the variance of the distribution was far too small to yield reasonable MUNEs. The results for these runs were also excluded from the analysis (6 runs in 4 subjects).

2.5 Discussion

2.5.1 Simulation study

The simulation model provides a simplified version of reality in that it assumes that MUs differ only by their recruitment threshold. Furthermore, we assumed these thresholds to be quite close together with respect to the width of the SI range over which the firing probability p of an individual MU increases from 0 to 1 (Fig. 2.4A). Hence, at intermediate stimulus intensities in particular, for a vast majority of MUs, this probability is larger than 0 and smaller than 1. Because the binomial method is based on the assumption that all MUs are probabilistically active, this agreement explains at least in part the good performance of the binomial MUNE method when applied to the simulation results (Figs. 2.5 and 2.6). In other words, the reliability of the model results presented here depends on the true size of the probabilistically active MU population at a given SI. As discussed in Appendix 2A, we have several reasons to believe that the variably active group is, indeed, large and that our model provides a sufficiently accurate description of the underlying physiology. Hence, its output can be used to assess the behavior of the MUNE with changes in the calculation method, stimulus intensity, window size, and window position.

When p is truly small, as is the case for low SIs, the Poisson estimate is as good as the binomial estimate (Fig. 2.5A), as expected on theoretical grounds. However, for most stimulus intensities, p cannot be that small. Consequently, the Poisson method severely underestimates the number of motor units. Changing window size or window position cannot adequately correct for this deficit. By contrast, the binomial method allows p to take any value between 0 and 1. In that way, it can accommodate the changes in the distribution characteristics that are the result of a rising stimulus intensity (Fig. 2.3). The resulting MUNE is much more accurate than the Poisson estimate.

Irrespective of the size of the variably active group of MUs or the calculation method used (Poisson or binomial), the statistical method of MUNE assumes that all MUs that are probabilistically active have the same activation probability p. Only when this condition is met is the distribution truly binomial (or Poisson). In the physiological situation, however, the observed variation will be determined by the combination of all individual probabilities of activation, $p_s(i)$, of all motor units at a particular stimulus intensity, s, and the result generally will not exactly follow a binomial distribution. That the observed CMAP size distribution at a certain SI would be binomial remains, therefore, an approximation. Nevertheless, the very good agreement between the model results and the binomial probability density function as presented in the middle row of Figure 2.3 indicates that it is a sufficiently good approximation indeed.

2.5.2 Experimental study

In its execution, the binomial test does not differ from the Poisson method (except for the selection of windows, which is superfluous), requiring but a minor change in the software algorithms that calculate the MUNE. However, as anticipated from the simulation study, the experimental MUNE values obtained with the binomial method (303; range 160-479) are much higher than those obtained with the Poisson method (88; range 65-137). Results for healthy subjects using MUNE techniques other than the statistical technique yield thenar MUNEs that range from low values between 150 and 200 (mostly for the spike-triggered averaging technique) and high values up to 360 for the increment counting method.[127] The median binomial MUNE of 303 fits well into this range.

Our results for the Poisson method are in fairly good agreement with previous results for this method.[79,80,101,129] In these studies, MUNE values between approximately 60 and 120 were found, with most values around 100. Although most of these results have been obtained for the hypothenar muscles, recent evidence[60] suggests that Poisson MUNEs obtained for the thenar and hypothenar muscles are similar, and hence that the aforementioned studies can be used to yield valid reference values for our study. In this comparison, it should also be recognized that, in determining the overall MUNE value of 88, we chose to use the median rather than the mean of the results of the 4 runs, because these results were not normally distributed. The mean was 102, which may be considered to be in even better agreement with previous results than the median value.

During the acquisition of the experimental data, we did not correct for drifts by slightly readjusting the stimulus intensity, as was done in some other studies.[60,101] Because we do not understand the nature of the cause of these drifts, we did not want to risk altering the variably active pool of MUs deliberately. The consequence of this choice was a large number of runs (12 out of 76) that had to be excluded from further analysis. For similar reasons, we did not repeat recordings at a different SI if we found steps to be present, but preferred to adhere to the predetermined settings of 10%, 30%, 50%, and 70%. In a clinical setting, of course, different choices may be made, which will yield a higher number of useful runs.

In six runs, extremely large binomial MUNE values were obtained (MUNE>1000). In these cases, Poisson values were also large (range, 127-519). Inspection of the corresponding distributions indicated that their width was very small. Because the width of a distribution is directly related to its standard deviation and hence to its variance, it follows from Equations (2.4) and (2.10) that MUNEs will be high. Most likely, in these cases only a relatively small number of the total population of MUs are variably active. Hence, the basic assumption of the binomial method is incorrect that all MUs are probabilistically active with equal probability. Future improvements of the binomial method should provide some measure to correct or at least warn for this situation. This problem has now been remedied by exclusion of runs yielding values above the somewhat arbitrary limit of 1000.

Finally, our simulation studies (Fig. 2.6) suggest that the binomial MUNE technique is more sensitive to a decrease in motor unit number than the Poisson method. Clinical studies are required to corroborate this. In this respect, it is important to note that the binomial MUNE method assumes a stable all-or-none response of motor axons following electrical stimulation. In this sense, it does not differ from the Poisson method. Any CMAP variability introduced by unstable MUAPs (such as in neurogenic conditions) cannot be separated from variability due to alternation and will affect the resulting MUNE.

Appendix 2A Number of simultaneously active motor units

Figure 2.1 shows the Poisson probability density function that follows from the assumption that only a small number of MUs (25 of a pool of 250) is probabilistically active with a small probability, p. It does not resemble most experimentally obtained distributions. Increasing the number of MUs will increase the absolute value of the mean of the Poisson distribution (assuming $p = 0.05$ and $n = 250$ will generate a Poisson distribution with mean $m = 12.5$; that is, a mean that is located in the middle of a 10% recording range with values from 0 to 25), but its value as percentage of the distributions' maximum observable value (250 instead of 25 in this example) remains the same. The long tail of the distribution, of values with a very small chance of being observed, is an integral part of a Poisson distribution and cannot be omitted. This is true even when this tail extends beyond the maximum observable value (maximum CMAP), leading to internal inconsistencies in the Poisson method. Because at higher stimulus intensities (SIs) this tail will extend further beyond the physiologically possible maximum, this internal inconsistency of the Poisson method becomes more pronounced with a rise in SI.

Furthermore, the aforementioned situation does not yet take into account the potential existence of a group of MUs that is never active at a particular SI. The size of this continuously inactive population cannot be estimated from the distribution, be it Poisson or binomial, because that would require registration of at least one occurrence of simultaneous activity of all probabilistically active MUs. As is illustrated in Figures 2.1 and 2.3, the probability of such an occurrence in a finite series of recordings is nil for all except the highest stimulus intensities. Conversely, this implies that the highest observed value generally does not reflect the combined activity of all probabilistically active MUs. Similarly, the smallest observed value in a series of recordings generally does not represent the situation in which none of the MUs is active either. Thus, from the information that is available in the distribution, it is impossible to determine the sizes of the always active, variably active, and never active groups of MUs. All that can be said is that the size of the variably active group is: (a) less than or equal to that of the total population; and (b) larger than or equal to the percent width of the observed CMAP size distribution. Both extremes (the first assumed in our methodology, the second in the conventional method) yield erroneous MUNE values, because physiologically at least two groups will exist at most stimulus intensities. However, one of the approximations will reflect physiology more accurately and, hence, result in a more accurate MUNE.

Little is known about the number of MUs (as percentage of the total number) that are probabilistically active at a certain SI, that is, about the extent of alternation. Work by Brown and Milner-Brown[17] showed that, beyond the 1 or 2 lowest threshold MUs, recruitment ranges quickly started to overlap. Although they were able to record some single MU stimulus-response curves, they could not determine how closely together the thresholds were for all except the lowest stimulus intensities.

Because of this lack of direct evidence for either of the two assumptions, we had to revert to indirect evidence instead. First, such evidence was found in the behavior of distribution width with stimulus intensity. If a large proportion of the MUs is probabilistically active with a probability that increases with stimulus intensity, then the width of the distribution will increase until intermediate stimulus intensities are reached and then decrease (Fig. 2.3). This behavior of distribution width with increasing stimulus intensity was experimentally confirmed. Second, support for a large variably active population and, hence, for the current model parameter settings, follows also from the good quantitative agreement between experimental results and the simulations – for instance, in the resulting MUNE values. Third, from our clinical experience with single-fiber EMG elicited by surface stimulation over the motor nerve, we know that recruitment ranges of individual muscle fibers tend to be in the same order of magnitude as the recruitment range of the muscle. This correspondence between the behavior of individual muscle fibers and of the muscle as a whole suggests that the MUs have stimulus-response curves that are very close together. Finally, we point out that a small distribution width percentage-wise is not necessarily related to a small group of probabilistically active MUs. It may equally well be the result of a large population of probabilistically active MUs (Fig. 2.3, lowest row). Based on the aforementioned evidence, we chose to implement and evaluate a binomial MUNE method that is based on the assumption that all MUs are probabilistically active.

3

A THREE-LAYER VOLUME CONDUCTOR MODEL AND SOFTWARE PACKAGE FOR APPLICATIONS IN SURFACE ELECTROMYOGRAPHY

On comparing multichannel surface electromyographic measurements of the m. biceps brachii with simulations performed with a previously developed two-layer volume conduction model, we found substantial discrepancies. To incorporate an apparent distorting effect of the skin tissue, the model was extended to three layers. This new model describes the potential resulting from an eccentric bioelectric source in a finite, cylindrical, and anisotropic volume conductor consisting of three layers, representing muscle, subcutaneous fat, and skin tissue. This chapter presents the governing mathematical equations of the three-layer volume conductor model as well as our approach to their solution. A comparison of various models shows that the three-layer model best describes measured potential distributions. Furthermore, we present the "Anvolcon" (analytical volume conductor) software package. This package has been developed to facilitate the use of the model for scientific and educational purposes.

JH Blok, DF Stegeman, and A van Oosterom
Annals of Biomedical Engineering 30: 566-577, 2002

3.1 Introduction

Surface electromyography (sEMG) is a non-invasive electrophysiological technique that provides information on central motor drive and the function of muscles. In sEMG, the recording electrodes are placed on the skin surface. The intermediate tissues act as conducting medium (volume conductor). Volume conduction results in the spatial spread of the electric field generated by the depolarized zone of a muscle fiber throughout the tissue in general and at the skin surface in particular. The nature of this spread strongly depends on the composition and conductivity of the tissue between the bioelectric source and the electrode. The resulting spatial (and temporal) behavior of the sEMG signal characteristics is complex and often counterintuitive. Yet, a proper understanding of these volume conduction aspects is essential for the correct interpretation of experimental results. As was shown by Roeleveld and co-workers,[121,123] the sEMG potential profile can be used to estimate motor unit location and size, the latter being a very valuable variable clinically. Via the potential distribution at the skin surface, changes in volume conductor characteristics can have a large impact on motor unit size estimates. To appreciate and understand this influence, as well as to guide the development and evaluation of new sEMG-acquisition and -analysis procedures, a computer model of volume conduction in human limbs is required. This model should be able to accurately simulate the potential distribution at the skin surface, irrespective of source depth and/or electrode position.

A number of surface EMG simulation models is currently available for various applications.[29,34,40,96,153] An advanced analytical volume conductor model for EMG in general was introduced by Gootzen et al.[57] It provided the mathematical description for an eccentric bioelectric source in a finite, anisotropic cylindrical volume conductor consisting of two layers. These layers were assumed to represent muscle tissue and subcutaneous fat. The two-layer model was developed to describe the effects of volume conduction on the action potentials of single muscle fibers, but could equally well be used to study motor unit action potentials (MUAPs). However, on comparing measured MUAPs from the m. biceps brachii with simulations performed with this model, Roeleveld et al. found substantial discrepancies.[119] The potential distribution over the skin surface in the direction perpendicular to the fibers was much smoother than the simulations predicted. Analysis methods based on inverse use of this model would result in (severe) overestimates of motor unit (MU) depth and, consequently, in underestimates of MU size.

To be able to describe a similar potential spreading or "blurring"[108] of the potential over the scalp, models of the electroencephalogram (EEG) usually take into account three different layers (brain, skull, and skin). In a previous paper,[119] we hypothesized that the potential spreading in sEMG was due to a similar cause as in EEG and extended the two-layer model to three layers. These three layers then can be taken to represent a large inner cylinder of muscular tissue, an intermediate layer of subcutaneous fat, and an outer layer of relatively well-conducting

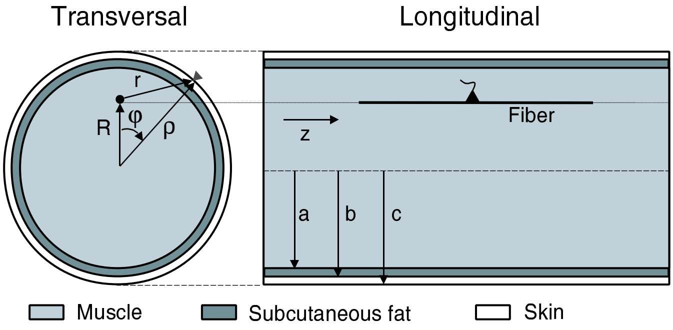

Figure 3.1: The three-layered cylindrical volume conductor configuration with eccentric source. The cross-section on the left (perpendicular to the cylinder axis) illustrates the relation between the local coordinates R and r, the cylindrical coordinates ρ and ϕ and the positions of axis, source and observation point. The cross-section on the right (parallel to and including the axis) shows the parameters a, b and c, describing the configuration, as well as the cylindrical coordinate z. The source (fiber) is shown with its motor endplate, i.e., the position of the neuromuscular transition, halfway along the fiber. The depth of the source equals $c - R$. Electrodes are dimensionless (point electrodes).

skin (see Fig. 3.1). This concept was followed by Farina and Merletti in their implementation of a three-layer model in Cartesian coordinates.[46]

The present paper describes the mathematical basis of the cylindrical volume conductor model, and discusses a number of aspects regarding its implementation. Throughout, the focus will be on volume conduction. The other essential ingredient of any sEMG model, an accurate description of the bioelectric source, is discussed in Appendix 3A at the end of this chapter. To facilitate the scientific and educational use of a well-tested version of the model in and beyond our own department, we developed a software package with a user-friendly interface. This analytical volume conductor (Anvolcon) software package is presented in Appendix 3B.

3.2 Methods

3.2.1 Mathematics of the three-layer bounded volume conductor

With sEMG models, we seek to understand certain phenomena observed in experiments. For that purpose, the models have to incorporate relevant “real-life” characteristics. It depends on the purpose of the model which these should be.[142] To reproduce volume conducted potential distributions properly, it is essential that the geometry of the model design reflects the recording configuration of experiments. Often, these experiments are performed on human limbs that, as a first approximation, may be considered cylindrical. They are finite, both in length and, more importantly, in radial extension. Since measured sEMG signals are dominated by the contributions of superficial motor units, the model should support the use of eccentric sources. It should also allow for the influence of the two tissue types – skin tissue and subcutaneous fat – that lie between the source and the recording electrode. In fact, especially for superficial sources, these two types may constitute the major part of the intermediate tissue and their combined effects on the volume conducted potential are certainly not negligible. Finally, tissue anisotropy needs to be incorporated, especially the anisotropy of muscular tissue with poor conductivity in the direction perpendicular to the fibers compared to that in the fiber direction.

In a human limb, the three tissue types are arranged in a more or less concentric configuration. For the construction of models, this cylindrical symmetry implies that it is possible to use an analytical description of the volume conducted potential. Thus, Heringa et al.[62] tackled the problem of an eccentric source in a finite, anisotropic but single-layer volume conductor. This configuration is realistic in the sense that it takes into account the finiteness of the volume conductor as well as the relatively superficial sources pertaining to experiments. The three-layer model presented here is an elaboration of the two-layer model described by Gootzen et al.[57] It incorporates all of the aforementioned elements and is based on the Poisson equation, a static approximation of the quasistatic volume conduction phenomena. Following the approach outlined in previous papers,[57,62,65] the general solution of this equation for each of the three layers of the configuration of Figure 3.1 is given by:

$$\begin{aligned}\Phi_1(\rho,\phi,k) = {} & \frac{d}{2\sigma_{1_r}} K_0\left(r\sqrt{\frac{\sigma_{1_z}}{\sigma_{1_r}}}|k|\right) G(k) \\ & + \sum_{n=-\infty}^{\infty} e^{-in\phi}\left[A_n(k) I_n\left(\rho\sqrt{\frac{\sigma_{1_z}}{\sigma_{1_r}}}k\right)\right]\end{aligned} \tag{3.1}$$

$$\begin{aligned}\Phi_2(\rho,\phi,k) = {} & \frac{d}{2\sigma_{2_r}} K_0\left(r\sqrt{\frac{\sigma_{2_z}}{\sigma_{2_r}}}|k|\right) G(k) \\ & + \sum_{n=-\infty}^{\infty} e^{-in\phi}\left[C_n(k) I_n\left(\rho\sqrt{\frac{\sigma_{2_z}}{\sigma_{2_r}}}k\right) + D_n(k) K_n\left(\rho\sqrt{\frac{\sigma_{2_z}}{\sigma_{2_r}}}|k|\right)\right]\end{aligned} \tag{3.2}$$

$$\begin{aligned}\Phi_3(\rho,\phi,k) = {} & \frac{d}{2\sigma_{3_r}} K_0\left(r\sqrt{\frac{\sigma_{3_z}}{\sigma_{3_r}}}|k|\right) G(k) \\ & + \sum_{n=-\infty}^{\infty} e^{-in\phi}\left[E_n(k) I_n\left(\rho\sqrt{\frac{\sigma_{3_z}}{\sigma_{3_r}}}k\right) + F_n(k) K_n\left(\rho\sqrt{\frac{\sigma_{3_z}}{\sigma_{3_r}}}|k|\right)\right]\end{aligned} \tag{3.3}$$

In these equations, the symbol Φ represents the potential as a function of position. The subscripts 1, 2, and 3 refer to the layers: a "1" attached to a quantity represents that quantity in the inner conductor or muscle tissue, a "2" and a "3" refer to the intermediate fat layer and the outer skin layer, respectively. The cylinder is supposed to be surrounded by nonconductive air. The radial positions of source, electrode, and cylinder axis are defined by three parameters (see the left

Table 3.1: Model parameters: symbols and default values

Symbol	Description	Default value
a	radius inner layer	32 mm
b	radius inner two layers	33 mm
c	cylinder radius	35 mm
σ_{1_z}	axial conductivity inner layer	0.5 $(\Omega\text{m})^{-1}$
σ_{1_r}	radial conductivity inner layer	0.1 $(\Omega\text{m})^{-1}$
$\sigma_{2_z} = \sigma_{2_r}$	conductivities middle layer	0.05 $(\Omega\text{m})^{-1}$
$\sigma_{3_z} = \sigma_{3_r}$	conductivities outer layer	1.0 $(\Omega\text{m})^{-1}$
R	distance axis-source	31 mm
$c - R$	source depth below skin	4 mm
	cylinder length	256 mm
	number of fibers	300
	muscle fiber conduction velocity	4 m/s
	mean fiber length	12 cm
	sample frequency	4000 Hz

side of Fig. 3.1). The parameter ρ is the radial distance between the central axis and the electrode. So, in the case of an electrode at the skin surface, ρ equals the cylinder radius, c. The second parameter, r, is the distance between the electrode and the line on which the source is located. Third, ϕ represents the angle between the radial directions (from the central axis) to the source line and the electrode.

The parameter k symbolizes spatial frequency in the axial direction. $G(k)$ is the Fourier transform of the electric current source function $g(z)$ to the spatial frequency domain. This source function describes the behavior of the current source density distribution along the active fiber with axial position z. The functions K_n and I_n are modified Bessel functions of order n, of the first and second kind, respectively, and $A_n(k)$, $C_n(k)$, $D_n(k)$, $E_n(k)$, and $F_n(k)$ are five unknowns which – for each n and k – have to be determined from the boundary conditions. The conductivity of the ith layer in the radial direction is represented by the parameter σ_{i_r}, that in the axial direction by σ_{i_z}. Each of the three layers is thus allowed to be anisotropic in the cylindrical coordinates ρ and z. Finally, d is the diameter of the fiber (source). An overview of the most important model parameters and their default values (taken from Roeleveld et al.[119]) is provided in Table 3.1.

Because the boundary conditions can be most easily expressed using the cylindrical coordinate ρ whereas the above Equations (3.1) to (3.3) are partly expressed in the local coordinate r, the following expansion of the K_0 term has to be used:[1]

$$K_0\left(r\sqrt{\frac{\sigma_{j_z}}{\sigma_{j_r}}}|k|\right) = \sum_{n=-\infty}^{\infty} e^{-in\phi} I_n\left(R\sqrt{\frac{\sigma_{j_z}}{\sigma_{j_r}}}k\right) K_n\left(\rho\sqrt{\frac{\sigma_{j_z}}{\sigma_{j_r}}}|k|\right) \tag{3.4}$$

The parameter R represents the radial distance between the central axis and the line on which the source is located (Fig. 3.1). This expansion applies only if $\rho > R$, which includes the case of an electrode at the skin surface and a source in the inner compartment. If an intramuscular (e.g., needle electrode) recording site is involved, the case $\rho < R$ has to be considered as well. For the relevant expansions, see, for example, Heringa et al.[62]

After substitution of the appropriate version of Equation (3.4) (i.e., with j =1, 2, or 3) into the corresponding equation of the set (3.1) to (3.3), the potential fields Φ_1, Φ_2, and Φ_3 are fully expressed in the cylindrical coordinates ρ, ϕ, and z (or k). Now, the following boundary conditions apply: at each transition between two compartments, the potential as well the current (which is proportional to the potential gradient) is continuous, meaning that:

$$\Phi_1\big|_{\rho=a} = \Phi_2\big|_{\rho=a} \tag{3.5a}$$

$$\sigma_{1_r}\frac{\partial\Phi_1}{\partial\rho}\bigg|_{\rho=a} = \sigma_{2_r}\frac{\partial\Phi_2}{\partial\rho}\bigg|_{\rho=a} \tag{3.5b}$$

$$\Phi_2\big|_{\rho=b} = \Phi_3\big|_{\rho=b} \tag{3.5c}$$

$$\sigma_{2_r}\frac{\partial\Phi_2}{\partial\rho}\bigg|_{\rho=b} = \sigma_{3_r}\frac{\partial\Phi_3}{\partial\rho}\bigg|_{\rho=b} \tag{3.5d}$$

$$\sigma_{3_r}\frac{\partial\Phi_3}{\partial\rho}\bigg|_{\rho=c} = 0 \tag{3.5e}$$

where a is the radius of the inner compartment, b the radius of the inner two compartments, and c the radius of the cylinder as a whole. Equation (3.5e) states that no current leaves the volume conductor.

Substitution of the modified version of Equations (3.1) to (3.3) into this set of boundary equations yields a set of five equations in the five unknowns A, C, D, E, and F for each value of n and k. The coefficients of the unknowns can be denoted as a 5×5 matrix. In principle, this set of boundary equations is solvable. When the five unknowns are determined for all n and k, a two-dimensional inverse Fourier transform finally yields the potential field. Unfortunately, because the K_n and I_n Bessel functions tend to very large or very small values for increasing values of n and for small or large values of k, the 5×5 matrix easily becomes ill-conditioned and its solution inaccurate. As described by Gootzen et al.,[57] it is possible to condition the linear system by rewriting it, using the following two characteristics of Bessel functions and of their combination with the unknowns $A_n(k)$ to $F_n(k)$:

1. From Equations (3.1) to (3.3) it can be seen that the combinations
    - $A_n(k)I_n(\rho\sqrt{\frac{\sigma_{1_z}}{\sigma_{1_r}}}k)$,
    - $C_n(k)I_n(\rho\sqrt{\frac{\sigma_{2_z}}{\sigma_{2_r}}}k)$,

   - $D_n(k)K_n(\rho\sqrt{\frac{\sigma_{2_z}}{\sigma_{2_r}}}k)$,
   - $E_n(k)I_n(\rho\sqrt{\frac{\sigma_{3_z}}{\sigma_{3_r}}}k)$, and
   - $F_n(k)K_n(\rho\sqrt{\frac{\sigma_{3_z}}{\sigma_{3_r}}}k)$

   contribute to the potential field and, hence, are restricted to physically acceptable values. Although the unknowns *A*-*F* and the Bessel functions I_n and K_n may independently yield unsatisfactory results, their combination counteracts instability.

2. The expressions

   $$I_l(x_1) \times K_m(x_2), \qquad \frac{I_l(x_1)}{I_m(x_2)}, \qquad \text{and} \qquad \frac{K_l(x_1)}{K_m(x_2)}$$

   are well-behaved as long as the value of $|l - m|$ is sufficiently small. The fraction $\frac{x_1}{x_2}$ should preferably be of order 1 for higher orders of l and m.

The set of five boundary equations can, therefore, be rewritten as:

$$\begin{pmatrix} \frac{I_n(a_1k)}{I_n(\rho_1k)} & \frac{-I_n(a_2k)}{I_n(\rho_2k)} & \frac{-K_n(a_2k)}{K_n(\rho_2k)} & 0 & 0 \\ s_1\frac{\mathcal{I}_n(a_1k)}{I_n(\rho_1k)} & -s_2\frac{\mathcal{I}_n(a_2k)}{I_n(\rho_2k)} & -s_2\frac{\mathcal{K}_n(a_2k)}{K_n(\rho_2k)} & 0 & 0 \\ 0 & \frac{I_n(b_2k)}{I_n(\rho_2k)} & \frac{K_n(b_2k)}{K_n(\rho_2k)} & \frac{-I_n(b_3k)}{I_n(\rho_3k)} & -\frac{K_n(b_3k)}{K_n(\rho_3k)} \\ 0 & s_2\frac{\mathcal{I}_n(b_2k)}{I_n(\rho_2k)} & s_2\frac{\mathcal{K}_n(b_2k)}{K_n(\rho_2k)} & -s_3\frac{\mathcal{I}_n(b_3k)}{I_n(\rho_3k)} & -s_3\frac{\mathcal{K}_n(b_3k)}{K_n(\rho_3k)} \\ 0 & 0 & 0 & s_3\frac{\mathcal{I}_n(c_3k)}{I_n(\rho_3k)} & s_3\frac{\mathcal{K}_n(c_3k)}{K_n(\rho_3k)} \end{pmatrix} \begin{pmatrix} A_n(k)I_n(\rho_1k) \\ C_n(k)I_n(\rho_2k) \\ D_n(k)K_n(\rho_2k) \\ E_n(k)I_n(\rho_3k) \\ F_n(k)K_n(\rho_3k) \end{pmatrix}$$

$$= \frac{G(k)\,d}{2} \begin{pmatrix} \frac{I_n(R_2k)K_n(a_2k)}{\sigma_{2_r}} - \frac{I_n(R_1k)K_n(a_1k)}{\sigma_{1_r}} \\ \sqrt{\frac{\sigma_{2_z}}{\sigma_{2_r}}}I_n(R_2k)\mathcal{K}_n(a_2k) - \sqrt{\frac{\sigma_{1_z}}{\sigma_{1_r}}}I_n(R_1k)\mathcal{K}_n(a_1k) \\ \frac{I_n(R_3k)K_n(b_3k)}{\sigma_{3_r}} - \frac{I_n(R_2k)K_n(b_2k)}{\sigma_{2_r}} \\ \sqrt{\frac{\sigma_{3_z}}{\sigma_{3_r}}}I_n(kR_3)\mathcal{K}_n(b_3k) - \sqrt{\frac{\sigma_{2_z}}{\sigma_{2_r}}}I_n(kR_2)\mathcal{K}_n(b_2k) \\ -\sqrt{\frac{\sigma_{3_z}}{\sigma_{3_r}}}I_n(kR_3)\mathcal{K}_n(c_3k) \end{pmatrix} \tag{3.6}$$

where the following notations have been used:

$$x_i = \sqrt{\frac{\sigma_{i_z}}{\sigma_{i_r}}}x \tag{3.7a}$$

$$s_i = \sqrt{\sigma_{i_z}\sigma_{i_r}} \tag{3.7b}$$

$$\mathcal{I}_n(x) = \frac{\partial I_n(x)}{\partial x} = \frac{I_{n-1}(x) + I_{n+1}(x)}{2} \tag{3.7c}$$

$$\mathcal{K}_n(x) = \frac{\partial K_n(x)}{\partial x} = -\frac{K_{n-1}(x) + K_{n+1}(x)}{2} \tag{3.7d}$$

On the right side of Equations (3.7c) and (3.7d), standard equalities have been used.[1] The set (3.6) results in stable solutions for all n and k. However, to avoid overflow and underflow problems in the calculation of the various Bessel functions that appear in this set, these functions are implemented using a dedicated addition and subtraction routine for the logarithms of modified Bessel functions.[57,61]

3.2.2 Modeling a cylinder of finite length

Equations (3.1) to (3.3) provide a continuous description of the potential in the spatial frequency (k) domain. The implementation of the inverse Fourier transformation of these equations, which is required to obtain the potential in the spatial (z) domain, involves a discretization of the spatial frequency scale. From Poisson's sum formula[112] it then follows that the resulting potential in the z domain has an infinite periodic continuation. Okada[109] and Heringa and Stegeman[61] have shown that one segment of this infinite, periodic potential distribution may provide a valid description of the potential in and on a cylinder of finite length. When a current source configuration has mirror symmetry around the center of the repeated cylinder segment, the repetition introduces virtual current sources which, by virtue of the method of images,[65] provide an equivalent description of the effect of the two insulating boundaries. To obtain this mirror symmetry in the repeated segment for a general source configuration, the cylinder containing the original source configuration must be mirrored once with respect to one of the two boundaries before repetition (see Figs. 3.2A and 3.2B). If this condition is met, and the double cylinder is used as input for the Fourier transforms, then the axial finiteness of the volume conductor is an inevitable result of the discrete spatial frequency description employed in the implementation of Equations (3.1) to (3.3). If it is not met, the potential gradient in the axial direction may not be zero as required at the position of the "boundaries".

Figure 3.2C illustrates the effect of mirroring (solid line) versus not mirroring (dashed). It shows the results of simulations with a single dipolar source at the central axis of a core conductor, i.e., a homogeneous, single-layer volume conductor with small radius compared to the source length. After mirroring, the potential is symmetric over the double (mirrored) cylinder segment, resulting in zero gradients at the boundaries. In contrast, the potential gradient is nonzero at the cylinder boundaries when the cylinder segment is not mirrored before performing the filtering and inverse discrete Fourier transform. The "background" potential with nonzero gradient physically implies a constant current flowing through the (infinite) cylinder.

Finally, in the implementation of the model, the source function (with N terms) is to and fro Fourier transformed. Therefore, an overall scaling factor of $1/N$ need be used.

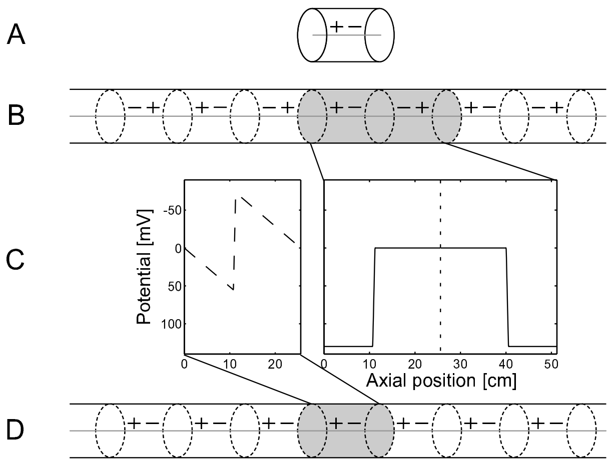

Figure 3.2: (A) and (B): Equivalent situations. (A) A cylindrical volume conductor with finite length, bounded by two parallel planes and enclosing a single dipolar source and (B) an infinitely long volume conductor without internal boundaries but with an infinite number of virtual images. The latter is, in fact, an infinite repetition of the light gray element, i.e., of the original configuration together with its image mirrored with respect to one of the (original) boundaries. (C) Effect of mirroring [solid line, right; resulting from the configuration in (B)] or not mirroring [dashed, left; resulting from the configuration in (D)] on the resulting surface potentials. Simulations were performed for a single dipolar source at the axis of a core conductor. The plot for the mirrored case shows the potential as a function of position in the original cylinder ($0 \leq z \leq 25.6$ cm) and one adjacent segment, with the dotted line marking the cylinder boundary and position of reference electrode. (D) Infinite repetition if the configuration is not mirrored.

3.2.3 Choice of source description and reference potential

To obtain potentials in volts as model output, an accurate, quantitative description of the bioelectric source is required. The source function $G(k)$ [see, e.g., Eq. (3.1)] represents the Fourier transform of the transmembrane current source density $g(z)$. This function $g(z)$ is proportional to the second (discrete) spatial derivative of the intracellular action potential (IAP). The constant of proportionality depends on the intracellular conductivity σ_i and the fiber diameter d [see Eq. (3.9) of Appendix 3A]. In the model, these are assigned the fixed values of 0.5 $(\Omega\mathrm{m})^{-1}$ and 50 μm, respectively. For modeling purposes, a number of mathematical approximations of recorded IAPs are commonly used.[31] Unless otherwise stated, the simulation results presented in this chapter have been generated with a mathematical function first proposed by Rosenfalck.[124] Since the source description can be considered independently from the volume conduction aspects of a sEMG model, it is not further considered here. Appendix 3A provides a more elaborate discussion of the source and its implementation.

Finally, attention has to be paid to the choice of the reference potential. In most infinite or semi-infinite models, potential differences ("potentials") are calculated between the electrodes and a reference at infinity, where the potential gradient equals zero. This implies that the influence of the reference potential can be incorporated by simply adding an arbitrary dc component, usually chosen to be zero. For a finite model there is no conductive path to infinity, meaning that the potential in and on the cylinder is "floating" (i.e., undefined) with respect to any position outside it. For that reason, a reference position has to be chosen in or on the cylinder itself. To remain close to results of simulations with other models, we have selected a reference point as far away as possible from the source: the lower-right-hand corner of the cylinder (with orientation as in the right of Figure 3.1). This choice is arbitrary, however, and may be adapted, for example, to mimic the reference electrode position in actually measured sEMG.

3.3 Results

With the completion of the three-layer model and its implementation in a software package (see Appendix 3B), a versatile tool has become available for a range of applications.[68, 119] Apart from the three-layer configuration, one- and two-layer volume conductors can easily be constructed by appropriately adapting layer conductivities. This model characteristic will be amply used in the results presented in this section, which aims to provide some examples of the model's possibilities, as well as some insight into its limitations. In all simulations, a dimensionless (point) electrode is assumed.

3.3.1 Extreme case 1: Core conductor

Consider a fiber at the axis of a homogeneous, single-layer cylindrical volume conductor. If both the intracellular and the extracellular radii are kept so small that any change of the potential in the radial direction can be neglected (core conductor), then the following equation holds:[2]

$$V_e(z) = -\frac{R_e}{R_i}[V_i(z) - V_{\text{rest}}]. \tag{3.8}$$

If the intracellular and the extracellular resistances R_i and R_e are equal, this implies that $V_e(z)$, the potential recorded at the cylinder surface, equals the opposite of the intracellular action potential $V_i(z)$, disregarding a dc shift (V_{rest}). As stated before, model input is not $V_i(z)$ itself, but $G(k)$, the Fourier transform of the transmembrane current source density (TCSD). This TCSD is proportional to the second spatial derivative of $V_i(z)$ (see Appendix 3A). The core conductor configuration with matched conductivities is, therefore, a double spatial integrator. More important in the context of this chapter is that it can demonstrate the influence on the signals of the discretization of the model in the axial direction. From a well-defined intracellular action potential (IAP), a TCSD can be calculated. When this TCSD is used as the program's input, any differences between the known IAP and the model generated output have to be due to rounding errors or other implementation problems such as inaccuracies in the solution of the set of boundary Equations (3.6).

Core conductor simulations were performed with identical conductivities for the three layers and a single muscle fiber [$\sigma_i = 0.5$ $(\Omega\text{m})^{-1}$ and $d = 50$ μm]. To obtain equal intra- and extracellular resistances at an extracellular diameter of 250 μm, all extracellular conductivities were set to 0.02 $(\Omega\text{m})^{-1}$. By comparing various IAP representations with the corresponding simulated potentials, it was found that the model indeed reproduces the IAP, except for some small differences (up to 3% of the signal's peak value for a tripolar source or 1.5% for the Rosenfalck source) at those positions where the second derivative of the IAP representation is high.

3.3.2 Extreme case 2: Superficial source

The previous case effectively circumvented most of the model's more complex mathematics. Since the source was located at the cylinder axis, all Bessel functions of order n with $n > 0$ vanished. This second case assesses model behavior in a configuration with a superficial source. In this situation, by contrast, very high spatial frequencies are present in the circumferential direction. To ascertain proper model function for realistic sEMG source depths (ranging from a few mm to two cm), a worst case scenario with a source depth of 1 mm was evaluated.

When a fiber is located very close to the curved cylinder surface, this surface seems approximately flat when viewed from the fiber's position. In a finite, homogeneous conductor this implies an approximate doubling of the potential at the skin surface (method of images) compared to the potential measured at the same distance from the fiber in an infinite conductor. Simulations show that differences between the total and the doubled infinite potentials [Eq. (3.3) and twice the contribution of the first term on the right-hand side of Eq. (3.3), respectively] are small indeed. For configurations with a fiber at a depth of 1 mm in a cylinder of radius 3.5 cm, they remain less than about 1% of the peak value. Taking into account the limited validity of the flat plane approximation of the cylinder surface, this implies that differences caused by rounding errors and other discretization problems can be neglected even for this extreme configuration.

3.3.3 Source depth

The model presented in this contribution allows for a detailed study of the potential fields resulting from a variety of volume conductor configurations. Figure 3.3 illustrates the effect of increasing fiber depth within a homogeneous, isotropic cylinder. Except for the most superficial source, the range of depths is a realistic one for sEMG. Note the rapid drop of potential amplitude with increasing distance. As is known from experiments,[122] the amplitude decline of the negative, upward peak is much stronger than that of the final positive (downward) peak, which is generated by the extinction of the action potential at the tendon. This results in a shifting dominance from the negative peak to this positive peak in the signals with increasing source depth.

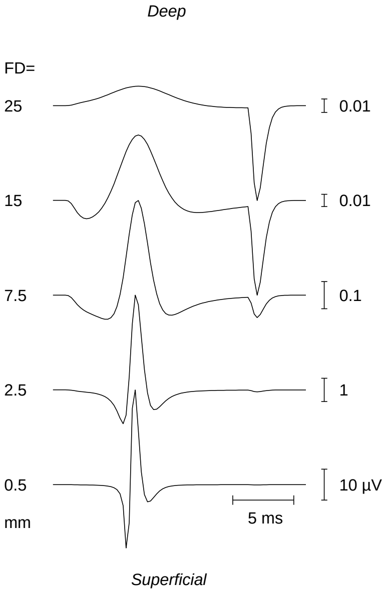

Figure 3.3: Surface single fiber action potentials in μV for varying fiber depth (FD) in mm in a homogeneous, isotropic volume conductor of radius 3.5 cm and with a conductivity of 0.5 $(\Omega m)^{-1}$. Simulation results are shown for an electrode 2 cm from the endplate zone. Following common usage in neurophysiology, negative potential values are plotted upward.

3.3.4 Three layers

To illustrate the effect of additional layers, Figure 3.4 shows surface potentials from a motor unit at a depth of 5 mm in a set of cylinder configurations. The electrode is right above the unit ($\phi = 0°$; see the left side of Fig. 3.1) and at an axial distance of 24 mm from the center of the endplate zone (i.e., the innervation region of the muscle fibers, see the right side of Fig. 3.1). The simplest, infinite volume conductor configuration is represented by the dashed curve (Inf). This conductor is assumed to be anisotropic with the conductivities of muscle tissue as shown in Table 3.1. The dotted line (M) shows the potential "recorded" on a finite volume conductor with a radius of 3.5 cm consisting solely of muscle tissue. Next, MF and MS illustrate the effect of replacing the outer 3 mm of muscle with an isotropic layer of subcutaneous fat or skin tissue, respectively. Finally, MFS presents results for the most complex, three-layer configuration. The amplitude of the negative peak of this curve (73 μV) is similar to that observed in sEMG recordings from motor units at a depth of 5 mm in the m. biceps brachii.[122]

Comparing the MF curve with the M curve, it can be deduced that the major effect of the poorly conducting subcutaneous fat layer is to enhance the potential amplitude while reducing signal width. The effect of the skin tissue, which conducts comparatively well, is exactly opposite: the signals are broadened and reduced in amplitude. The combined effect of fat and skin depends on the thicknesses of the

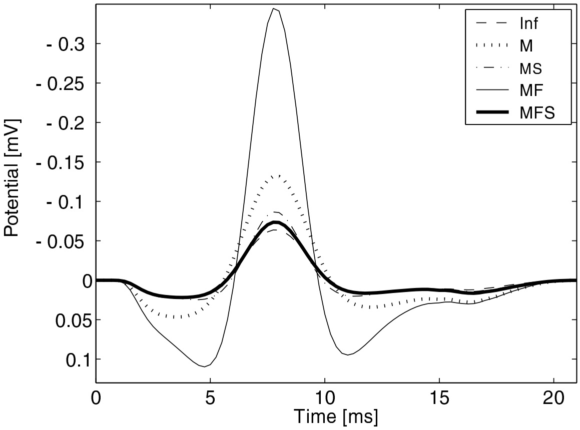

Figure 3.4: Model comparison. Simulation results for a variety of volume conductor (VC) configurations and a motor unit (300 fibers) at a depth of 5 mm. "M" indicates muscle, "F" subcutaneous fat, and "S" skin tissue. Configurations range from an infinite VC (Inf) with the conductivity values of muscle tissue, via a single anisotropic muscle layer (M) and two two-layered models (MF and MS), to a complex three-layered structure (MFS). Each of the indicated layers has the default conductivities indicated in Table 3.1. At a source depth of 5 mm, recorded motor unit potentials on average have a negative peak amplitude of approximately 50 μV.[122]

two layers and their respective conductivities.

In Figure 3.4, the effects of different model choices on the sEMG signal are demonstrated for signals as a function of time, but they can also be observed as a function of space, e.g., in the circumferential direction. This is illustrated in Figure 3.5 for the average volume conductor configuration as observed by Roeleveld et al.[119] Figure 3.5 shows the decline in sEMG amplitude in the direction perpendicular to the fibers. The signals with the largest amplitude are recorded right above the fibers ($\phi = 0°$); the other curves represent signals at the same axial position as in Figure 3.4, but spaced at $\Delta\phi = 9.8°$ intervals.

Apart from the results for the three-layer model (MFS), Figure 3.5 also shows the results for the two extreme cases of Figure 3.4: the infinite volume conductor and the two-layer MF configuration. Although Figure 3.4 suggests that the results of the infinite model approximate those of the three-layer model quite well, this is true only for the particular configuration chosen (small source depth and small electrode to source distance). By adapting this configuration, for example, by increasing the source depth or by shifting the electrode laterally, we might have made a match with any of the other models as well. For each of these, with the exception of the three-layer model, changing the configuration results in large deviations between the simulated and recorded potential distributions. This is illustrated in Figure 3.5. None of the one- and two-layer models is able to produce the slow decline of sEMG amplitude (large potential spreading) as observed in experiments (right; reproduced from Roeleveld et al.[119]) and simulated with the three-layer model. Recorded data are available only for distances of 0, 12, and

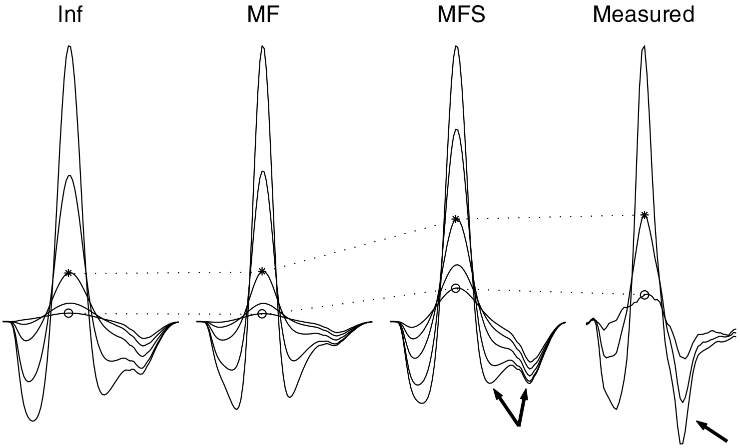

Figure 3.5: The decline of the sEMG potential over the circumference of the cylinder, for three of the configurations of Figure 3.4 and for experimental results (right). Negative potential values are plotted upward. Electrodes are spaced 9.8° apart, the first being right above the source (i.e., at $\phi = 0°$; see Fig. 3.1). The amplitude of the negative peak of this first signal is used for normalization (for absolute amplitude values, see Fig. 3.4). The decline with increasing ϕ values is slowest in the three-layer model, and similar to that observed in experiments. The experimental results are reproduced from Roeleveld et al.,[119] for electrodes spaced 12 mm apart. Identical positions (12 mm and 24 mm) are marked with "*" and "o", respectively, in all results, and are connected by the dotted lines. For the arrows, see the Discussion.

24 mm from the top (corresponding to $\phi = 0°$, 19.6°, and 39.2° in the simulations). These recordings were made simultaneously with scanning EMG[133] and multichannel sEMG. The scanning EMG recording allowed accurate determination of the location of individual MUs, and enabled spike-triggered averaging of the multichannel sEMG.

3.4 Discussion

This chapter has presented a three-layer analytical volume conductor model for applications in sEMG. To our knowledge, no experimental evidence exists that clearly demonstrates the effects on the sEMG of skin and/or subcutaneous fat. Such a study would probably require an *in vivo* comparison of the different volume conductor configurations presented in Figure 3.4. Instead, we used a comparison of recorded and simulated potential distributions at the skin surface. We believe this to be a good alternative for direct validation, since we set out to establish a proper match between the two distributions, particularly to support further development of data-acquisition and -analysis methods. The results of this "physiological" validation already were provided by Roeleveld et al.[119] Using a partly qualitative comparison of simulation and measurement results from the human m. biceps brachii, it was judged how well the model is able to reproduce the recorded potential distributions. Although limited to a small number of recordings, the rate of amplitude decline with increasing source depth of the recorded and simulated signals was similar, both for the negative peak that corresponds to the propagating component of the action potential and for the final positive peak that results from the termination of the action potential at the tendon. As reflected in the simulation results of Figure 3.3, measurements show a shifting dominance from the negative, upward peak to the positive, downward peak with increasing source depth. Remaining differences between measurements and three-layer model results consistently were a slightly slower decline of the recorded potential amplitudes with depth, of both peaks.

When the source depth remains fixed and the distance between source and electrode is increased by a lateral shift of the electrode position, a related decrease of signal amplitude can be observed. The potential distribution over the surface in the direction perpendicular to the fibers is much smoother than the two-layer simulations predict (Fig. 3.5; compare MF with Measured). In fact, none of the one- or two-layer models is able to describe this extensive spreading of the potential over the skin. However, with the addition of a third layer, it has become possible to reproduce this behavior quite accurately. From Figure 3.5, this is obvious for the negative peak. Positive peak behavior cannot be directly compared between simulation and experimental results. In the presented recording, two positive peaks add up (single arrow in Fig. 3.5, Measured), probably because of a short average fiber length: the third, positive phase of the propagating component of the signal and the positive peak that corresponds to action potential termination. For reasons of clarity, in the simulated signal these two components (marked by the two arrows in MFS) are separate, as is also commonly observed in experiments.

Still, the spatial spread of signal amplitude generally remains somewhat stronger than the simulations predict. Possibly, but not necessarily, this effect has the same origin as the unexpectedly small source depth dependence noted above. In part, both effects may be caused by an inaccurate combination of conductivity values as assumed in the model. Especially the value of the skin conductivity is somewhat ambiguous since reference values in the literature are scarce.[55, 152] Another explanatory factor may be the lack of a radially distributed source. To avoid the lengthy computations that would result from a source with scattered fiber positions, the representation of the source that we use places all fibers in the same radial position. A more realistic source that includes the effect of an increased circumferential spread of the fibers thus far has not been implemented.

The above indicates that the presented three-layer model is the method of choice for applications that strongly depend on an accurate description of the potential distribution at the skin surface. When the effect of the volume conductor is less important, other, less complex models may suffice. We advise against the use of a two-layer model with muscle and subcutaneous fat tissue (MF), since it artificially elevates potential amplitude and narrows the signal's propagating component (Fig. 3.4). A better option is the use of a two-layer configuration with muscle and skin tissue (MS). However, since this model is only slightly less complex than the three-layer version, there is not much to gain through its use. A similar argument would plead against the one-layer model (M) and for a (semi-) infinite model (Inf or 2×Inf). In this respect, it is interesting to compare the MFS curve with the Inf and M curves in Figure 3.4, the latter being approximately equal to the 2×Inf curve resulting from a semi-infinite model. Assuming that the three-layer model provides the best description of the sEMG potential, Figure 3.4 indicates that for small distances between source and electrode the much-used semi-infinite description of the volume conductor provides a worse estimate of sEMG amplitude than does the infinite model. Apparently, in this configuration, the effect of the additional layers is strong enough to counteract the doubling of the potential that is due to the cylinder boundary.

During the construction of the model, we also studied a four-layer version, incorporating a central bony structure. When put to use, we found its solutions to be unstable (most notably resulting in oscillations in the potential profile in the circumferential direction), especially for superficial sources. Apparently, the solution adopted for the numerical problems, i.e., the use of logarithmic Bessel functions and the redefinition of the matrix terms, no longer provides a sufficiently strong stabilizing influence. Furthermore, for those cases where stable solutions could be obtained (deeper sources), these did not differ markedly from the results obtained with the three-layer model presented in this contribution. Just like the addition of the two outer layers has its strongest influence on the signals of superficial sources, differences due to an inner fourth layer can be expected to be less for superficial sources than for deeper ones. We therefore believe that, with the construction of the three-layer model, we have about reached the maximum complexity in the analytical modeling of passive cylindrical volume conductors that significantly adds to the understanding of sEMG potentials. Probably, the most logical next step would be the incorporation of capacitive effects.[56] In fact, an example of a three-layer rectangular volume conductor model that can incorporate capacitive tissue characteristics has already been described by Farina and Merletti.[46] As of 2002, these authors did not actually study the influence of the frequency dependent conductivities on the sEMG, probably because for most applications the quasistatic or passive approach to volume conduction in muscle tissue remains a widely accepted one.

Finally, one intrinsic advantage of the presented model and its implementation is that it provides the full spatial distribution of the surface potential with a single run of the program. The effect of finite electrode size can easily be approximated by off-line averaging of the potential over the relevant surface samples. Furthermore, there is no need to repeat calculations for different electrode positions. This makes the model particularly apt for studying volume conducted distributions of potentials and their application in motor unit characterization.

Appendix 3A The myoelectric source

The input for the volume conductor transfer function is a description of the transmembrane current source density (TCSD), represented by the function $g(z)$ or its Fourier transform $G(k)$. On the assumption that the muscle fiber is a core conductor, the TCSD equals:

$$g(z) = \frac{\sigma_i (d/2)}{2} \frac{\partial^2 V(z)}{\partial z^2} \tag{3.9}$$

with σ_i the intracellular resistance and d the diameter of the fiber.[2] In the presented model, these are assigned the values 0.5 $(\Omega\text{m})^{-1}$ and 25 μm, respectively. $V(z)$ represents the intracellular action potential (IAP) as a function of axial position.

In the literature, three mathematical descriptions of the TCSD are commonly used (although many more have been proposed; see Ref. [31] for an overview): a dipole and a tripole or quadrupole description as well as the more realistic function based on the work of Rosenfalck.[124] These three representations differ in their approximation of the IAP. For the Rosenfalck description, an analytical expression is used that closely approximates the shape of measured IAPs:

$$V(z) = 96 z^3 \exp(-z) - 90 \ \text{ mV (for } z \geq 0 \text{ and } z \text{ in mm)} \tag{3.10}$$

In the case of the tripolar source, the IAP description is triangular. The dipole source corresponds to an (unphysiological) steplike IAP. All three source descriptions have been built into the Anvolcon software package (see Appendix 3B). The program also allows input of a user-defined TCSD.

Any discrete description of the TCSD has to start with a discrete description of the IAP. If, instead, a discrete TCSD is obtained through sampling of a continuous TCSD [irrespective of whether this TCSD was recorded or provided as a mathematical expression such as Equation (3.9)], in general the net dipole moment of all current sources together does not equal zero. Translated to the IAP, this implies that the potential does not return to its resting value after a complete cycle of depolarization and repolarization. On the other hand, starting from the IAP description assures that the potential returns to the same resting value.

The resulting TCSD consists of multiple, three, or two monopoles, respectively, for the Rosenfalck, the tripolar, and dipolar source descriptions. In Anvolcon, the time dimension is incorporated by assuming that these monopoles remain at a fixed distance from each other and move along the muscle fiber with a constant propagation velocity. For each new source configuration, different functions $G(k)$ are used while the volume conduction transfer function remains the same as long as the fiber depth does not change. Since the model is based on the assumption that the conducting medium is purely resistive, this simple way of incorporating time by considering each instance independently suffices. The effects of the generation and extinction of the action potential at the motor endplate and the tendon are described by dipole sources of varying strength. An extensive description of our implementation of these processes has been provided by Roeleveld et al.[119] Dimitrova et al.[29,31] have proposed an alternative for the time-consuming calculation of the independent time samples. Their proposal includes a simplified (but basically equivalent), dipole-layer based description of the generation and extinction effects. This elegant alternative has not been implemented yet in Anvolcon.

When the source function is thus defined at the single fiber level, the next step is to generate a motor unit as a set of related single fiber sources. For each of the fibers, the motor endplate position and the two muscle-tendon transitions are drawn at random from a normal distribution. All fibers have the same propagation velocity and are merged onto a single line to avoid the lengthy calculations that would result from a spatially more realistic distribution: for each different location, the volume conduction transfer function needs to be recalculated.

Finally, as has been demonstrated in a number of studies,[30,42,75,113] after the extinction of the propagating component of the action potential at the muscle-tendon transition, the IAP does not immediately return to its resting level. Instead, due to a slow repolarization, the IAP decreases approximately exponentially to zero. This so-called “negative after-potential” is not yet incorporated in any of the implemented source models.

Appendix 3B The Anvolcon software package

The functionality and usefulness of a model not only depend on its intrinsic properties and the assumptions it is based on, but also on how easy it can be implemented and operated. With source and volume conductor combined, the model counts many user-definable parameters. Most of these have to be bound by upper and/or lower limiting values to ensure proper model functioning and meaningful results. Ease of model operation then requires an orderly presentation of the parameters and their settings, together with a check on their crossing limiting values. Furthermore, the three-layer cylindrical volume conductor model is a valuable tool that can be used for many applications, but we felt that the complexity of its implementation might prohibit use of the model beyond our own department. The combination of these factors lead us to develop a software package with a user-friendly interface. This “Anvolcon” software package contains our implementation of the mathematics and numerical aspects presented in this chapter. Anvolcon was developed with LabWindows/CVI, a product of National Instruments Inc., for a Microsoft Windows environment. The package facilitates widespread use of a well-tested version of the model for both scientific and educational purposes. Its graphical user interface includes a limited viewing function for the simulation results. The complete set of results can be stored to disk for further analysis and comparison of multiple simulation results. For a simulation with default parameters, the results file has a size of approximately 25 MB, which takes somewhere between half a minute (e.g., with a 800 MHz Pentium III PC) and two to three minutes (with a 166 MHz Pentium PC) to calculate. A free copy of the program, in the form of a stand-alone executable with manual and sample analysis file, will be sent upon request to interested readers.

Part III

High-density surface EMG system

4

A HIGH-DENSITY MULTICHANNEL SURFACE EMG SYSTEM FOR THE CHARACTERIZATION OF SINGLE MOTOR UNITS

An electromyography (EMG) system is presented that non-invasively records the electrical activity of a muscle with 126 densely spaced skin-surface electrodes. The electrodes are arranged in a two-dimensional array, and integrated in a single container for ease of application. Signals are recorded “monopolarly”, with a reference electrode placed at a distance from the array. With this recording configuration, the surface EMG (sEMG) potential distribution can be described not only as a function of time, but also topographically. The availability of topographical information opens up a range of applications. Some of these have been described previously. However, the system presented is unique in that it allows exploration of all clinical and scientific possibilities of topographical sEMG. In its design, special attention was paid to user-friendliness and flexibility. With high-density multichannel sEMG, both the properties of a whole muscle and those of single motor units, the functional units of a muscle, can be studied. The latter belong to a realm that was long considered accessible only by needle-EMG, a conventional, invasive diagnostic technique. It is demonstrated that the additional topographical information can be used to characterize motor units in a way that is partially superior to needle EMG.

JH Blok, JP van Dijk, G Drost, MJ Zwarts, and DF Stegeman
Review of Scientific Instruments 73: 1887-1897, 2002

4.1 Introduction

Clinical electromyography (EMG) is a neurophysiological technique used to study the structure and function of peripheral nerves and muscles. An important part of the routine EMG procedure is the recording of the muscle's electrical activity with an intramuscular needle EMG electrode. Many methods have been developed over the past 40 years that allow interpretation of the needle EMG signals in terms of the most important characteristics of the contributing motor units (MUs).[133] Furthermore, with years of practical training and scientific experience, it is possible to relate the needle-recorded electrical activity of MUs to pathological conditions.[41,67] Regardless of how important needle EMG may be, it could be very beneficial for various reasons (see Paragraph 1.4) to replace the present invasive EMG technique at least partially by a non-invasive alternative, yielding similar diagnostic information. It has long been known that the phenomenon of volume conduction enables the electrical activity of superficial muscles to be registered at the skin surface. Yet, the single surface EMG (sEMG) signal that is commonly recorded contains little information about the level of single MUs. It is, therefore, necessary to extend the sEMG. This can best be achieved by increasing the number of recording electrodes, covering a larger part of the muscle. As is known from EEG and ECG, increasing the number of electrodes adds spatial information that is largely independent of the temporal information in the signal.

By extending the number of electrodes in a single direction to form a linear array, Lynn showed that it is possible to estimate the propagation velocity of the electrical activity along the muscle fibers.[85] The linear array was soon applied in normal and pathological conditions, but it never became a widely accepted clinical diagnostic tool. Although there was appreciation of the new variable (muscle fiber conduction velocity or MFCV),[155,156] linear arrays could not address most of the clinically relevant issues regarding the properties of single MUs. Later, two-dimensional arrays with a larger number of electrodes appeared.[87,115,118,123,150] Generally, these were designed for a specific purpose, such as the detection of the innervation or motor endplate zone,[87,89] the enhancement of the activity of superficial MUs[118] or the estimation of MU size and location.[120,123] Only in a very limited number of cases was an attempt made to use a multi-electrode array for diagnostic purposes. Kumagai et al. developed a grid consisting of 60 electrodes.[72,150,151] The spatiotemporal information they obtained in this way was used to calculate more reliable estimates of the MFCV in patients and in controls, by selecting the electrode column with the highest amplitude ("go-where-the-action-is" principle). They were also able to show abnormal propagation patterns in patients with Duchenne muscular dystrophy, a myogenic disorder, along with diminished discharge patterns and MU potentials with abnormally high amplitude in neuropathy. Huppertz et al. used two columns of electrodes flanking a central column to enhance the activity of superficial MUs in the signals of the central electrodes.[64,117] From these signals, several measures were calculated for both patients and controls and their value for diagnostic purposes was assessed.

The availability of topographical information opens up a whole range of possible applications, of which the above are merely examples. The goal of the developments laid down in the present chapter was the design of a system that would allow exploration of the clinical and scientific possibilities of topographical sEMG. To enable us to compare the power of this new technique with that of needle EMG, we chose to focus on its possibilities in MU analysis. At the same time, we sought to make maximum use of the additional information that multichannel sEMG may yield on the whole muscle. These goals naturally led to requirements concerning both data acquisition and analysis of the sEMG. As discussed in the next section, some of the design specifications are an immediate consequence of the sEMG signal characteristics themselves. Others follow from technical or operational demands and will be discussed in Sections 4.3 and 4.4. These sections also provide an overview of the data-acquisition system realized. Most of the presently available data-analysis tools are described elsewhere (e.g., in Chapters 5 to 7, and Refs. [123,37]). However, before discussing the performance of the system in Section 4.6, we will present an example of an application, illustrating the use of many of these tools in the characterization of single MUs (Section 4.5).

4.2 Translation of sEMG signal characteristics into design demands

The relatively large distance between the muscle fibers and the sEMG electrode implies that factors such as intermediate tissue composition and muscle morphology gain in importance compared to needle EMG. These factors differ from muscle to muscle and the sEMG signals change accordingly. Understanding why and how the recorded signals change, helps in determining the ideal recording configuration for a specific muscle. This first section therefore provides a brief introduction to the factors that influence the characteristics of the recorded signal. These characteristics logically lead to a set of design demands tailored to the needs of multichannel sEMG recordings.

4.2.1 The sEMG signal

The characteristics of any electrophysiological signal, independent of the type of electrode used to record it, depend on two major factors: the properties of the bioelectric source and the conductive properties of the tissue between this source and the electrode. In muscular tissue, the electric activity is generated at the outer membrane of the muscle fibers (the sarcolemma). From the motor endplate, the electric activity propagates along the membranes of both fiber halves toward the two tendons. At the tendons, it extinguishes.

Physically, during propagation, the myoelectric source has the character of a linear quadrupole. During the processes of generation and extinction, it can be described using dipole sources of varying strength (see, e.g., Ref. [119]). Since a quadrupolar

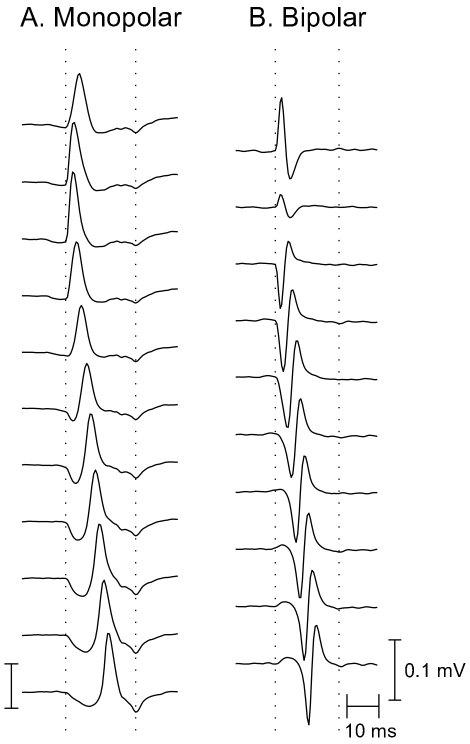

Figure 4.1: Surface EMG signals derived from a single column of electrodes, placed parallel to the fibers of the m. biceps brachii. Signals are averaged over multiple firing instances to improve signal-to-noise ratio (see also Section 4.5). Notice the presence of stationary components (marked with the dotted lines) in the monopolar signals (A) and their near-absence in the bipolar montage (B), which is constructed by subtracting the signals of consecutive electrodes in fiber direction. In contrast, the propagating component changes in space and in time for both derivations.

potential field decreases much more steeply with distance than a dipolar field, the components that correspond to action potential generation and termination often dominate the sEMG signal. These components are non-propagating, i.e., they occur for each electrode at the same instance in time (left of Fig. 4.1, dotted vertical lines). In contrast, the propagating component of the action potential varies, both with time and with position (see Fig. 4.1, left) and shows maximum amplitude when the activity passes beneath the consecutive electrodes.

The potential fields caused by myoelectric activity are shaped by the tissue surrounding the source. Although they can be studied both with needle EMG and with sEMG, the recorded signals are very different. These differences are mainly caused by the distance between the source and the electrode, and the composition of the intermediate tissue. In needle EMG, the subcutaneous fat and skin layers are of little influence. The amplitude and, to a lesser extent, the shape of the needle EMG signal are mostly determined by the distance between the source and needle electrode. For sEMG, the combination of poorly conducting subcutaneous fat and well-conducting skin is of major importance (Chapter 3). Together with the comparatively large distance between source and electrode, it results in strong low-pass filtering of the action potential's propagating component. The primary effect of this filtering is spatial, leading to increased smoothing or blurring of the potential profile. However, since it is easy to convert the space and time dimensions into one another, using the propagation velocity as a conversion factor ($z = Ut$), one can observe in time a similar broadening of the propagating component of the action potential with source depth.

4.2.2 Consequences for temporal and spatial sampling

While needle EMG is commonly recorded with a temporal sample frequency of about 50 kHz, for sEMG a lower rate of 2 kHz suffices. The highest temporal frequency components of the sEMG are around 400 Hz. These are observable in recordings from very superficial muscles with short fibers, such as the m. abductor pollicis brevis in the hand. Although for these recordings a sampling rate of 1 kHz meets the Nyquist criterion (sample frequency $>$ 800 Hz), it is more convenient to use a temporal sample frequency of at least 2 kHz.

To obtain an adequate resolution in the spatial domain, i.e., to ensure that rapid changes in the potential distribution over the skin surface can be recorded, the density of the electrodes has to be high enough to meet the spatial version of the Nyquist criterion for both directions involved.[86, 89] For the direction parallel to the muscle fibers, the Nyquist criterion demands that the propagating component be sampled in time with a minimum of 800 Hz (see above), i.e., at sample intervals of 1.25 ms maximum. Assuming a constant propagation velocity over the fiber of 4 m/s, it follows that the propagating component should be spatially sampled with a maximum IED of 5 mm. Unfortunately, no experimental results are available to corroborate this estimate, although results of Masuda et al. suggest that, at least for the fiber direction, an IED of 5 mm is adequate.[89] In their opinion, for the direction perpendicular to the fiber, the IED should be no more than 2.5 or 3 mm for detailed studies of the motor endplate zone.

Simulation studies using the dedicated volume conductor model described in Chapter 3 further support these estimates. The simulations indicate that small, superficial muscles require a high electrode density (IED of 2.5 to 3 mm), for both directions. For larger and/or deeper muscles, an IED of 5 mm suffices. These values correspond to values suggested by Rau and Disselhorst-Klug, based on a different model.[117]

In conclusion, it is our opinion that for the recording of the sEMG of small and/or superficial muscles, the IED should not exceed 3 mm. For larger muscles, an IED of 5 mm is acceptable, though 3 mm might be preferred for studies of the motor endplate zone.

4.2.3 Consequences for recording montage

The sEMG is often recorded bipolarly, using two electrodes attached to the skin above the muscle. A bipolar lead suppresses activity common to the two electrodes (primarily non-propagating components; see Fig. 4.1B). This spatial high-pass filtering effect is even stronger for higher order montages.[33,118] The advantage of these types of recording is that they single out the (high-frequency) contribution of superficial sources and focus on the action potential's propagating component. At the expense of a decreased signal-to-noise ratio, they yield a relatively "quiet" sEMG signal, in which it is fairly easy to detect the activity of single MUs.

By contrast, using a monopolar montage in which the electrodes over the muscle are referenced to an electrode at some distance, all components of the potential field are recorded. This includes the contribution of deeper sources and the non-propagating components of the action potentials. When a multichannel recording is made monopolarly, it remains possible to construct higher order montages, if required for a particular question. Reconstructing monopolar signals from a bipolar (or higher order) recording is, on the other hand, impossible. Furthermore, particular applications, such as the estimation of MU depth or average fiber length, are best performed using monopolar signals.[121] In our opinion, high-density multichannel sEMG data should, therefore, be acquired monopolarly, with a reference electrode placed at sufficient distance from the array (as in EEG).

4.2.4 Consequences for data presentation

From the above, it should be clear that the sEMG is a three-dimensional signal. Apart from the temporal dimension, it involves two spatial dimensions. For muscles with straight, parallel fibers it is most convenient to distinguish between the fiber direction and the direction perpendicular to the fibers. Since action potential propagation occurs only in fiber direction, the two directions yield different information. Generally, the three-dimensional nature of the sEMG signal requires selection of – or compression to – two dimensions before it can be presented comprehensibly on a computer screen. The choice of dimensions will depend on the question at hand (see also Sections 4.4.1 and 4.4.3). The data-display facilities should, therefore, allow easy switching between various modes of presentation.

4.3 Hardware

One of the guiding principles in the design of the multichannel sEMG system was that it should be flexible and serve multiple purposes. It should be a convenient tool in a research environment as well as easy to use in a day-to-day clinical setting. The following paragraphs in this section and the next provide an overview of "lessons learned" during the development and first years of use (1997-2001) of the system. They may serve as a list of (technical) aspects of a sEMG system

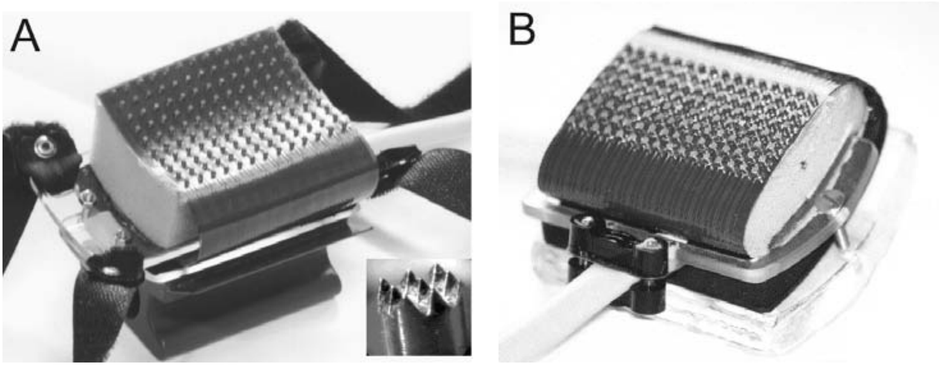

Figure 4.2: (A) Large electrode grid with 130 electrodes and interelectrode distance (IED) of 5 mm for use on larger limb muscles. The inset shows a close-up of an electrode. The serrated structure ensures a comparatively large contact area (and, thus, low impedance) at small electrode diameter. (B) Small electrode grid with 128 electrodes and IED of 3 mm for use on hand and foot muscles.

that we believe are essential in its proper functioning as a diagnostic or research tool.

4.3.1 Electrodes

For high-density multichannel sEMG in principle dry electrodes should be used, both to reduce the risk of short-circuiting the electrodes and to improve ease of use. The main disadvantage of dry electrodes, especially when they are of the small size required by the short interelectrode distance, is their high electrode-to-skin impedance, which results in increased noise levels and instability of the signals. Consequently, optimal high-density sEMG electrodes combine small size with low impedance.

The electrodes we use are adapted from commercially available printed circuit board testing probes (type "serrated contact"; see the inset in Fig. 4.2A), acquired from Farnell, Inc. They have a diameter of 1.52 mm, which is sufficiently small to allow the electrodes to be placed at a heart-to-heart interelectrode distance of 3 mm. From a range of probes with equal diameter but differing contact structure, the serrated contact had the lowest impedance.[12] This probably is the result of the comparatively large contact area/electrode diameter ratio. In contact with human skin and with sufficient pressure applied, these electrodes on average have an electrode-to-skin impedance of approximately 150 kΩ at 100 Hz. All electrodes are referenced to a single electrode at some distance from the muscle (monopolar recording). This reference electrode is a gold-coated but otherwise conventional (EEG) cup electrode of 1 cm diameter.

4.3.2 Grid design

To cover a large limb muscle with electrodes spaced as close as 3 or 5 mm, the number of electrodes required might well run into the hundreds. As yet, this would make the system inappropriately expensive and result in huge amounts of data that might or might not yield relevant information. Therefore, as a compromise, we chose to use 126 electrodes in two different configurations (see Fig. 4.2). The first is intended for measurements on larger limb muscles such as the m. biceps brachii and m. vastus lateralis. It has 13 electrodes in fiber direction and 10 electrodes in perpendicular direction, creating 13 "rows" of electrodes and 10 "columns". Corner electrodes are not used. In both directions, the interelectrode distance (IED) of this large grid is 5 mm. The second configuration has 16 rows of 8 electrodes, with IED of 3 mm. This slightly adapted layout was chosen to accommodate the more elongated shape of small muscles such as the m. abductor pollicis brevis. In the small grid, two of the corner electrodes (in one column) are not connected.

To allow the electrodes to be used routinely in a clinical setting, they have to be easy to apply. We therefore chose to integrate them gridwise in a single container, which can be pressed to the skin or, for the large grid, tied around a limb with Velcro. The electrodes of the large grid are mounted on a single flexprint and are connected to the cable at the other side of the print. A strain relief protects the fragile connections between cable and flexprint from high pressures and movements. To allow sufficient flexibility of the electrode configuration, the side of the flexprint with the electrodes is mounted on a 25 mm thick layer of foam. Thus, the grid can follow the muscle morphology to a large extent. The flexprint of the small grid is mounted on a thinner layer of foam. To avoid inaccurate interelectrode distances in fiber (propagation) direction, the grids are much more flexible in row direction than in column direction. "Semi-loops" in the flexprint (see, e.g., Fig. 4.2A) allow the print to move when the foam is compressed, without mechanically loading the electrodes or print-to-cable contacts. For optimal manageability and flexibility of the grids, we prefer to use a single, flexible and lightweight cable. The type used for both grids (Junflon PFA coaxial round cable, manufactured by W.L. Gore & Associates Inc.) contains 132 leads within a single cable of 8 mm diameter. All 132 leads are individually shielded, yet cable capacitance is low (110 pF/m at 1 kHz). The length of the cable is 1 m, i.e., sufficient for almost every application.

4.3.3 Data-acquisition hardware

The topography of the sEMG is only valuable if the small changes in the potential from one electrode to the next can be measured accurately. Furthermore, signal components that are common to an electrode and the amplifier ground are of no interest and should be suppressed (high common mode rejection). The Mark-6 128-channel BioSemi Inc. recording system that we use for our sEMG measurements is specifically designed with these physiological requirements in mind.[99,100] Of the available channels, 126 are used for multichannel sEMG, one for the recording of the reference potential and one for checking data storage. Input impedance is >100 MΩ.

In this amplifier system, signals are preamplified with a gain of 153 in an isolated and battery-powered front-end. They are filtered with a bandpass filter of bandwidth 3.2-400 Hz (high-pass: first order Bessel, low-pass: fourth order Bessel), and are simultaneously digitized (synchronous sampling). The signals are sampled at 2000 Hz with a resolution of 0.5 μV over a range of ± 16 mV. Data flow is 0.5 MB/s. Data are transferred from the front-end to a receiver via an optical fiber connection and then to a 450 MHz Pentium II PC, which is used to register the sEMG signals as well as to control the experiments.

4.3.4 Additional hardware

Many of the research-oriented applications of high-density sEMG require stable, isometric contractions. Therefore, the sEMG recordings are often combined with force measurements using specially developed ergometers (Fig. 4.3). Thus, we are able to provide the subject/patient with visual feedback about the contraction. Equally important is that in many cases the simultaneously recorded force adds valuable information to the sEMG measurements (see, e.g., Ref. [37]).

In clinical practice, the sEMG is often recorded from the muscle's response to electrical stimulation of the motor nerve, instead of from voluntary activity. With stimulated activation, the – often troublesome – analysis of the EMG interference pattern can be avoided. Furthermore, stimulated recordings require less patient cooperation. To accommodate this increase in versatility of the sEMG system, it was equipped with a constant-current stimulator. This stimulator was specially developed for electrophysiological experiments by the Equipment Services Department of the Nijmegen University Medical Center.

4.4 Software

To increase the flexibility of the sEMG system further, a variety of data-acquisition tools was developed, the most important of which will be discussed in this section. Most of the quantitative data analysis is still performed off-line, with algorithms that are described elsewhere (see, for example, Chapters 5 to 7, and Refs. [37,121, 123]). This section will conclude with a brief listing of possibilities regarding the analysis of the data.

Figure 4.3: Example of a recording with the large high-density surface EMG grid on the m. vastus lateralis. The reference electrode is attached to the knee. The leg is fixed in a specially designed ergometer to ensure an isometric contraction and to allow the simultaneous recording of delivered force. The white piece of equipment on the left is the amplifier system's front end.

4.4.1 User Interface

As in needle EMG, for the experienced clinical neurophysiologist the on-line inspection of the raw multichannel sEMG data provides a wealth of information regarding the condition of the patient. In contrast to needle recordings, however, more data are available than can be presented comprehensibly on a single screen. With 126 signals, containing both spatial and temporal information, a selection of the most relevant data is required. Besides, it often is impossible to determine in advance which data should be displayed. The display mode needs to be adjusted ad hoc, according to the findings in a particular investigation. This requires a versatile, flexible user interface that can easily make the switch from one way of presenting the recordings to another.

The data-acquisition and -display software presented here can be used for many different types of recordings, and continues to develop. The modular structure of the software, written in CVI/LabWindows (National Instruments, Inc.), allows easy implementation of new possibilities. However different the required display facilities may be, a common feature of all types of data acquisition is that the sEMG signal itself is the central source of information. Therefore, the major part of the graphical user interface (GUI; see Fig. 4.4) is used for displaying the raw data, as well as for several options to change the main features. The latter facilitate zooming of the displayed signals, both in horizontal (time) and vertical (potential amplitude) direction.

Since it should always be clear with which electrodes the displayed signals were recorded, the GUI shows a schematical picture of the electrode grid, which highlights the selected electrodes (Fig. 4.4A, upper left). From the 126 monopolar signals (or slightly less if higher order montages are used), a selection can be made row-wise (showing the signals of a single row of electrodes, perpendicular to the fiber direction; see Fig. 4.4A) or column-wise (showing the signals of a single column of electrodes; Fig. 4.4B).

The settings of the hardware and the parameters that determine the course of a measurement are placed more in the background, yet are easily accessible through the toolbar at the top of the GUI. They include both the controls of additional, PC-controllable hardware such as the constant-current stimulator mentioned in Section 4.3.4, and several settings for signal display and storage, e.g., for the triggered data-acquisition mode. This mode stores for all 126 channels those data that lie in a predefined interval around triggers.

4.4.2 Quality check

The quality of the information contained in a recording strongly depends on the placement of the electrode grid. Grid positioning involves two elements: obtaining a high signal-to-noise ratio, and properly placing the electrodes relative to the muscle and its fibers. The acquisition software supplies visual feedback of the recorded signals in a form that allows the user to assess both of these aspects during the preparatory measurements.

To guarantee a good signal-to-noise ratio and to keep crosstalk between amplifier channels negligible, the impedance between electrode and skin should be as low as possible. We consider an impedance of less than 300 kΩ, if obtained for the majority of electrodes, acceptable for our recording configuration. In people with dry skin, impedance can reach 500 kΩ or more. In these cases, a small amount of conductive electrode cream (Siemens Elema AB) is rubbed into the skin, while care is taken not to leave any on the skin to avoid short-circuiting the electrodes. In our experience, once the electrode-to-skin impedance is below 500 kΩ, it will continue to decrease during the experiment. Repeated application of gel is, therefore, unnecessary.

In general terms, the electrode grid is correctly placed if it covers the potential distribution sufficiently. To assess the quality of the recorded signals in this second respect, they can be viewed both column-wise and row-wise, as indicated in the previous paragraph and in Figure 4.4. In this way, it is possible to ascertain that the correct muscle or part of a muscle is located below the grid. Many applications further require that the columns of the electrode grid be aligned with the fiber direction. If they are not, signal shape and amplitude vary from one electrode to the next. This complicates, for example, the detection of single MU

A

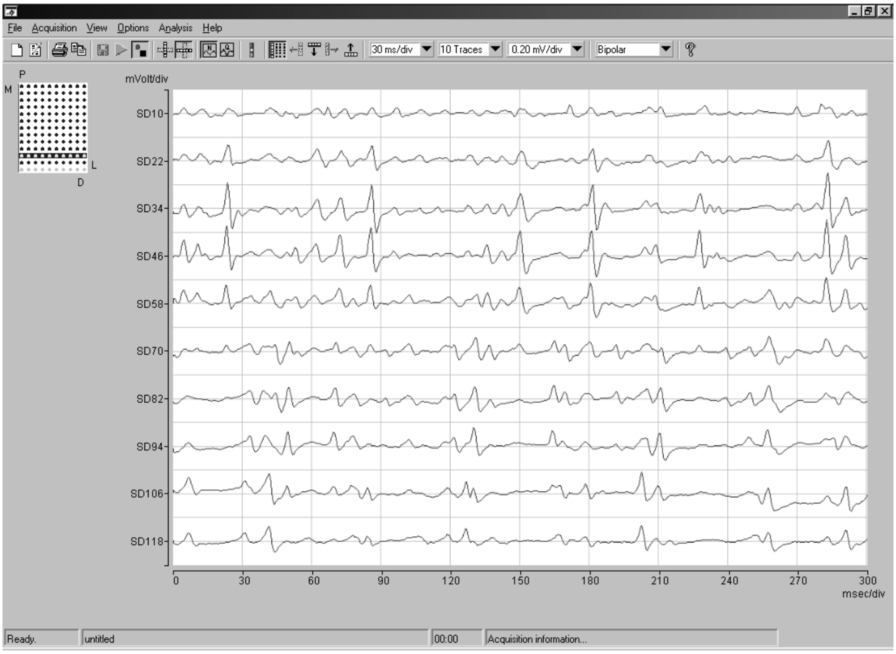

30 ms/div | 10 Traces | 0.20 mV/div | Bipolar

Ready. | untitled | 00:00 | Acquisition information...

B

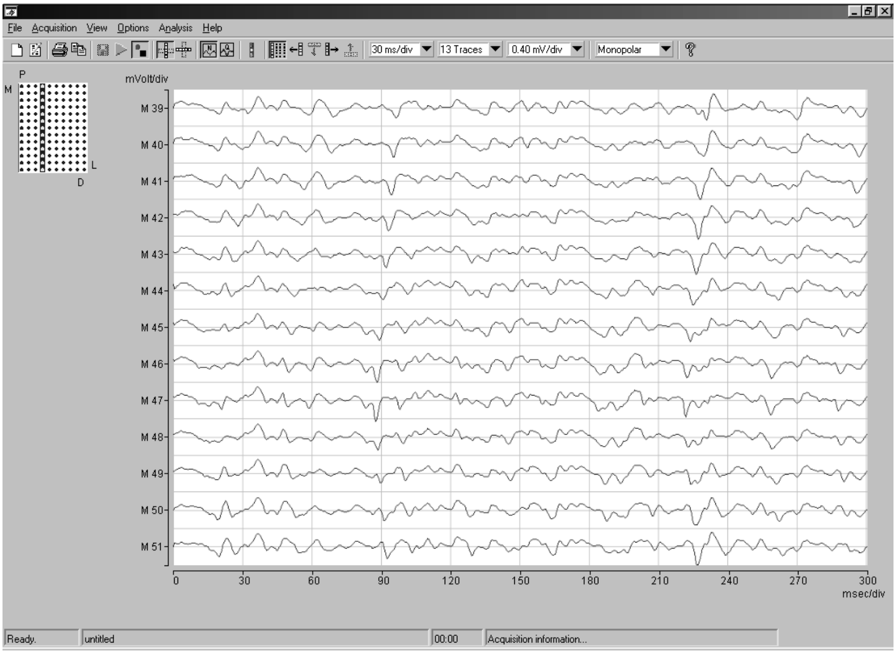

30 ms/div | 13 Traces | 0.40 mV/div | Monopolar

Ready. | untitled | 00:00 | Acquisition information...

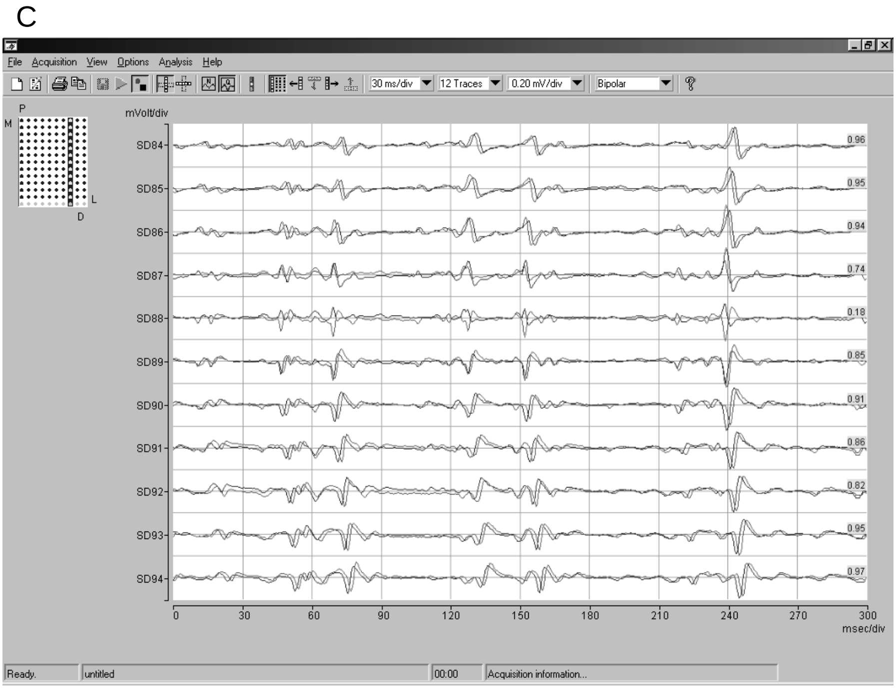

Figure 4.4: The graphical user interface that is used for data acquisition in three different viewing modes. The major part of the screen shows the signals from a single row [(A) bipolar signals] or column [(B) monopolar signals] of electrodes. This row or column is highlighted in the schematical representation of the grid on the upper left side of the screen. Zooming in on or out of the signals as well as switching between display modes can be performed using the various other buttons. (C) Data quality check by a pairwise superimposition of consecutive bipolar signals in fiber direction, together with their cross-correlation value.

potentials and prohibits an accurate determination of the muscle fiber conduction velocity (MFCV). Therefore, a visual feedback tool was developed that – pairwise – superimposes consecutive signals in fiber direction, together with their cross-correlation value (i.e., the maximum of the cross-correlation function, calculated and updated on-line for each 0.5 s of data). See Figure 4.4C. This tool helps to evaluate whether the signals are sufficiently similar in shape and amplitude for accurate analyses to be made, and guides the repositioning of the electrode grid if the signal correspondence is found to be insufficient.

4.4.3 Data analysis: available tools

When a needle EMG examination is performed, most of the relevant information is gained on-line, during the recording. The interaction with the patient and the (auditory and visual) feedback on manipulation of the needle electrode generally provide enough information to draw clinical conclusions. Although some quantitative (on-line or off-line) analyses, such as a turns/amplitude determination,[78] may also be made, for clinical routine most of these are auxiliary, not central. In a sense, the same applies to multichannel sEMG. Although the way of looking at and interpretation of these signals is quite different from that applied to needle EMG, on-line data inspection in conjunction with patient interaction still can provide a wealth of qualitative information. Many of the previously mentioned versatile display facilities were, therefore, developed with this specific goal in mind. They allow assessment of the sEMG interference pattern and, hence, muscle recruitment and central drive mechanisms up to the highest level of voluntary contraction, which cannot easily be attained with needle EMG.

Yet, a qualitative assessment is often insufficient. Pathological changes do not always translate into distinctive changes in the sEMG that are noticeable at a (trained) glance. A quantitative analysis is then required. For this purpose, there are various software tools available that can yield several estimates of MU and muscle characteristics. The next section will discuss the possibilities for single MUs. With respect to the muscle as a whole, the software includes tools for the following:

- Automatically detecting the main motor endplate zone in the raw sEMG. This morphological information might provide a better insight into the process of denervation and reinnervation in patients with neurogenic disorders, although this hypothesis still awaits confirmation for sEMG.
- Determining and mapping of amplitude and median frequency, both as a function of time and of position. This type of mapping can be used to determine position-dependent fatiguing or to study other space- and time-dependent properties of the raw data.
- Tracing peaks in the sEMG interference pattern to determine amplitude behavior both in space and in time. Drost et al. have shown that this type of algorithm can be used to characterize propagation disturbances over the muscle fiber membrane.[37]
- Determining the MFCV, both on individual peaks and on signal segments. As was pointed out by several authors,[72,155] this variable can be quite sensitive to pathological changes of the muscle fibers. It can also be used as an indicator of fatigue.[95]

Finally, as was mentioned in Section 1.3, a characteristic pathological change that can take place in a muscle affected by a neurogenic disorder is a reduction in the number of MUs. High-density multichannel sEMG can play an important role in estimating this number (Chapter 6).

4.5 Characterization of single motor units

Multichannel sEMG already has proven its value in a variety of applications. Instead of rediscussing them here, we will illustrate some of the system's capabilities via an application that combines many of the data-analysis techniques presented elsewhere: characterization of single MUs, obtained from a voluntary contraction.

In Chapter 5, it is shown that, at least for low contraction levels, the firing moments of individual MUs can be accurately determined from high-density multichannel sEMG (see also Ref. [68]). Using the topographical differences between the MUs that contribute to the sEMG, an advanced peak detection and classification algorithm can decompose the sEMG interference pattern. First, this provides non-invasive access to central MU firing characteristics during voluntary contractions. Furthermore, averaging the sEMG over the detected firing instances for all electrodes yields a low-noise template of the potential profile.[32] Figure 4.5 shows the results of this procedure for a multichannel recording from a sustained, isometric contraction of the m. biceps brachii, at 5% of the subject's maximum voluntary contraction. Results are shown for one out of five MUs detected. This unit fired with an average frequency of 11 Hz during the four minutes that the recording lasted. The potential that could be recorded when this MU fired, is shown for each of the electrodes in the grid, both for a monopolar (A) and for a bipolar montage (B). The signals presented in Figure 4.1 are a selection of these data (column 6).

From these templates, several spatiotemporal MU characteristics can be determined. As was recognized by Masuda et al.,[87] the position of the motor endplate zone of the MU can be detected from the bi-directional propagation pattern of the action potential, which results in low amplitude at and opposite signal polarity on both sides of the endplate in the bipolar montage (arrow in Fig. 4.5B). From the motor endplate, the action potential travels toward the two tendons with a velocity that in healthy conditions remains approximately constant over the length of the fibers. This MFCV can be determined from the time shift of the propagating peak, as observed with consecutive electrodes in fiber direction. To estimate the MFCV value, often a cross-correlation technique is used.[104, 107] For the MU of Figure 4.5, this yields an MFCV of 3.9 m/s.

From Figure 4.5A and, more easily, from Figure 4.1, it can be seen that the monopolar signals show a non-propagating component 20 ms after the generation of the action potential (marked with dotted lines in Fig. 4.1). This non-propagating component results from the extinction of the action potential at the tendon. Hence, using the MFCV value determined above, this implies that the distance between motor endplate and distal tendon is approximately 78 mm.

As was shown by Roeleveld et al.,[123] the amplitude distribution of the propagating component can be used to determine MU location. From the rate of decline of the (monopolar) amplitude of this peak in the direction perpendicular to the fiber, an indication of the depth of the MU beneath the skin surface can be obtained. Roeleveld et al. found that the distance over which this peak amplitude is halved

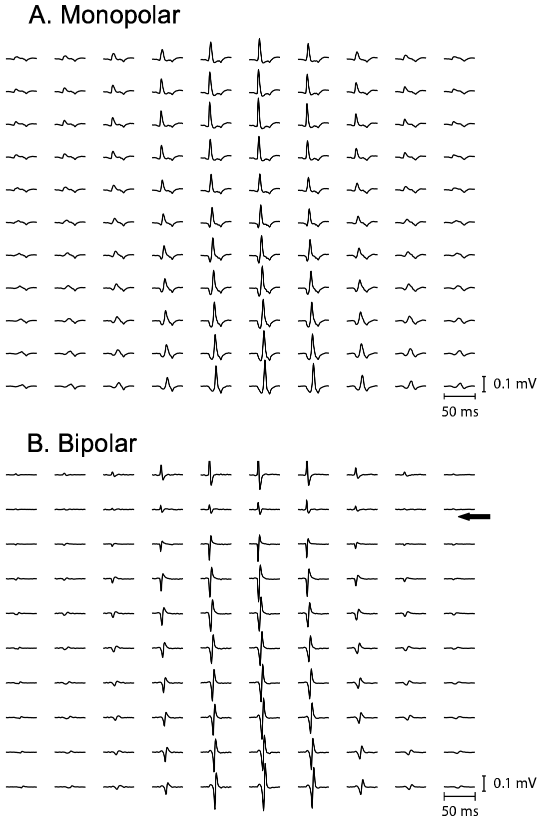

Figure 4.5: (A) Monopolar template ("fingerprint") of a single motor unit action potential, as analyzed from an m. biceps brachii sEMG interference pattern with the decomposition algorithm described in Chapter 5. The template results from averaging the sEMG interference pattern over all detected firing instances. (B) Idem, but now for a bipolar montage. The arrow indicates the estimated position of the motor endplate.

is approximately equal to twice the MU depth. In this case, the MU's estimated location was 3-4 mm below the skin surface.

One of the clinically very important properties of a MU is its size, defined as the number of fibers it contains. Since MU potential amplitude increases approximately linearly with this number, the maximum amplitude of the template (0.35 mV) might well be used as an indicator of MU size. However, besides MU size, several other factors determine potential amplitude, the most important being MU depth.[149] With known depth, the amplitude can be normalized to that of a MU at a depth of 1 mm, allowing comparison of MUs.[121] For this MU, the normalized amplitude (or MU size) equals 3.5 mV.

The previous listing includes a major part of the clinically relevant MU information that is present in needle EMG (firing characteristics, electric size). It also includes properties that cannot easily be accessed without a topographical technique. Some of the mentioned characteristics, such as average fiber length, as yet have no clinical value but might be useful in functional anatomical studies. Others, such as the MFCV, firing pattern, and MU size, have already found their way into research applications and are awaiting more widespread use in a clinical setting.

4.6 Discussion

4.6.1 Use of topographical information

There are many uses of the topographical information that becomes available through the recording of high-density sEMG. For some of these, a linear array of electrodes suffices,[94, 96] but most require a two-dimensional configuration. They may be divided into three global categories:

1. Going-where-the-action-is: on-line or off-line selection of electrodes with high amplitude or other interesting characteristics for further (more accurate) analysis of only one or a few signals.[72]
2. Use of the spatial dimensions of the signal in data analysis
    - to suppress the activity of deep parts of the muscle and thus to enhance superficial activity;[64]
    - as a more powerful discriminator between MUs than the temporal information, to recognize the contributions of single MUs in the sEMG interference pattern (Chapter 5).
3. Use of the spatial information contained in the signal
    - to estimate functional and anatomical MU characteristics, such as size and location;[103, 123]
    - to study spatial muscle inhomogeneities, by analyzing the signals for changes as a function of space and time.[37]

The major difference between the second and third categories is that the second uses the spatial dimension of the signal for a technical purpose, whereas in the third category the spatial MU or muscle properties themselves are the object of study. With full exploit of the indicated possibilities and, especially, by combining them, high-density sEMG can answer a large number of clinical and research questions regarding peripheral muscles.

4.6.2 Subjects and muscles

Surface EMG has the intrinsic disadvantage that it can only be measured from relatively superficial muscles. As may be deduced from the work of Roeleveld et al., the monopolar sEMG can be recorded from MUs at depths of less than approximately 2 cm within a muscle that lies directly beneath the skin.[122] Potentials from MUs at larger depths become smaller than the system's noise level, although non-propagating action potential components may be recorded from larger distances. Contrary to what might be expected, the thickness of the subcutaneous fat layer is of little influence for this range of the monopolar signals. Low conductivity limits the potential drop over this layer (Chapter 3 and Ref. [119]). For similar reasons, the recording of sEMG from MUs at any depth becomes extremely difficult in the presence of well-conducting subcutaneous edema.

For many of the applications mentioned above, a relatively simple muscle morphology is a prerequisite. An important indication of such a morphology is the presence of bi-directional propagation patterns. Masuda et al. studied 26 muscles accessible with surface electrodes.[88] Of these, 19 showed bi-directional propagation patterns, three did not, and four did show bi-directional patterns, but only at low contraction levels. Although it remains to be confirmed in the ongoing process of evaluation of the system, their results provide an indication of the muscles that may be fully characterized with the analysis tools mentioned in this chapter.

A third factor that determines system performance with regard to a specific application is the type of contraction performed. The optimal level of contraction is application dependent. For example, the detection of the activity of single MUs is possible only with low contraction levels (generally less than 10% of the maximum voluntary contraction). On the other hand, the characteristic changes in the sEMG of patients with generalized myotonia congenita proved to be most pronounced at the 60% MVC level.[37] In general, therefore, it is not possible to determine a priori the optimal contraction level for a new application. Furthermore, our recordings have thus far been limited to isometric contractions. Using multichannel sEMG to record activity of muscles during dynamic contractions would place additional demands on the system, especially with regard to the fixation of the electrode grid, the stability of the signals and the reduction of motion artifacts.

As to subjects, the recordings require cooperation. Other than that, however, no special criteria are used. In practice, we have chosen to exclude children from our preliminary studies. Although they form an important target population for the new system because they are likely to benefit most from the non-invasive nature of sEMG, the time-consuming nature of the evaluation experiments made them less apt candidates.

A limitation of the present system is that, for the m. biceps brachii (the muscle that we most extensively investigated) of 20-30% of women, it is difficult to obtain high-quality bipolar signals with clear propagation patterns. In those cases, the detection of activity of single MUs becomes difficult or even impossible. The percentage varies from muscle to muscle. It is (much) lower for more superficial muscles such as the m. abductor pollicis brevis. The exact factors that determine this effect remain uncertain, but the extent and constitution of the (sub)cutaneous layers are certainly among them.

4.6.3 Electrodes and montages

Since many electrodes are required in the construction of one grid and even more if several grids are to be used, the electrodes should be inexpensive and easy to obtain. Also, they should be made of a hard metal (rather than silver) to withstand the pressures applied to the grid, and, as indicated previously, they should have the lowest possible impedance. These are the main reasons for our selection of the commercially available probes used. The choice of the electrode material for sEMG is not very critical. Any instability caused by unstable electrode to skin contacts is likely to be in the low-frequency range of the spectrum (0-3 Hz), which is not important for sEMG measurements. Indeed, at random intervals, arbitrary channels can show low-frequency disturbances that last from several tens to hundreds of ms. They are of the same order of magnitude as the sEMG itself, but can be removed by high-pass filtering.

The small size of the dry electrodes results in high impedance values compared, for example, to standard EEG electrodes. This means that the noise in the sEMG signals is dominated by the thermal noise of the electrodes (1.4 μV RMS for an electrode impedance of 300 kΩ). Amplifier noise is 0.8 μV RMS. This produces a total noise level of 1.6 μV RMS, or about 10 μV peak-peak (pp). Noise therefore remains less than the size of the smaller MU potentials (order 15-20 μV pp).

A large number of superficial muscles can be studied using the two grids currently available (Fig. 4.2). The limitation to two grids has not yet restricted the flexibility of the recording, in the sense that the present grids would not adequately cover the topography of a specific muscle of interest. We expect that for the near future the two grids will suffice for all 126-channel recordings. However, when required, new grids can be developed relatively easily using the flexprint methodology, to accommodate the external morphology of other muscles or, for example, for use on children.

As indicated in Section 4.2.3, monopolar signals are most inclusive in the sense that they show sEMG components both different from and common to the electrodes. The presence of the contributions of the many non-propagating components in the interference pattern precludes, however, that individual MUs can be identified. Therefore, the monopolar montage is most important for averaged data, in which the contributions of other MUs are effectively averaged out (Section 4.5). A higher order montage should be used for viewing and analysis of the interference pattern, especially for its decomposition into the contributions of single MUs. In practice, we found it hard to predict which montage should be used for a particular application (Fig. 4.6). In principle, the higher the order of the montage, the greater the suppression of deep activity and thus the clearer the activity of the remaining superficial MUs. On the other hand, higher order montages result in decreased signal-to-noise levels. The optimal montage appears to depend strongly on the muscle, as well as on the composition of the intermediate tissue. In general, the smaller the distance between MU and electrode, the higher the order of the montage that can be used effectively. In practice, we generally prefer to use a simple bipolar derivation, both for on-line viewing of data and data quality, and for off-line analysis and interference-pattern decomposition.

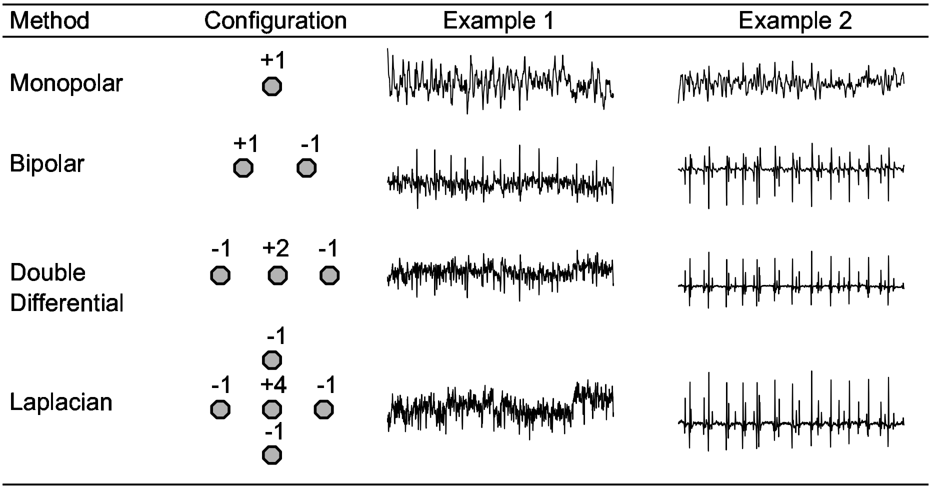

Figure 4.6: Illustration of electrode montages and their effect on surface EMG signals, showing the required electrode configuration and weights on the left. The third and fourth columns indicate their effect on sEMG signals recorded on the m. biceps brachii of two different, healthy individuals. The monopolar results are derived with the reference electrode at the elbow (infinity). In our experience, the montage with the highest signal-to-noise ratio is difficult to predict, yet for the majority of recordings the bipolar montage provides best results.

4.6.4 Use and userfriendliness

At present, the hardware functions properly in a technical sense. However important this may be, clinical use of the multichannel system makes demands that go beyond technical functioning. In particular, attention has to be paid to use and user-friendliness. In its present form, a single individual can operate the system, whether it be a clinical neurophysiologist or a research assistant. Thus far, most of our measurements were performed in a research setting. Although this often implied a stricter protocol than is used in the average diagnostic investigation (which is at least partially guided by ad hoc findings), we believe that much of our experience can be transferred to the clinical diagnostic setting.

The preparations for the recordings have proven to be of fundamental importance for data quality. They include proper placement of the grid and assessment of electrode impedance (see also Section 4.4.2). These preparations generally take five to ten minutes, the major part of which is taken up by finding the correct grid position. Less time is required if the alignment of the grid columns with the muscle fibers is not too important. Technical preparations, such as preparation of the skin and connection of the electrodes, only take a few minutes. In our experience, after completion of the preparations, the measurements can generally be performed in less than half an hour, although this duration strongly depends on the study protocol.

The major difficulty regarding the meaningful use of multichannel sEMG does not lie in technical aspects but rather in the interpretation of the recorded signals. As long as the data analysis is not fully automated, it will require experience and training to translate the multichannel sEMG into diagnostically relevant information. In this respect, sEMG is not different from needle EMG.

Finally, we have shown that the system presented can be used to study both the properties of a whole muscle and those of single motor units, the latter belonging to a realm that was long considered accessible only with needle-EMG. We do not claim to present a thoroughly validated alternative for needle EMG. Rather, we believe that we have developed a system that might provide an alternative for some specific applications. Equally important are the many possibilities that high-density sEMG has to offer beyond those of needle EMG, possibilities that we have only just begun to explore.

5

MAGNETIC STIMULATION-INDUCED MODULATIONS OF MOTOR UNIT FIRINGS EXTRACTED FROM MULTICHANNEL SURFACE EMG

The non-invasive assessment of motor unit (MU) firing patterns on the basis of topographical information from 126-channel high-density surface electromyography (sEMG) is reported. First, multichannel MU action potential (MUAP) templates are obtained by clustering detected firing events according to the surface topography of the MUAP. Second, a template-matching algorithm is used to find all firings of a MU, including the superimpositions of MUAPs. From a single recording, the firing pattern of up to five MUs could be derived. The modulation of MU firing by transcranial magnetic stimulation was analyzed in peri-stimulus time histograms. The results are similar to previous results of transcranial magnetic stimulation (TMS) obtained by needle electromyographic (EMG) recordings. The method can be used to investigate MU firing patterns in patients with central motor disorders. An additional advantage of the technique, apart from its non-invasiveness, is the structural and functional information that it provides on the MUs, which is not obtained by needle EMG.

BU Kleine, JH Blok, R Oostenveld, P Praamstra, and DF Stegeman
Muscle & Nerve 23: 1005-1015, 2000

5.1 Introduction

The excitability of the motor cortex and the corticospinal connections is reflected in postsynaptic activity of the spinal motoneuron pool.[110] This postsynaptic activity can be estimated from externally induced changes in the firing probability of motoneurons.[3] Therefore, studies of the central motor system via motoneuron activity need two basic elements: the controlled excitation of cortical neurons and a way to monitor the altered motoneuron firing patterns.

The most common way to induce changes in the human central nervous system is the application of transcranial magnetic stimulation (TMS). TMS can be used to "probe" cortical excitability. It modulates the firing of steadily discharging spinal motoneurons to a degree that depends directly on the excitability state of the cortex.[148] To monitor this modulation at the other end of the neural pathway, the motoneuron activity has to be recorded very accurately. In general, recording of single-cell responses of the human nervous system is problematic. However, the discharge of a spinal motoneuron leads to an action potential in all muscle fibers innervated by its axon, i.e., in the whole motor unit (MU). The muscle fibers belonging to a spinal motoneuron can thus be used as a "natural electrical amplifier". Their combined electrophysiological activity, known as the motor unit action potential (MUAP), may be larger by two to three orders of magnitude than the single nerve fiber action potential and can be registered with either needle or surface electromyography (sEMG).

The application of TMS and needle electromyography (EMG) in patients with amyotrophic lateral sclerosis revealed changes in cortical excitability. Hyperexcitability of the motor cortex was observed in the early stages and might precede the degeneration of cortical motoneurons.[3, 148] The technique was also used to measure the timing of descending waves in the corticospinal tract that were produced by TMS exciting the pyramidal cells directly (D-waves) or indirectly through interneurons (I-waves).[22, 53, 59, 102] As yet, no other technique is able to provide this type of information on the intact human brain in an experimentally accessible way.

Considering its high potential and its elegance, the number of applications for the TMS/sEMG technique is still relatively small. One reason might be that needle electrodes are a cause of pain and tension to subjects and certainly also to patients. They often hinder the maintenance of the steady MU discharge patterns that are required for the type of experiment just described. Moreover, they can hardly be used for follow-up studies. So, it can be argued that the combination of TMS with sEMG would open a unique non-invasive window on the temporal properties of the central nervous system, a window that can be used for a variety of purposes.

sEMG usually is discarded as an alternative to needle EMG, because it generally contains the intermingled contributions of many MUs. The resulting sEMG interference pattern is not expected to enable the detection of all firing events of single MUs. For conventional sEMG techniques this remains true. Single-channel needle electrodes are sufficiently selective to distinguish MUs by their wave shape.[92, 134, 135] However, the selectivity of a single (bipolar) signal derived from two surface electrodes per muscle does not allow reliable recognition of single MU firings. To improve decomposition accuracy of needle electrodes, LeFever et al.[76, 77] added spatial information by using three-channel recordings from a special needle electrode. The extra spatial (or topographical) information helped to resolve the signals from MUs that were similar in a temporal, but different in a spatial sense. In the study reported here, we analogously added topographical information to sEMG. The additional information from multiple sites on the skin surface makes the differences between MUAPs more pronounced.[11]

For needle EMG, adding spatial information is an improvement of an already fairly accurate technique. It allows a number of difficult cases to be better resolved. For sEMG, it is the only possible way of obtaining differences between MUAPs that are large enough to allow these MUAPs to be classified according to the MU that generated them. In addition, topographical sEMG, as will be described here, has an important advantage over needle EMG techniques: its wider view. Different MUs at different locations within the muscle can be separated very well by their skin surface topography.[123] Since multichannel sEMG can cover a large skin area, the spatial differences between the recorded MUAPs become much larger than between needle MUAPs, which all result from muscle fibers close to the electrode. Apart from MU location, the skin surface topography of a MUAP also relates more directly to often relevant anatomical and physiological properties of the underlying MU (Section 4.5; Ref. [120]). Thus, the addition of topographic information was expected to be especially valuable in sEMG.

The present study reveals the possibilities of using topographical information in the determination of the firing pattern of individual MUs. Our ultimate goal is to use multichannel sEMG together with TMS on a regular basis, so providing a truly non-invasive tool for functional motor studies. For this purpose, we put forward the following research questions:

1. how can the available topographical information be optimally used to decompose the sEMG interference pattern into the contributions of MUs;
2. how reliable are the results; and
3. how do the TMS-sEMG results compare to the results obtained with needle electrodes?

5.2 Methods and experimental setup

5.2.1 Subjects

Five healthy volunteers (age, 23-59 years) without signs of neuromuscular disorders were investigated. All subjects gave their informed consent. The experimen-

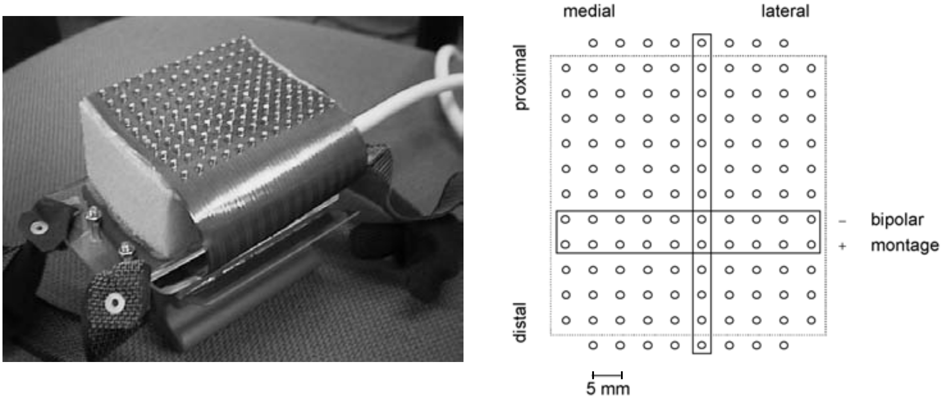

Figure 5.1: (A) The electrode grid as used for the sEMG measurements. Corner electrodes are not connected. (B) Schematic view of how the electrode grid (10 columns, 13 rows) is used in this study.

tal protocol was approved by the local ethics committee.

5.2.2 sEMG acquisition

The myoelectric signal was recorded with a multichannel electrode grid (Fig. 5.1A), in which the gold-coated electrodes are arranged in a 10 × 13 rectangular matrix with an interelectrode distance of 5 mm. A schematic view is given in Figure 5.1B.

The dry grid was applied above the belly of the biceps brachii muscle without skin preparation. The 10 columns of 13 electrodes each were oriented parallel to the muscle fibers. In total, 126 monopolar EMG signals (corner electrodes are not connected), each referenced to the olecranon, were amplified, bandpass filtered (3-400 Hz), AD-converted with a resolution of 0.5 μV/bit at a rate of 2 kHz/channel, and stored on the hard disk of a personal computer using a 128-channel amplifier system (Mark6, Biosemi Inc., Amsterdam, The Netherlands).

During the measurement, a column (11 or 13 electrodes in fiber direction) or a row (8 or 10 electrodes perpendicular to the fiber direction) of channels can be selected for on-line visualization. Bipolar derivations are obtained by subtracting the monopolar signals measured at two adjacent electrodes of the same column, which reduces the number of channels in each column by one. Due to their higher spatial selectivity, bipolar signals are more suitable than the original monopolar signals in the stage of separation of MUAPs. In this application, the signals measured from the most proximal and distal rows were not included in the MUAP templates, leaving 100 channels (dotted square in Fig. 5.1B).

5.2.3 Protocol

After proper application of the electrodes, a row (perpendicular to the fibers) of bipolar signals between the endplate region and the tendon was selected for visual feedback.

Once a stable pattern of several active MUs was achieved, the subject was instructed to keep the force constant. The force of the flexion of the left elbow was measured by a strain gauge ergometer attached to the wrist. The force signal was displayed on a monitor to help the subject maintain a steady contraction. The required force level, i.e., the level at which several MUs are recruited while their sEMG pattern remains separable, was lower than or of the order of 5% of the maximum voluntary contraction. The isometric contraction had to be maintained for some minutes, during which 100 magnetic stimuli were given with intervals of approximately 2 s.

5.2.4 Magnetic stimulation

Magnetic stimuli were applied with a Magstim 200 (The Magstim Company Ltd., Whitland, UK) using a standard circular coil (90 mm diameter) centered above the vertex with the "B"-side visible. Each stimulus induces a current flowing anticlockwise (as viewed from above) resulting in a posterior-anterior current flow in the right hemisphere. During a slight but steady voluntary contraction of the subject's biceps, the stimulation strength was increased in steps of 5% of the maximum stimulator output until a clear response was visible in the sEMG. Stimulus strength then was reduced again by 5%. The first stimulation intensity that produced a clear motor evoked potential also elicited a visible twitch. In this way, TMS intensity was just subthreshold for a visible contraction.[5]

5.3 Data analysis

All of the data analysis was performed off-line. It involved three main steps: (1) obtaining relatively noise-free MUAP-templates of the MUs that contribute to the EMG interference pattern; (2) using the templates to find all the firing instances of those MUs; and (3) relating these firing instances to the TMS pulses and analyzing the changes in firing behavior.

5.3.1 Template Construction

To be able to recognize the firings of a particular MU in the interference pattern, it is necessary to obtain a virtually noise-free template of the MUAP generated by this MU. MUs can be differentiated by their position, size, and depth. These factors mainly influence the amplitude distribution of the MUAPs in the medial-lateral direction.[123] A large part of the available topographical information is

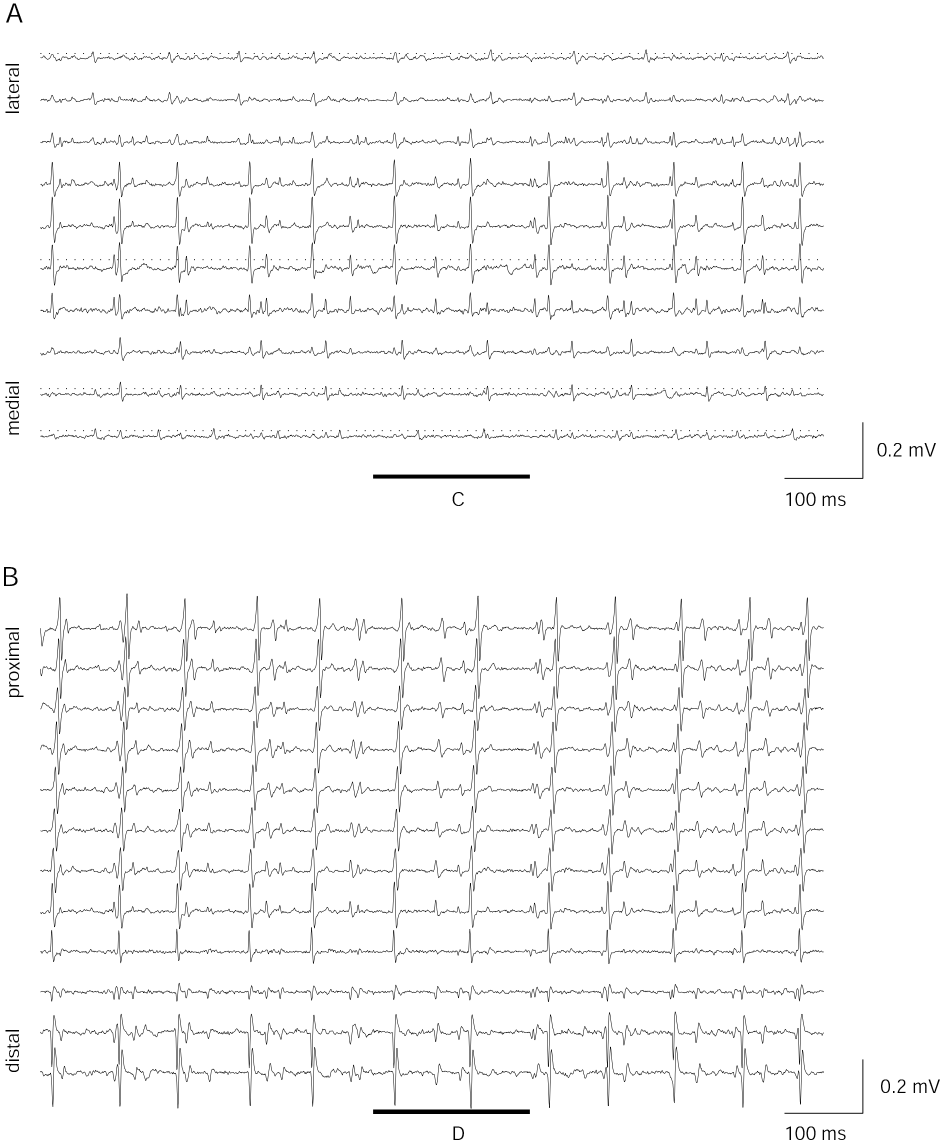

Figure 5.2: Example of 1 s of sEMG recorded during an isometric contraction of the biceps brachii muscle at low force. (A) The bipolar signals constructed from the fifth and sixth electrode row (perpendicular to muscle fibers; horizontal box in Fig. 5.1B). Dotted lines indicate peak-detection thresholds for channels 1, 2, 5, and 10. (B) The bipolar channels taken from the sixth electrode column (parallel to muscle fibers; vertical box in Fig. 5.1B). The segments indicated by the solid bars in (A) and (B) are expanded in (C) and (D), respectively (next page).

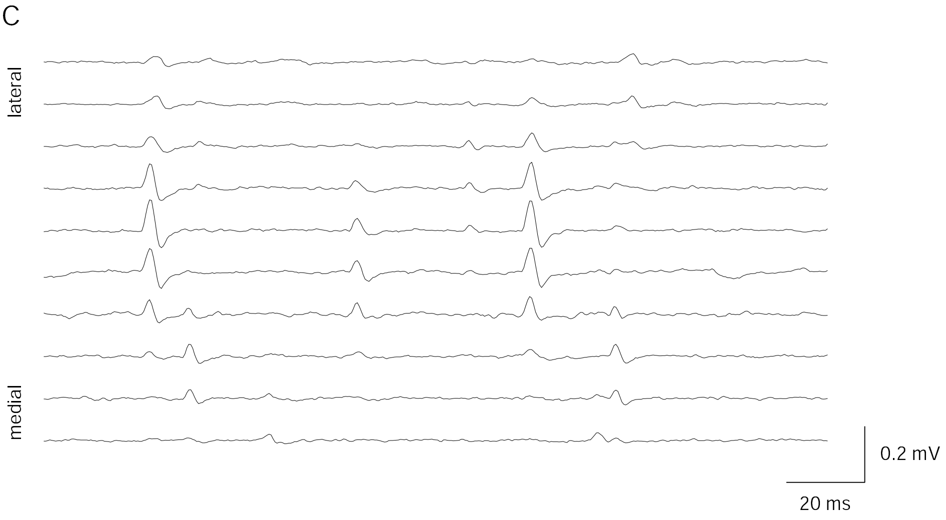
C
lateral
medial
0.2 mV
20 ms

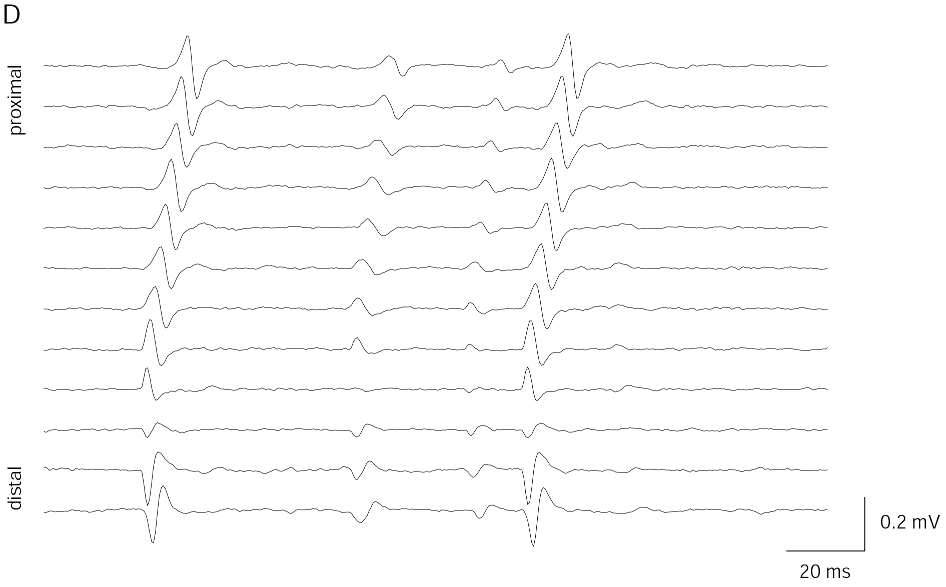
D
proximal
distal
0.2 mV
20 ms

thus already included in an appropriately selected single row of bipolar signals. When superimpositions of MUAPs are excluded, the topographical differences within one row of bipolar signals appeared sufficient to distinguish the MUAPs generated by different MUs.

Therefore, the construction of MUAP templates started with the experimenter selecting a single row of bipolar signals with a high signal-to-noise ratio and clear topographical and amplitude differences. Care was taken to avoid endplate regions, where the bipolar sEMG amplitude is low and MUAPs might be missed. Next, the data of a selected time segment of 40 s were read from the file for the two rows of monopolar (2 × 10) electrodes that constituted the chosen bipolar ensemble of signals (in the example presented, the fifth and sixth row were taken; see horizontal box in Fig. 5.1B). The bipolar montage for the 40 s sEMG was then calculated and digitally high-pass filtered at 20 Hz to remove slow baseline drifts. An example of such an ensemble of signals (1 s) is shown in Figure 5.2.

The MUAPs in the bipolar signals were isolated from the background activity by a peak detection procedure. Once the amplitude of the signal exceeded a user-defined threshold, the sample number of the peak extremum was added to a list. Due to their topographical differences, not all MUAPs were visible in all channels. Therefore, the peak detection was carried out for several of the 10 channels to find all MUAPs. In the example, four channels (and different amplitude thresholds, dotted levels in Fig. 5.2A) were chosen for the peak detection. Note that the endplate region can be recognized in a proximal-distal view along the fiber direction as presented in Figure 5.2B. Channels and thresholds were adjusted for each subject to include the MUAPs that could be distinguished by eye. The potential problem of multiple detections of the same MU firing across channels can be avoided by the proper selection of channels and thresholds. If two peaks were detected within a time interval of less than 7 ms, both were removed from the list. This step removed most complex wave shapes produced by superimpositions of MUAPs, since a main MUAP peak usually is shorter than 3.5 ms.

The TMS produces a sharp artifact that is present in all channels. It could be misclassified as an additional MUAP or disturb the templates. Therefore, the TMS artifact was detected in the reference signal from the olecranon, where no MUAP activity is expected. Peaks detected in the bipolar channels close to the TMS artifact were also removed from the list.

After completion of the peak detection, a data segment of 3.5 ms (seven samples) around each of the listed peaks was used to group the MUAPs. Longer segment-duration did not increase classification accuracy. Each peak was thus represented by 70 datapoints (10 channels × seven samples). Peaks which had similar topographical and temporal characteristics were assumed to be generated by the same MU. As a measure of similarity, the Euclidean distance between peaks was taken. This distance can be calculated by taking the square root of the sum of the squared differences between the 70 datapoints from each pair of peaks. The Euclidean distances between all possible pairs of peaks were then fed into a Wards clustering algorithm.[44] This clustering algorithm sorts the peaks into groups ac-

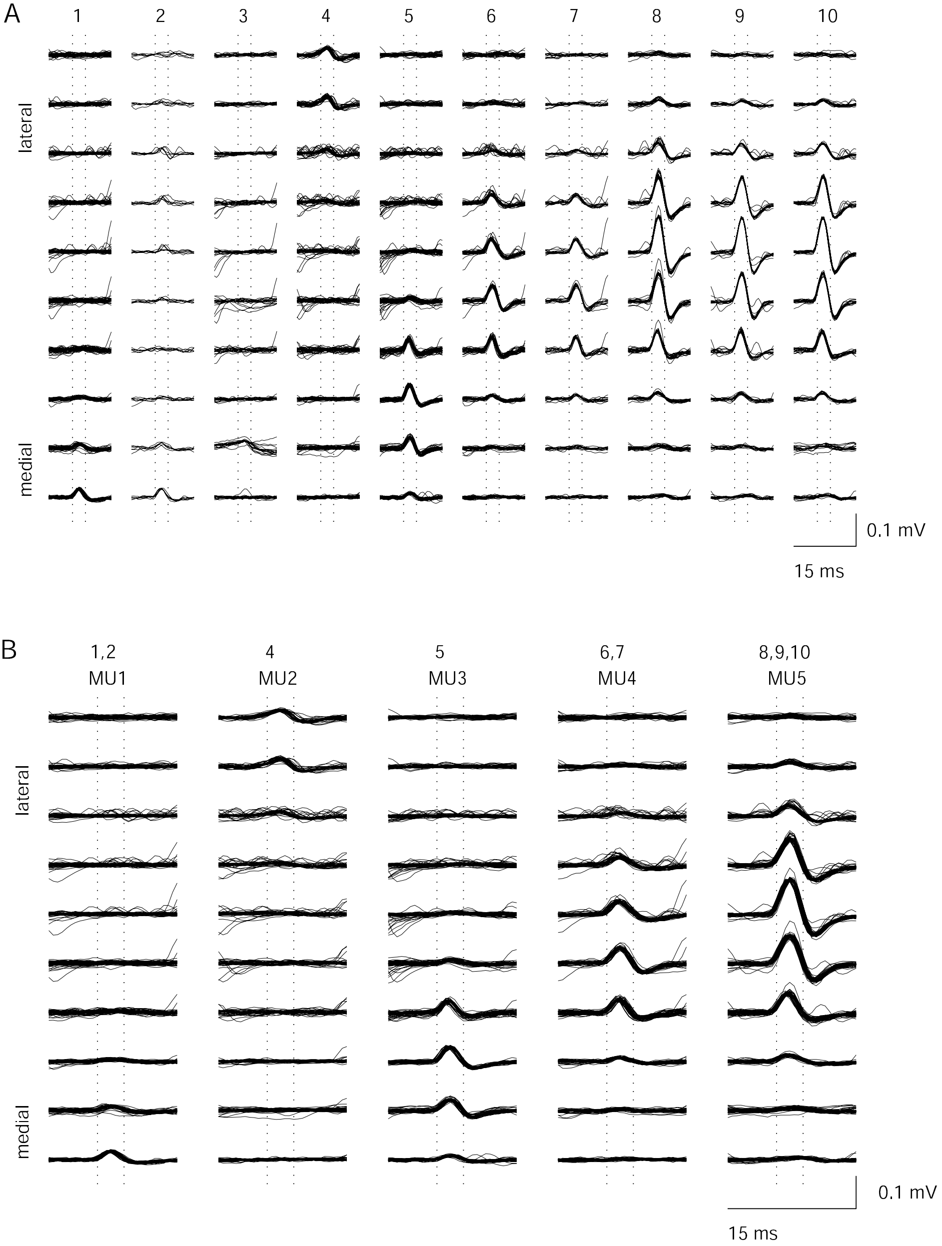

Figure 5.3: Example of the result of the clustering algorithm. Each of the columns 1-10 in (A) shows the superimposition of the wave shapes clustered by the procedure into one group. The 10 medial to lateral traces show the 10 channels from one electrode row (see Fig. 5.1 and Fig. 5.2A,C). The dotted lines indicate the 3.5 ms around the peak that were fed into the Wards clustering algorithm. The merged clusters (1,2), (6,7), and (8,9,10) are shown in (B). Cluster 3 in (A) is removed.

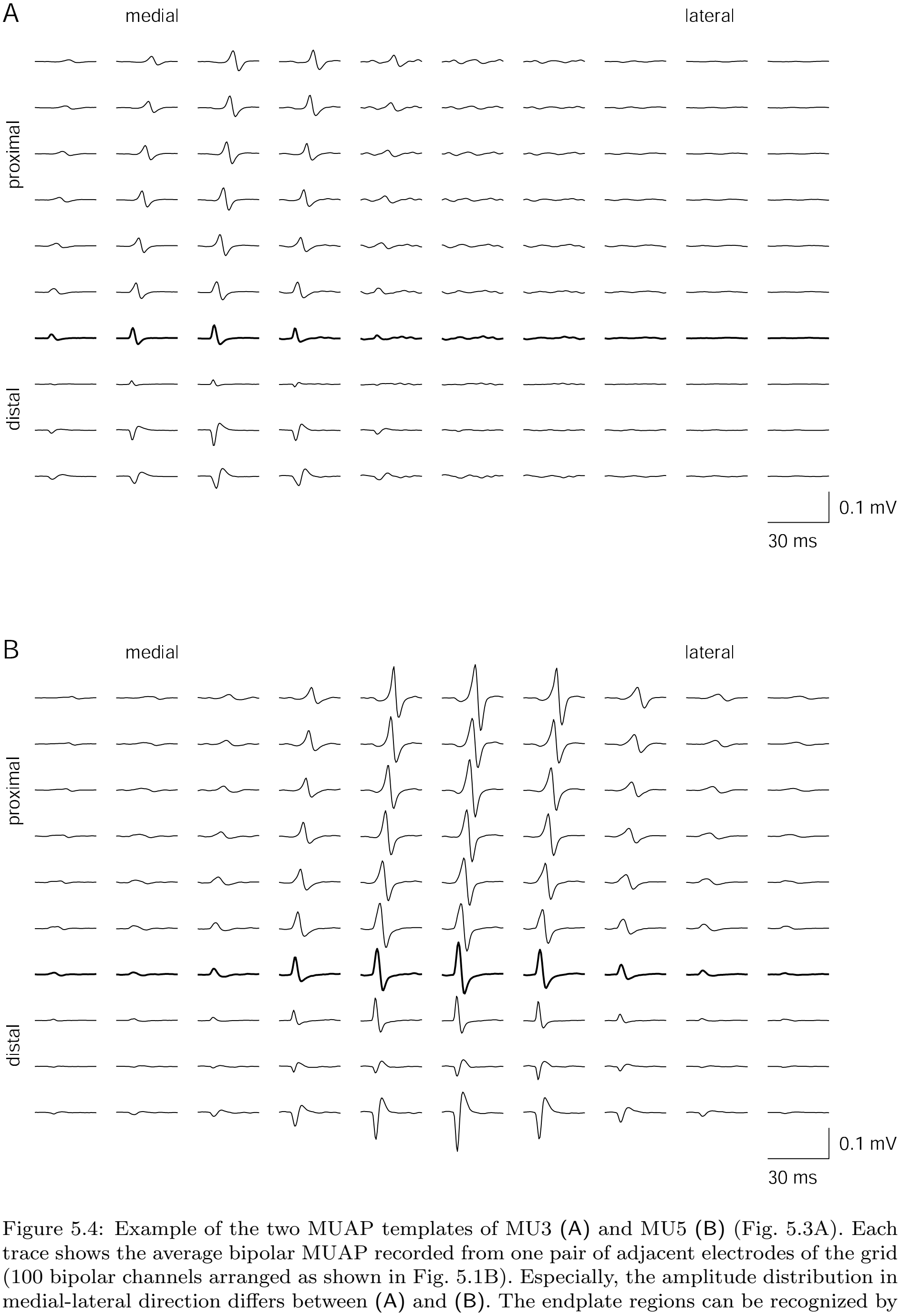

Figure 5.4: Example of the two MUAP templates of MU3 (A) and MU5 (B) (Fig. 5.3A). Each trace shows the average bipolar MUAP recorded from one pair of adjacent electrodes of the grid (100 bipolar channels arranged as shown in Fig. 5.1B). Especially, the amplitude distribution in medial-lateral direction differs between (A) and (B). The endplate regions can be recognized by low amplitudes and phase reversal. Bold lines highlight the row used for the clustering step.

cording to their similarity. Wards algorithm merges the peaks with the smallest distance, i.e., with the most similar wave shapes, into one cluster. Similar clusters and peaks are further merged until a user-defined number of clusters remains. We found it efficient to stop at about twice the number of MUAPs that was expected from visual inspection of the signal.

As a third step in this first stage, the result was checked manually by the experimenter by plotting the wave shapes of each cluster superimposed (Fig. 5.3A). Clusters could be removed or two clusters could be merged into one (Fig. 5.3B). In this step, some a priori knowledge about the firing pattern was used. For instance, peaks with too short an interval cannot be generated by the same MU and should not belong to the same cluster. Furthermore, clusters that contained a small number of peaks or that could not be merged with another cluster for physiological or other reasons, were removed (cluster 3 in Fig. 5.3A). In Figure 5.3, it is shown how the clusters obtained from the sEMG of the same subject as in Figure 5.2 (subject 1 in Table 5.1) were merged [(1,2), (6,7) and (8,9,10)]. Clusters containing a small number of peaks are generated either for superimposed MUAPs or for a MU that was not continuously active during the whole recording. In the latter case, errors in the template-matching can occur. The number of clusters used is a compromise between false-positives and false-negative firing detections in the later template-matching step. The result of this procedure was a list of firing times for each identified MU.

As a final step towards template formation, the data from 100 sEMG channels were read from the file and averaged using peaks from one of the lists as a time-lock. The resulting template included the sEMG from 11 electrode rows and 10 columns (dotted in Fig. 5.1B, first and last row are not used; the bipolar montage reduced the number of rows by one). For each channel, the samples of the 50 ms around the detected peak were stored, which included the complete MUAP profile. In the example, the above process resulted in five averaged multichannel MUAPs (templates), two of which are shown in Figure 5.4.

5.3.2 Detection of MU Firings

To measure changes in the MU firing behavior caused by TMS, the interspike intervals before and after the cortical stimulus have to be compared. The final goal is thus to accurately estimate the firing pattern of each contributing MU. However, particularly after the TMS pulse, superimpositions of MUAPs are likely to occur, since all active MUs have a higher probability to fire in response to the corticospinal volley. For that reason, the peri-stimulus data segments were excluded from the previous analysis stage. Previously unclassified peaks and, especially, superimpositions of MUAPs have still to be resolved.

For the following steps in the analysis, the 100-channel templates described above (Fig. 5.4) were used. The increased number of channels added further spatial and temporal information, in particular about the propagation of the action potential

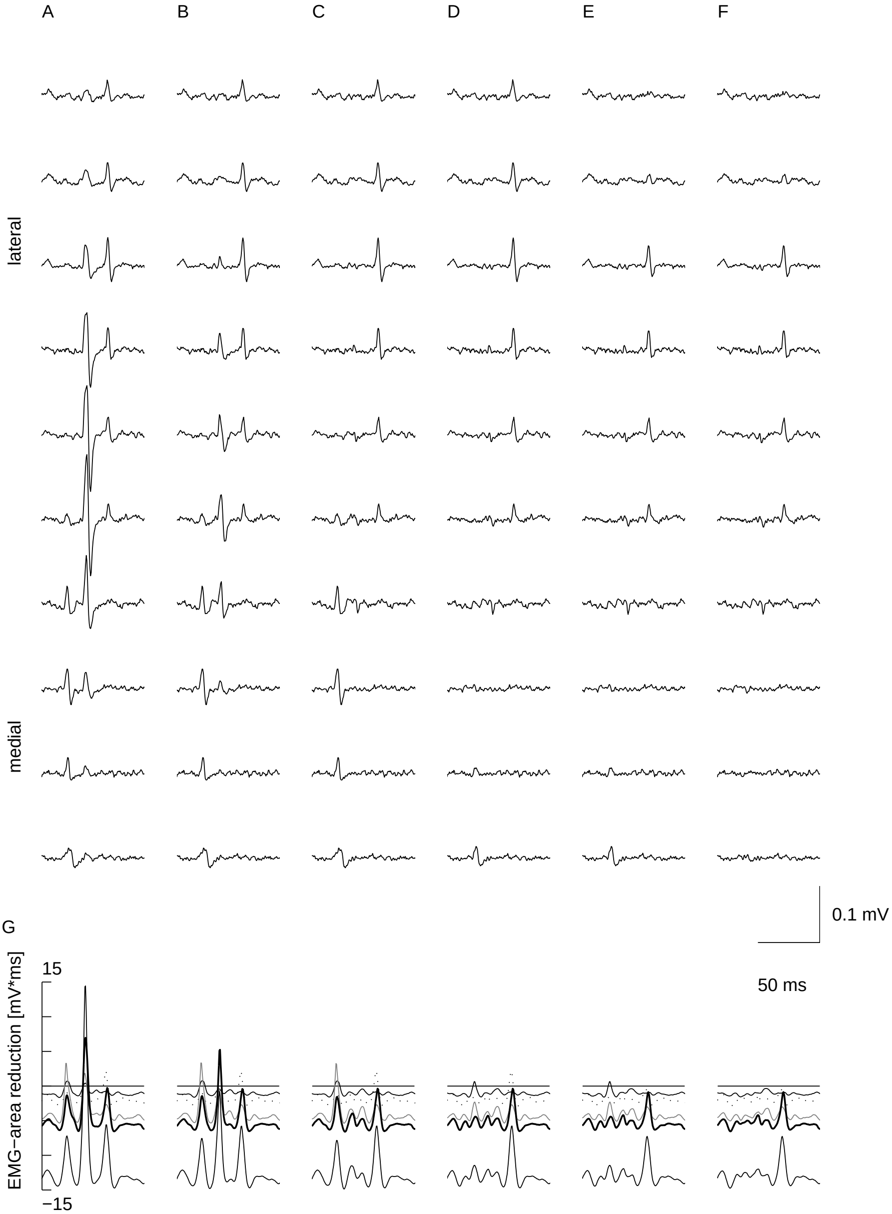

Figure 5.5: Example of the MU detection. (A) 80 ms of raw sEMG signal (10 bipolar channels perpendicular to muscle fibers). The highest area reduction results from the fifth template [corresponding to the lower thin solid line in (G); each line type in (G) refers to a different MU template]: a firing of MU5 is detected. (B) Template 5 is subtracted, and the template matching is performed again. Repetition of template subtraction [(C) MU4; (D) MU3; (E) MU1] and template-matching results in the wave shapes in (F). The peak still visible is not explained by any template and the procedure stops. The peak in (F) was generated by a inconstantly firing MU for which no template was constructed.

and the endplate position in the proximal-distal direction (Fig. 5.2D). The difference between MUAPs increased as did the signal-to-noise ratio, since noise is not expected to be correlated to the MUAP.

The continuously recorded EMG was divided into segments comprising the time from 300 ms before to 300 ms after each of the 100 TMS pulses. The first segment was read from file, all channels were high-pass filtered, and the proximal-distal bipolar montage was calculated for all rows. Each template was subtracted from the measured sEMG, sample point by sample point. The reduction in absolute sEMG area measures the quality of the template-matching. Where the maximum area reduction occurs, that specific template is most suitable to explain the measured sEMG and that MU is supposed to have fired. At this position in time, the template is subtracted from the sEMG and the procedure is repeated for the remaining signal. In this way, the MUAPs were removed step by step from the signal. A MUAP with a smaller amplitude, that was obscured by one of higher amplitude, may now become visible so that superimpositions can be resolved. The procedure stops when none of the templates gives a further reduction in sEMG area for any moment in time. The progress in this procedure is illustrated in Figure 5.5A-F. To shorten the timeconsuming template-matching, a preceding peak detection was introduced. The thresholds were lowered and arbitrarily set at 80% of the levels used for the template construction. The template matching was performed only for the 5 ms (10 sample points) around the newly found peaks.

After completion of the template matching for the 600 ms segment around the first TMS pulse, the next sEMG segment was read and processed, and so on. As a result, the firing times of the MUs before and after the TMS pulse were known for the 100 trials.

Up to this stage, the MU firing times were measured using a peak in an arbitrarily selected row of channels. However, the latency of this peak with respect to the TMS stimulus also depends on the propagation of the action potential along the muscle fiber membrane and thus on the distance between the endplate region of the MU and the electrode row used for the template construction procedure. In the monopolar version of the template, the electrode above the endplate region of the MU records an initially negative potential with a short rise-time from which the onset can be measured most easily (example in Fig. 5.6). The onset coincides with the arrival of the activity at the neuromuscular junction and can be directly compared to motor evoked potential onsets that are measured in a monopolar tendon-belly montage. Thus, the delay from the true onset of the MUAP to the peak used for triggering was measured from the monopolar version of the template, and the firing times were corrected to the onset of the MUAP recorded closest to the endplate.

In the absence of a true gold standard for EMG decomposition, the performance of the algorithm was checked by extensive visual inspection. This final visual judgment was convincing in the sense that each firing was eventually classified without conflicting with physiological and physical a priori knowledge (firing intervals, differences between wave shapes). The 10 bipolar channels that had already been

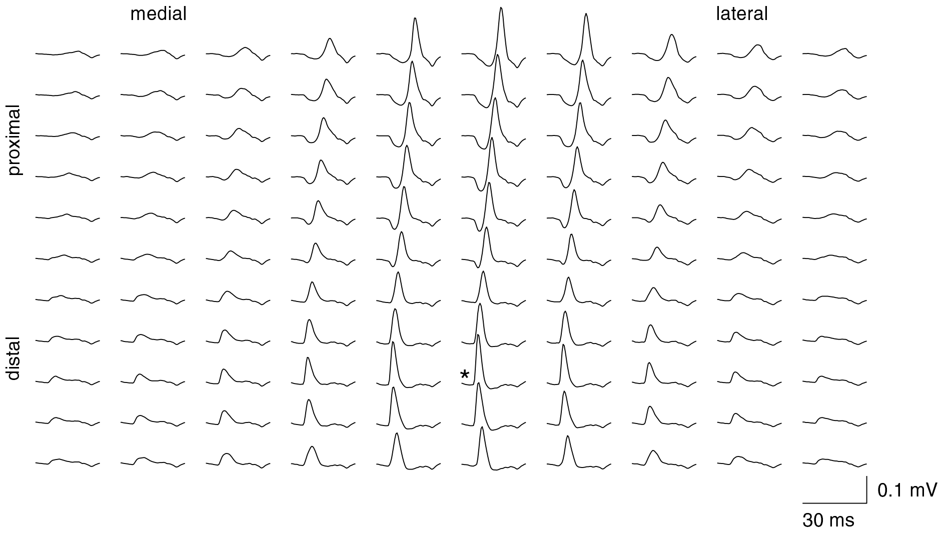

Figure 5.6: Example of the monopolar MUAP templates of MU5 (see Fig. 5.4B) over the whole electrode grid. The asterisk indicates the start of action potential propagation over the muscle fiber membrane at the endplate region, which sharply defines the arrival of the motoneuron activity at the muscle fibers.

used for the template construction were redisplayed. The recomposed signal, constructed by summation of the MUAP templates at the firing times found by the template matching algorithm, was superimposed on the measured signal. The program allowed a stepwise subtraction of the templates to visualize the MU detection. Furthermore, the reduction in sEMG-area achieved by the subtraction of the detected best-matching template could be printed out. By visual inspection of the measured signal, the recomposed signal, and the firing intervals, errors were detected. MUAPs were added to, or removed from, the firing times list using a mouse cursor. For each MU, the number of firings missed (false-negative) or erroneously detected (false-positive) was calculated.

5.3.3 Firing Pattern Analysis

The result of the procedure thus far comprises the firing times of the different MUs in relation to the TMS pulse. Spike trains were corrected for any detection error found in the visual performance evaluation procedure. In the final stage of the analysis, the spikes from all 100 trials were plotted in a peri-stimulus time histogram (PSTH) with a time resolution of 1 ms for the interval of 100 ms before to 200 ms after the TMS pulse. From the firing pattern of each MU, the displaced impulses function (DIF in extra firings/stimulus) and the interspike interval change function (IICF in ms) were calculated according to Awiszus.[3,4] Both methods use the 100 firing patterns just before the stimulus to estimate an expected firing behavior and compare it to the actually observed firing behavior.

Both functions are similar to the cumulative sum of the PSTH (CUSUM).[43] The advantage of IICF, however, is its independence of the prestimulus spike density. Furthermore, it provides an estimate of the average postsynaptic current induced by the TMS pulse in the spinal motoneuron.[3,4] DIF and IICF were first averaged over the MUs within one subject and then over subjects.

5.4 Results

After some minutes of practice, all subjects could contract the biceps brachii muscle so that only a few MUAPs were visible in the sEMG. The sEMG pattern was highly dependent on the position of the wrist. Slight changes in forearm-supination could derecruit firing MUs and recruit new MUs without changing the elbow flexion force. However, with unchanged arm position and constant force, some MUs can be kept firing at a regular rate for 3-5 min. An example of 1 s of such a regular sEMG pattern is shown in Figure 5.2.

Up to five MUs could be differentiated within one sEMG recording. In the present, still experimental, arrangement, the analysis of one recording takes about 1 to 2 days for the analysis itself and another 1 or 2 days for the visual evaluation of results (depending on the number of MUAPs). In total, 17 MUs were measured from five subjects. Multichannel templates were used to find the firing moments of the MUs. An overview of the accuracy of the algorithm as checked by visual inspection is given in Table 5.1. On average, 97% of the firings were correctly identified. Generally, very few firings were missed. The number of false-positives was higher than the number of false-negatives (missed firings). False-positives were particularly likely to occur when MUs did not fire continuously during the recording. For these MUs, no template was constructed, because the number of firings was too low. An example is shown in Figure 5.5F. The peak remaining after the subtraction of all five templates was generated by a sixth MU. Its topography was most similar to that of MU2 and MU4. In some cases, such similarity led to misclassifications. The number of errors was lower for templates with large amplitudes and areas, but also depended on the topographical similarity between MUAPs. In the example illustrated in Figures 5.3 and 5.5, the smallest MUAP1 was detected with a high accuracy, since it was clearly separated from the other MUAPs by its medial amplitude distribution.

All MUs showed an increased firing probability at latencies of 11-14 ms after the TMS pulse (Figs. 5.7 and 5.8). This interval is referred to as the primary peak of the PSTH.[13] This primary peak corresponds to the steep increase in the DIF and IICF. After the primary peak, there was a period of decreased firing probability. In some MUs, a secondary peak at latencies of 45-65 ms was present. The primary peak leads to an increase in DIF and IICF, followed by a decrease. At latencies longer than 65 ms, DIF and IICF become negative in some cases, indicating an additional inhibitory process.[3] At longer latencies, the differences between MUs become larger. However, the DIF and IICF of MUs of the same subject show very similar patterns.

Table 5.1: Accuracy of the decomposition procedure, checked by visual inspection. The accuracy was measured for the total recording (300 ms before until 300 ms after TMS) and separately for the primary peak (PP, 8-16 ms after TMS). Percentages are indicated in parentheses.

Subject and MU	Template area [mVms]	Firings		Correct detections		False negatives (missed)		False positives	
		Total	PP	Total	PP	Total	PP	Total	PP
1-1	2.99	695	42	686 (98.7)	40 (95.2)	9 (1.3)	2 (4.8)	2 (0.3)	0 (0.0)
1-2	4.40	572	33	555 (97.0)	32 (97.0)	17 (3.0)	1 (3.0)	299 (52.3)	2 (6.1)
1-3	7.19	631	33	631 (100.0)	33 (100.0)	0 (0.0)	0 (0.0)	0 (0.0)	0 (0.0)
1-4	8.34	570	34	564 (98.9)	34 (100.0)	6 (1.1)	0 (0.0)	59 (10.4)	6 (17.6)
1-5	17.04	661	29	661 (100.0)	29 (100.0)	0 (0.0)	0 (0.0)	1 (0.2)	0 (0.0)
2-1	5.55	614	33	608 (99.0)	32 (97.0)	6 (1.0)	1 (3.0)	36 (5.9)	3 (9.1)
2-2	5.16	724	39	583 (80.5)	26 (66.7)	141 (19.5)	13 (33.3)	833 (115.1)	36 (92.3)
2-3	12.24	665	32	655 (98.5)	32 (100.0)	10 (1.5)	0 (0.0)	10 (1.5)	0 (0.0)
3-1	11.06	697	38	637 (91.4)	34 (89.5)	60 (8.6)	4 (10.5)	356 (51.1)	14 (36.8)
3-2	15.90	549	40	540 (98.4)	40 (100.0)	9 (1.6)	0 (0.0)	126 (23.0)	8 (20.0)
3-3	14.92	770	39	738 (95.8)	35 (89.7)	32 (4.2)	4 (10.3)	131 (17.0)	8 (20.5)
3-4	33.55	703	27	703 (100.0)	27 (100.0)	0 (0.0)	0 (0.0)	9 (1.3)	4 (14.8)
4-1	9.20	372	5	372 (100.0)	5 (100.0)	0 (0.0)	0 (0.0)	0 (0.0)	0 (0.0)
4-2	23.45	581	25	581 (100.0)	25 (100.0)	0 (0.0)	0 (0.0)	58 (10.0)	8 (32.0)
5-1	10.18	758	31	725 (95.6)	24 (77.4)	33 (4.4)	7 (22.6)	32 (4.2)	2 (6.5)
5-2	12.36	701	17	678 (96.7)	17 (100.0)	23 (3.3)	0 (0.0)	13 (1.9)	4 (23.5)
5-3	9.22	622	42	620 (99.7)	41 (97.6)	2 (0.3)	1 (2.4)	180 (28.9)	14 (33.3)

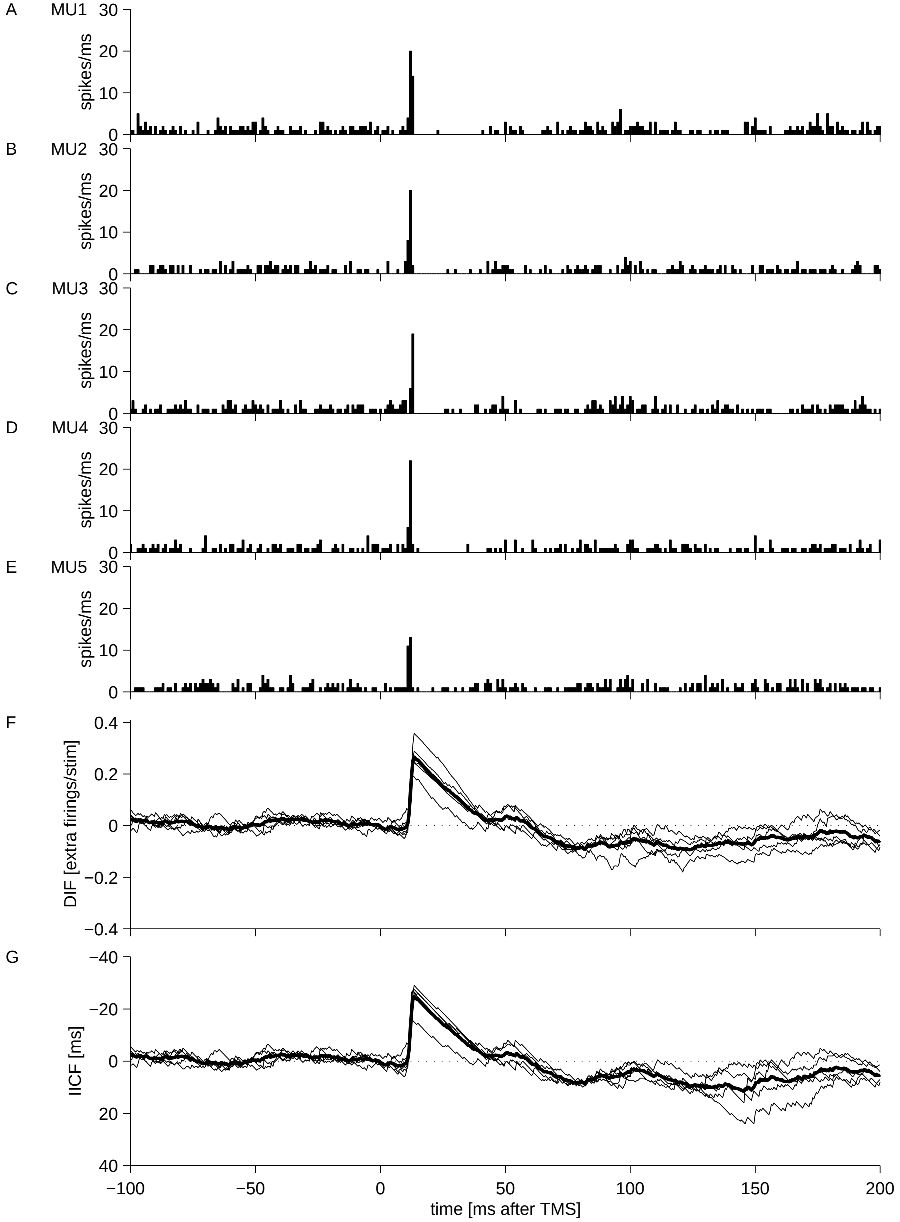

Figure 5.7: Influence of TMS on the firing pattern of the 5 MUs recorded simultaneously in subject 1. The TMS pulses were given at $t = 0$ ms and 100 trials were recorded. (A-E) Peristimulus-time histograms (PSTH) of the 5 MUs (binwidth 1 ms). (F) Displaced impulses function (DIF) of the 5 MUs (thin lines) and mean DIF (thick line) of the 5 MUs. (G) Interspike interval change function (IICF) of the 5 MUs (thin lines) and mean IICF (thick line) of the 5 MUs.

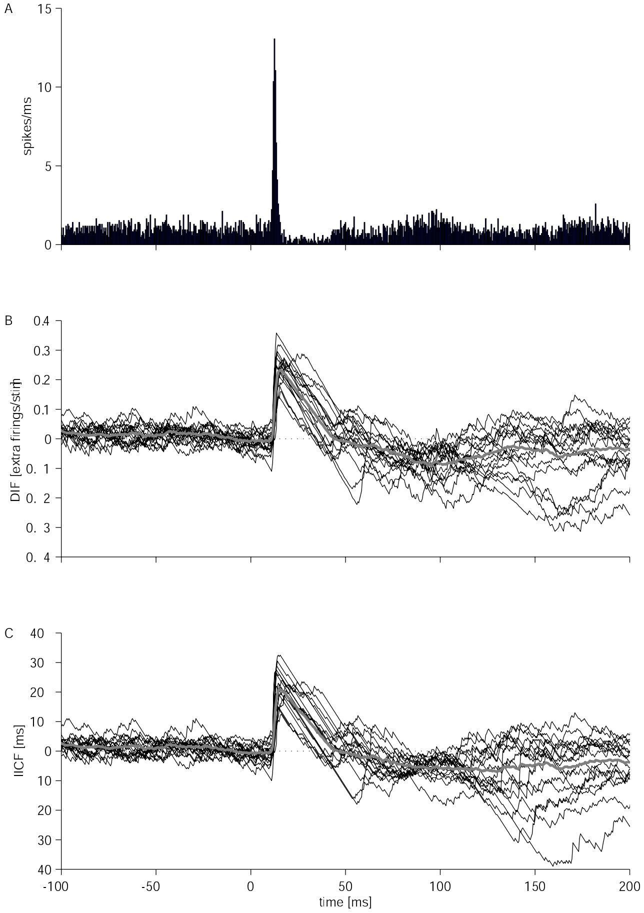

Figure 5.8: Pooled results of the 17 MUs recorded from the five subjects. The TMS pulse was given at $t = 0$ ms and 100 trials were recorded. (A) PSTH of all pooled firings (binwidth 0.5 ms). (B) DIF of all 17 MUs (thin lines) and DIF averaged over the five subjects. (C) IICF of all 17 MUs (thin lines) and IICF averaged over the five subjects.

5.5 Discussion

To measure the firing pattern of motor units, the EMG has to be recorded and decomposed into the individual contributions of these motor units. Previously described methods are based on an invasive recording with a concentric needle electrode[21,45,82,91,134,138] or with a specially designed three-channel needle.[76] The invasiveness of these methods, together with the limited possibilities for follow-up studies and the hindrance when maintaining a steady contraction, has limited single MU studies of the central motor system. In principle, therefore, sEMG is preferable. However, MUAPs generated by different MUs show a relatively uniform temporal morphology when their activity is recorded with conventional sEMG. Single-channel sEMG recordings are not sufficient for EMG decomposition. But each MUAP has a characteristic spatial distribution at the surface depending on the endplate position, the fiber length, and the position and depth of the muscle fibers.[122,123] In this article, we show that high-density sEMG allows the use of spatial information for sEMG decomposition.

It is necessary to (1) differentiate MUAPs from noise, and group them to extract low-noise MUAP templates; and (2) decompose superimpositions of MUAPs into the contributing templates and reconstruct the MUs' firing patterns. When only the morphology of the MUAPs and the average firing rate is of interest, step (1) is sufficient.[91,134,139] For our application, the measurement of TMS influence on firing probability, step (2) is especially important, since the TMS pulse induces an increased firing probability of all active MUs in the primary peak, leading to an increased chance of superimposition.

Step (1) included a peak detection in selected channels. We found the interactive selection of channels and thresholds to be superior over absolute criteria or some percentage of average amplitude, since the amount of "background-activity" (sEMG that was generated by MUs that could not be classified reliably) differed between subjects and recordings. The choice is somewhat arbitrary. Usually the selection of a neighboring row led to nearly identical results. Independent of the choice made, the selection did not use all available spatial information. The MUAPs recorded from neighboring rows have similar wave shapes with a similar topography, but are shifted by the time necessary for propagation along the muscle fiber. If more channels are included, the total duration of the MUAP is therefore increased. This leads to a higher number of superimpositions, which complicates the classification procedure. Furthermore, the restriction to 10 channels has some computational advantages. The lower need of memory and computational power makes it possible to use long recordings and to average more than 100 peaks per template, which results in a good signal-to-noise ratio in the templates.

The detected peaks were clustered using a Wards clustering algorithm. Since there was no possibility to define the minimal distance between peaks of different MUs and the maximal distance between peaks of the same MU beforehand, clustering had to be stopped at an arbitrarily defined number of clusters. When this number of clusters is set larger (approximately two times) than the number of MUAPs expected to be present in the recording, it is unlikely that MUs are missed by erroneously merging two clusters. Apparently, for the biceps brachii, the differences between the consecutive MUAPs of a single MU are relatively small compared to the differences between MUAPs generated by different MUs. This seems to be valid even in diseased and in smaller distal muscles (Chapter 6), but has to be further evaluated systematically. Some of the above-mentioned needle EMG decomposition methods include a template updating step to account for the changes in the MUAP wave shapes introduced by slight shifts of the needle. The position of the electrode grid with respect to the muscle fibers is sufficiently constant. The MUAP does not change and the same template can be used to decompose sEMG measured over several minutes.

The accuracy of the decomposition process was assessed visually. As can be seen from Table 5.1, very few MU firings were missed, whereas the number of extra firings found was relatively large. These false-positives were often caused by MUs that were not continuously active, so that no MUAP template was generated. In this case, the area reduction was always somewhat lower than for the correct MUAPs (Fig. 5.5). Often, it would have been possible to exclude most of the erroneous findings below a threshold value without losing correctly identified firings. However, the determination of this threshold is difficult. For the MUAPs with high amplitude, the detection was very accurate, so that it is possible to analyze the firing pattern without checking the firings manually. For the most difficult cases, it is necessary to edit the spike trains by hand before analyzing them with PSTH, DIF, and IICF. This manual editing step is the most time-consuming of all steps in the analysis procedure.

Before calculating PSTH, DIF, and IICF, the spike trains were corrected to the onset of the monopolar MUAP. This step uses MUAP information that can easily be extracted from the monopolar template, but that is not available when recording with needle electrodes. In needle EMG recordings, the latency of the PSTH peaks depends on the action potential propagation time within the muscle, which in turn depends on the position of the needle relative to the motor endplates. Thus, in needle EMG, this source of variation cannot be eliminated.

The spike trains were analyzed using PSTH, DIF, and IICF. The results we found – a sharp primary peak at latencies of 11-14 ms and a subsequent period of low firing frequency, which can be followed by a secondary peak – are similar to the findings reported in the literature.[6, 13, 53, 102, 148] With the methods presented in this chapter, it was possible to analyze the firing of up to five MUs during the same session. This is more than has been reported for needle EMG techniques. We therefore believe that it is possible to replace the needle electrode with a multichannel surface electrode without consequences for the main experimental outcome. The method of analysis presented here is definitely more (computer) time-consuming than the corresponding needle EMG method and requires more user-intervention. On the other hand, it is easier to use and more comfortable for the subject during the measurement itself. Furthermore, as discussed earlier, the latencies that result from the sEMG-method are more accurate. The MUAP also provides information on structural (endplate position, length of fibers) and physiological (muscle fiber conduction velocity) parameters of the underlying MU, which can be related to the motor control principles. The possibility to investigate the peripheral and central components of the motor system within one experiment seems especially interesting for the study of motoneuron disease.

The recording of simultaneously active MUs has the additional advantage that it allows the analysis of synchronization between MUs, which may be changed in central motor disorders.[7, 25, 48] This article has focused on the application of TMS and the analysis of resulting changes in the firing pattern of MUs. However, in a more general sense, the presented method provides a way to study single cell responses in the human motor system non-invasively.

Part IV

Applications

6

MOTOR UNIT ACTION POTENTIAL TOPOGRAPHY AND ITS USE IN MOTOR UNIT NUMBER ESTIMATION

High-density multichannel electromyography (EMG) recordings add spatial information to the temporal information content of the surface EMG (sEMG) signal. This study explores the potential value of such multichannel information at a single motor unit level, in particular for the improvement of motor unit number estimation (MUNE) techniques. It is shown that multichannel recordings make it easier to distinguish motor unit action potentials (MUAPs) and that MUAP combinations can be better resolved. Furthermore, the spatiotemporal information allows a quantitative assessment of the representativity of the mean of the recorded MUAPs in relation to the maximum CMAP, i.e., for the muscle as a whole. In general, this is practically impossible on the basis of temporal information alone. For these reasons, we expect that high-density sEMG has the potential to address several methodological limitations of single channel surface EMG recordings. This is specifically illustrated in this study for one of the MUNE techniques in use, the F-response method.

JH Blok, JP van Dijk, MJ Zwarts, and DF Stegeman
Muscle & Nerve 32: 280-291, 2005

6.1 Introduction

Differences in the spatial properties of motor units (MUs), for example in their size and position, result in spatial differences in surface motor unit action potentials (MUAPs). Consequently, at the skin each MU has its own spatiotemporal "fingerprint" (Fig. 6.1B-D), which can be picked up by a two-dimensional array of densely spaced electrodes (Fig. 6.1A). For low levels of contraction, up to 10% of the maximum voluntary contraction, the unique spatiotemporal MUAP characteristics can be used to decompose the surface EMG interference pattern (Chapter 5), just as characteristic temporal MU properties can be used to decompose the needle EMG signal.[24, 91, 136] The temporal information contained in the sEMG signal is by itself insufficient for this purpose. Hence, the spatial information in the fingerprint plays a crucial role in the detection of the contributions of individual MUs. For that reason it may prove valuable in many applications of voluntary muscle activity as well as in electrically elicited sEMG. This article addresses potential advantages of high-density sEMG for such applications, by focusing on motor unit number estimation (MUNE).

Since the introduction of the basic idea of MUNE by McComas et al. in 1971,[90] several MUNE methods have been developed.[14, 18, 23, 36, 52, 66, 71, 126, 137, 140] As yet, no gold-standard technique is available, and a variety of techniques is still in use today. A comprehensive overview of their underlying assumptions and advantages and disadvantages is beyond the scope of this report and has been provided by Doherty et al.[35] and more recently by Shefner.[127] The various methods differ in their approach to the central problem of MUNE: how to obtain a sufficiently accurate estimate of the mean MUAP, based on the acquisition of a limited number of possibly not representative individual MUAPs. The solutions offered by the original increment-counting technique,[52, 90] and the multiple-point stimulation,[18, 66] spike-triggered averaging,[14, 137] and F-response[140] methods differ in many respects. They have in common, however, that at some point during recording, the problem is encountered as to whether a particular MUAP has been recorded previously. A decision is always made using the wave shape (especially amplitude) information in the MUAP. The spatiotemporal profiles that result from multichannel recordings of the surface EMG contain much more information that is characteristic of a particular MU than a single channel temporal wave shape. As will be shown, this offers the possibility of improving the detection and recognition of MUAPs. Furthermore, we will demonstrate how the availability of a mean MUAP in spatiotemporal terms provides a tool to assess whether an identified subpopulation of individual MUAPs is representative of the muscle as a whole. The consequences of a less than perfect agreement on MUNE will be illustrated, together with the use of this representativity measure in quantifying the reliability of MUNE in individual subjects.

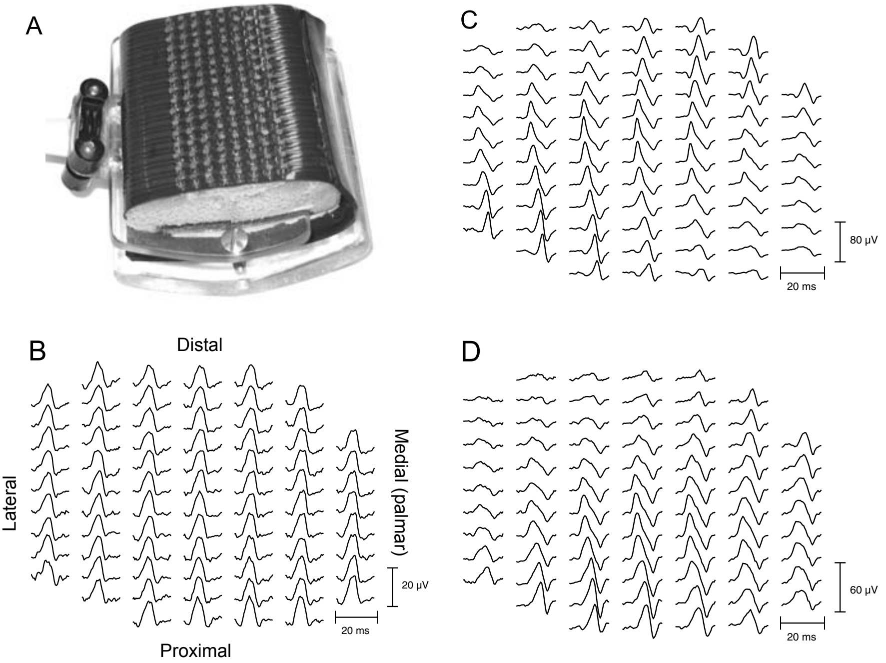

Figure 6.1: (A) The electrode grid with 128 electrodes and an interelectrode distance of 3 mm. (B) - (D) Spatiotemporal profiles of three monopolar MUAPs obtained from a single subject (averaged F-responses of single motor units). Each signal position in the profile corresponds to the position in the grid of the electrode that was used to record the signal. Signals from electrodes that were in poor contact with the skin (1 column and 4 rows of electrodes, plus some additional electrodes in the grid corners) are not shown. (B) indicates the orientation of the grid over the left hand. This orientation is identical in all figures.

6.2 Methods

To demonstrate the general principle that topographical information aids the detection and recognition of MUAPs, we chose to combine the multichannel approach with one of the MUNE techniques. According to Doherty et al.,[35] of the MUNE methods used on distal muscles, the MPS method and the F-response method (FRM)[49, 140] seem to suffer least from limiting assumptions and technical problems. Since the FRM recordings can be more easily automated than those of MPS, we chose to employ high-density sEMG in combination with the FRM.

6.2.1 Subjects

The experiments were performed on the thenar muscle group of the left hand of nine normal subjects (five men, four women) aged 22-51 years (mean, 31) with no history of neuromuscular disease. All subjects gave their informed consent. The experimental protocol was approved by the ethics committee of the Radboud University Nijmegen Medical Centre.

6.2.2 Stimulating and recording systems

Electrical stimuli were delivered to the median nerve at the wrist, using a constant-current stimulator that was specially developed at our institution for electrophysiological experiments. Circular self-adhering electrodes, 1 cm in diameter, were used as stimulating electrodes. The stimuli were constant-current pulses with a duration of 200 μs, delivered at 2 Hz. The topographical surface EMG was recorded with the system described in Chapter 4. The electrode grid has 16 rows and 8 columns of electrodes. Two corner electrodes are not connected. In both directions the interelectrode distance is 3 mm. The acquisition software was developed in-house. Apart from flexible on-line inspection of the data, it allows PC-based control of the constant-current stimulator. For all 126 channels, the sEMG data from 15 ms before to 85 ms after each stimulus were stored.

6.2.3 Experimental protocol

The skin was slightly abraded and the grid was placed over the abductor pollicis brevis muscle. The electrodes were referenced to a single electrode on the first metacarpophalangeal joint of the left index finger (monopolar recording). This reference electrode is a gold-coated but otherwise conventional electroencephalographic cup electrode, 1 cm in diameter. An amplitude map of the compound muscle action potential (CMAP) was made after a strong but not necessarily supramaximal stimulus to the median nerve to assess whether the topography of the CMAP was well-covered by the grid (Fig. 6.2). If required, grid position was adjusted such that the CMAP's maximal amplitude was located approximately in the center of the grid. After an impedance check, electrode gel was rubbed into the skin if necessary (the majority of the electrodes should have an impedance of less than 300 kΩ), while care was taken not the leave any on the skin to avoid short-circuiting the electrodes. If both grid position and electrode impedance were acceptable, the grid was fastened using Velcro straps.

Following the protocol as described by Stashuk et al.,[140] stimulus strength was gradually increased until visual inspection indicated that approximately one of three responses showed an F-wave. At this intensity, which generated a CMAP with an amplitude between 20% and 50% of the amplitude of the maximum CMAP, the triggered multichannel sEMG was recorded for 5 - 8 minutes (548-983 responses; see Table 6.1), until on-line visual inspection suggested that at least a few different F-waves had been registered. Finally, the responses to three supramaximal stimuli were recorded. Throughout data acquisition, subjects were encouraged to relax in order to avoid voluntary sEMG activity interfering with the F-responses.

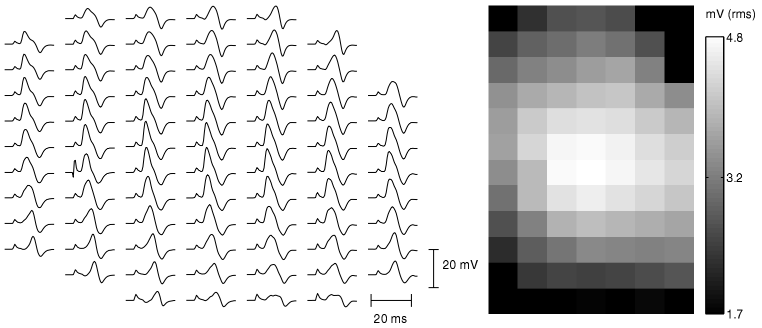

Figure 6.2: Example of a maximal CMAP. Signals are presented in two modes: as a spatiotemporal profile (left) as in Figure 6.1, and as an root-mean-square (rms) amplitude map (right). The latter focuses on the spatial distribution of the CMAP over the muscle. It was calculated from the signals within a temporal window of 15 ms, starting 1 ms after the stimulus artifact (visible as the first small negative peak in each of the signals).

6.2.4 Data analysis

The signals recorded at the electrodes in the most dorsal column and the two most distal and the two most proximal rows were systematically excluded from the analysis, because inspection of the recorded data revealed that several electrodes on the edges of the electrode grid often had made poor contact with the skin. As shown in Figure 6.3A, this left a maximum of 84 signals [any remaining electrodes with poor contact, mostly in the corners of the grid, were also excluded, leaving N electrodes for further use ($64 \leq N \leq 82$, depending on the subject)].

Data analysis was performed off-line using Matlab (The MathWorks, Natick, Massachusetts). As a first step in the data-analysis procedure, the signals were analyzed for the presence of an F-response. For this purpose, the topography of the sEMG is of less interest than its signal-to-noise ratio. To optimize this ratio, signals were averaged over multiple electrodes. Averaging over all N electrodes yields the lowest noise, but also reduces the resulting F-response amplitude compared to that of the single-electrode, maximal amplitude F-response. An optimal trade-off between noise reduction and amplitude reduction was obtained by averaging the signals per row of electrodes. To accommodate varying MU site below the grid, this procedure was followed for seven consecutive rows, centered around the row with the highest monopolar root-mean-square (rms) value of the maximum CMAP (Fig. 6.3B). It allowed improved detection of low-amplitude MUAPs with small spatial extent compared to a single large electrode over the muscle belly.

Because each electrode averages the potential distribution beneath it, averaging over electrodes has an effect similar to increasing electrode size. Therefore, this first step created the (near-)equivalent of a recording configuration consisting of seven strip electrodes of approximately 2 mm × 20 mm. Within the temporal window relevant for F-waves, the maximum area below the (absolute value of the) seven averaged signals and between successive zero-crossings was determined.

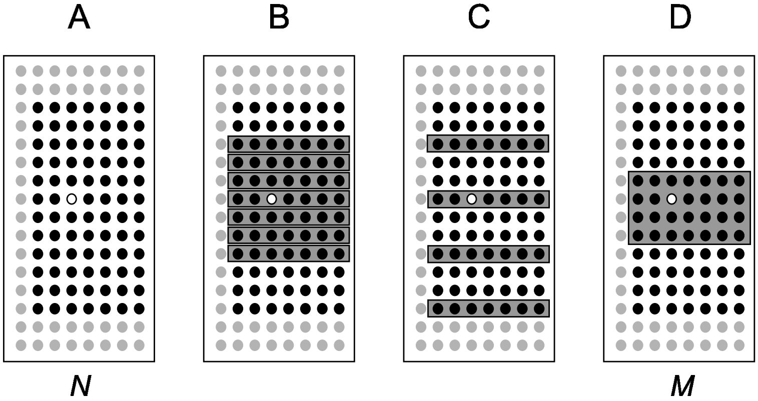

Figure 6.3: Flexible use of available electrodes. The white dot marks the position of the electrode with the highest CMAP rms value. (A) Grid representation with the $N \leq 84$ electrodes that generally are in good contact with the skin indicated in black. “Gray” electrodes are not used. (B) The 7 × 7 electrodes whose signals are averaged row-wise around the row containing the highest rms amplitude, for F-response detection. Each average yields the approximate signal of a larger strip electrode (better signal-to-noise ratio than any of the 7 single electrodes, but less topographical information). (C) Rows of electrodes used for classification. Together, the selected 28 electrodes cover much of the available topographical information. (D) The M signals that are used for the calculation of the overall MUNE and for “large electrode calculations”.

If any of these seven area values exceeded a subject-dependent threshold of 10-20 μVms, an F-wave was assumed to be present and that response was kept for further analysis.

Next, the data-analysis procedure identified identical F-waves in the remaining set of 203 to 351 responses. For that purpose, the addition of the topographical information becomes particularly important. Our experience showed that there is redundancy in the topographical information recorded with the N electrodes. The detection of identical MUAPs does not require the use of the data contained in all signals. We used four rows at 9 mm intervals as depicted in Figure 6.3C. These rows cover adequately both the topographical differences in fiber direction and those perpendicular to the fiber. The F-responses recorded with these 28 electrodes (4 × 7) were clustered using a clustering algorithm that groups the recorded MUAPs according to similarity. This algorithm is essentially the same as the algorithm for voluntary contractions described in Chapter 5. It is conservative (strict) to make sure that all responses within a cluster are indeed generated by the same MU. The disadvantage of such a strict algorithm is that multiple clusters may be formed for a single MUAP, which differ between one another only by noise. To avoid inclusion of such multiples, and, hence, bias in the MUAP selection, we discarded the class with the least number of members if any two classes in the algorithm's output appeared very similar on visual inspection.

Once all F-waves had been assigned to a cluster or group, the signals in the groups with three or more nearly identical responses were averaged. At this stage of the analysis, we returned to the full set of N electrodes: for each of them, the group or cluster average was determined, yielding MU fingerprints as presented in Figure 6.1. Next, the available spatial and temporal template characteristics were used to check for each of the templates whether it could be composed of a combination of two of the others. If so, or if any doubt remained, the template was discarded. The above procedure ascertained that we were dealing with templates of MUAPs from single MUs only.

At this stage of the analysis, we had a sample of MUAPs similar in size to the sample that might have been obtained using the conventional FRM. The multichannel sample may be somewhat larger because of the inclusion of conventionally undetectable MUAPs, or it may be smaller because of more accurate detection and subsequent exclusion of multiple occurrences of the same MUAP or of MUAP combinations. An additional difference is, of course, that for each of the MUAPs not one, but N temporal wave forms were available. The identified MUAPs were averaged for each of these N channels separately. Ideally, this averaging should be performed after alignment of the templates on the basis of their M-wave latency, which is unknown from the F-wave. As an approximation to this ideal situation of known latencies, the templates were aligned on the basis of signal onset before they were averaged. A single MUAP onset value was used per MUAP template. It was determined from the signal with the largest peak amplitude and the shortest latency, recorded above the motor endplate zone.

The maximal multichannel CMAP was taken as the average of the data recorded in response to the three supramaximal stimuli. From the mean multichannel MUAP and this multichannel CMAP, a MUNE could be calculated for each electrode by dividing the former into the latter. More specifically, we determined the MUNE as an amplitude-weighted sample by sample average of the division of the two signals:

$$\mathrm{MUNE}_e = \sum_t w_e(t) \times \frac{\mathrm{CMAP}_e(t)}{\mathrm{MUAP}_e(t)} \tag{6.1}$$

with the subscript e denoting electrode, t the sample (time), and $\mathrm{CMAP}_e(t)$ and $\mathrm{MUAP}_e(t)$ the amplitudes of the maximum CMAP and of the mean MUAP at electrode e and sample t, respectively. The sum was performed over all samples in the signals. The weights $w_e(t)$ were determined from the amplitude of the mean MUAP:

$$w_e(t) = \frac{\mathrm{MUAP}_e(t)^2}{\sum_t \mathrm{MUAP}_e(t)^2} \tag{6.2}$$

That is, we calculated a MUNE for each sample t and averaged the outcome to obtain a single MUNE value for each electrode e. By the weighing with $w_e(t)$ we let the samples with high amplitude contribute more in this averaging than those with small amplitude, because for the latter the influence of noise is larger. This approach uses all information available in the signals, yields similar results to the division of signal areas that is more commonly used in MUNE methods, but does not depend on the exact location of onset and offset of each of the N signals. As we followed this procedure for each of the N electrodes, N MUNE values per subject were obtained. An overall MUNE was calculated by averaging the M MUNE values from the electrodes in the four consecutive rows with highest CMAP rms values ($M \leq 28$; see Fig. 6.3D). The use of only these four rows prevents the signals at the edges of the grid, where signal size is small (and, hence, the reliability of the MUNE value is limited), from making a significant contribution to the outcome.

The assessment of the representativity of the subset of MUAPs could now be implemented as follows. A sampled set of MUs being representative for the muscle as a whole implies that the spatiotemporal profiles of the averaged MUAP and the maximum CMAP match. In that case, the M MUNE values, taken from the different electrode positions, hardly differ. The less representative the sample, the larger the difference between the two profiles, and the larger the standard deviation of these M simultaneously obtained MUNE values. This standard deviation as a measure of reliability is provided together with the overall MUNE value.

Finally, we simulated an approximation of the mean MUAP and the maximum CMAP as a conventional electrode placed over the belly of the muscle would record them. These large-electrode signals were calculated as the mean of the signals of the M electrodes of Figure 6.3D. From this single mean MUAP signal and single maximum CMAP signal, a single MUNE value was determined. To some extent (differences in MUAP sample composition are not taken into account), this MUNE value allows comparison of our results with literature data, since the rows on which it is based are located where a rectangular electrode of about 1 cm × 2 cm would be in conventional measurements.

6.3 Results

6.3.1 Detecting and classifying MUAPs

Figures 6.1 and 6.4 illustrate that the differences in the spatial properties of MUs translate into topographical differences over the skin surface between the corresponding MUAPs. The latter figure shows rms amplitude maps for the 14 different monopolar MUAPs detected in a single subject. In each case, the grayscale is normalized to the MUAP's minimum and maximum rms values over the grid. The largest negative peak amplitude recorded with any of the electrodes is indicated in microvolts above each of the maps. The signal presented below each map is the approximation of the MUAP as a large conventional strip electrode (large-electrode signal; see paragraph 6.2.4) would record it.

The topographical differences are pronounced. The profiles are most distinctive for the larger MUAPs. The smallest MUAPs often have a fairly homogeneous topography, as is the case for the first MUAP in Figure 6.1 and the first three MUAPs in Figure 6.4. This implies that the difference between the largest and the smallest of the N rms values is relatively small. Noise or small artifacts can significantly alter these rms profiles, explaining their patchy look. Somewhat

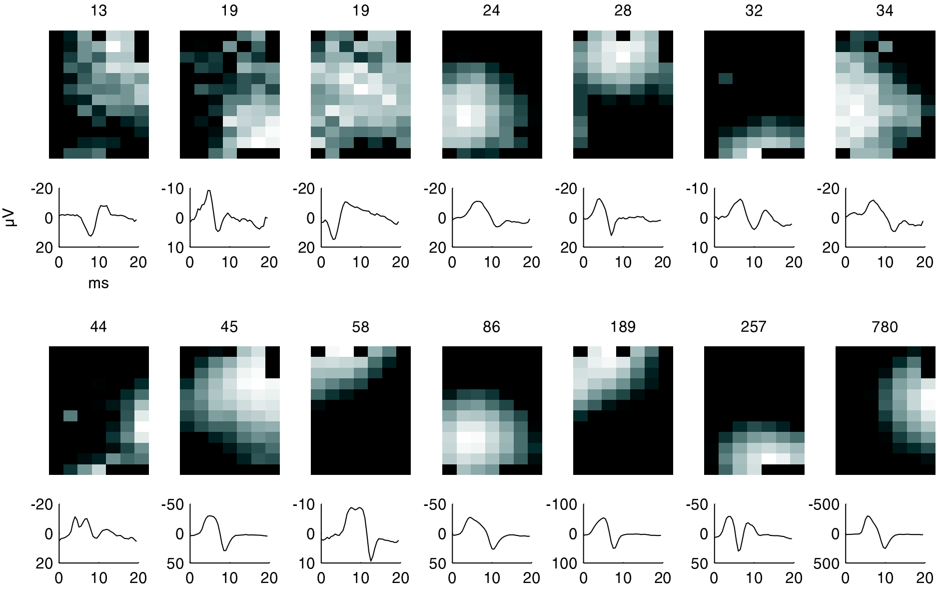

Figure 6.4: Rms maps for each of the 14 MUAPs recorded from subject 3. Note the large differences in the profiles. The number above each map indicates the negative peak amplitude (in μV) of the largest of the N signals. The plots below the maps show the MUAPs that would be recorded when a single large (conventional) electrode is used. The signal of this electrode is calculated as the mean of the signals of the M electrodes of Figure 6.3D. Note the giant MUAP (last in bottom row)!

surprisingly, the MUAPs' maxima do not seem to be preferentially located where the CMAP's maximum is. MUAPs appear to be generated anywhere below the grid. This was true in all subjects studied.

As suggested in Section 6.1, the spatiotemporal information indeed simplifies the MUAP classification stage of the analysis, increasing its reliability. Judging from the large electrode or temporal profiles alone, it might be difficult to state with certainty that, for example, the second, fifth and sixth MUAP in Figure 6.4 are different (as the topographical information demonstrates them to be), especially if it is taken into account that in Figure 6.4 only relatively low-noise averages of clusters are shown.

The objective of the F-response method that, after clustering and averaging the responses, the resulting templates represented single MUAPs was usually realized. However, in some cases a template appeared that was generated by the superimpositions of two MUAPs. As an additional advantage of the multichannel recordings, the available spatiotemporal information allowed fairly easy detection of these cases. Figure 6.5 shows three templates (same subject as in Fig. 6.4). It can be seen both from the full spatiotemporal profiles (left) and from the rms maps (right) that the template presented in Figure 6.5B is a combination of the two MUAPs shown in Figure 6.5A1 and Figure 6.5A2. The similarity between

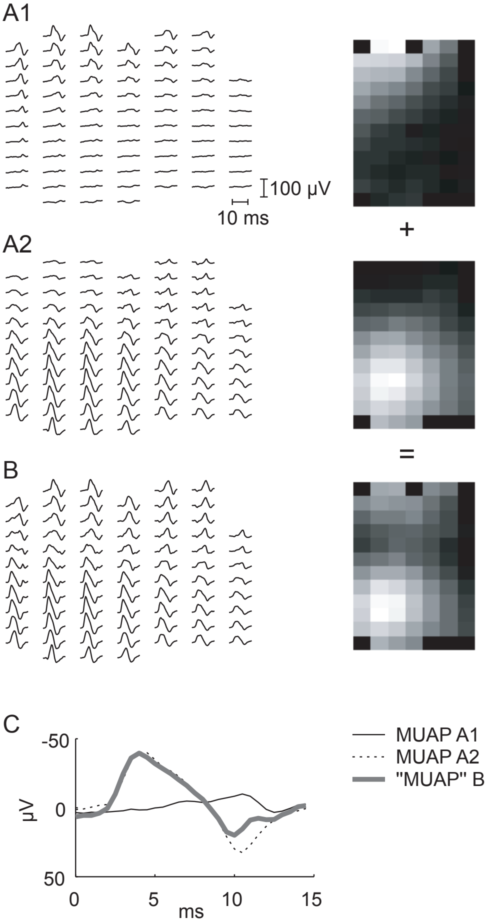

Figure 6.5: Topographical information aids the detection of MUAP combinations. Template (B) is a combination of the two single MU templates (A1) and (A2). This observation can be made both from the full spatiotemporal profiles (left) and the rms maps (right), but not so easily from the temporal profiles of the MUAPs [(C) large-electrode averages, rows 5 to 8]. The three profiles have been plotted with the same amplitude and time scaling.

the wave shapes of Figure 6.5C illustrates that this conclusion cannot be drawn as readily on the basis of the corresponding large-electrode signals.

One of the nine subjects was unable to relax. As it was impossible to tell F-waves apart from voluntary activity, the resulting recording could not be analyzed. All subsequent results are, therefore, obtained from the eight remaining subjects. In these subjects, between 7 and 19 different MUAPs could be detected (Table 6.1). In two cases, less than 10 MUAPs were obtained. The reason was that one or two of the MUs generated an F-response with a persistency that was several times higher than that of the other MUs.

Table 6.1: MUNE results for eight subjects, ordered by standard deviation in the multichannel MUNE (i.e., by representativity of the mean MUAP)

Subject	Number of stimuli	Number of F-responses	Number of MUAPs (n)	Mean MUAP amplitude[a] (μV)	Multichannel MUNE[b]	Large-electrode MUNE[c]
1	548	302	19	53	255 ± 35	253
5	868	301	15	26	404 ± 56	416
6	939	337	18	34	230 ± 56	222
3	631	213	14	43	295 ± 57	307
8	816	351	13	33	399 ± 103	404
2	873	271	12	21	470 ± 158	616
4	983	252	8	27	491 ± 164	427
7	734	203	7	28	592 ± 193	709

[a] Calculated by averaging n detected MUAPs; mean MUAP amplitude is presented for the electrode at which the CMAP was maximal.

[b] Determined as the average and within-grid standard deviation of M single electrode MUNE values (Fig. 6.3D).

[c] Estimated for a single large (constructed) electrode, based on the same n MUAPs.

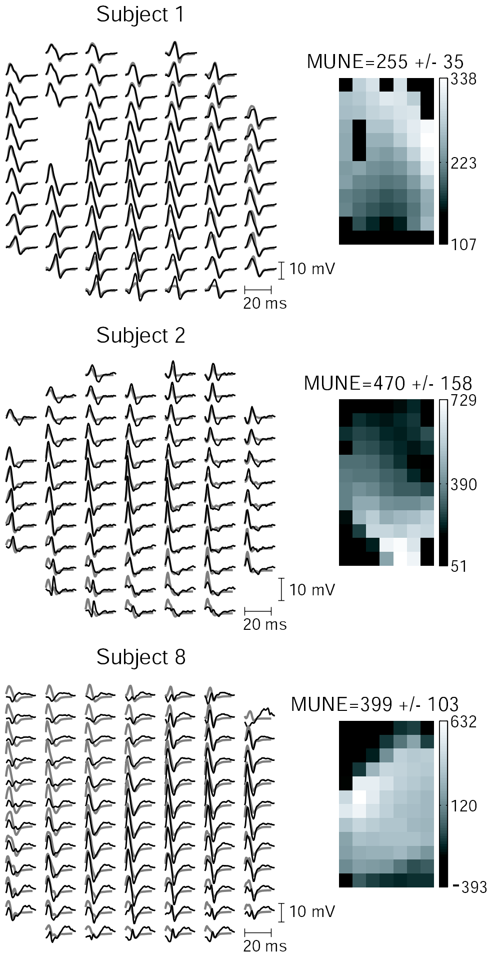

Figure 6.6: The effect of a good (top) or poor (middle and bottom) match between the mean MUAP and maximum CMAP on individual electrode MUNEs. Left: Topographical profiles of the mean MUAP (multiplied by the mean MUNE; black line) and the supramaximal CMAP (gray line) for three subjects. Right: Maps showing the MUNE for each of the electrodes in the grid separately. The numbers above each map show the mean of the M MUNE values of Figure 6.3D and their standard deviation. If the mean MUAP is perfectly representative, the map contains only one color or value.

6.3.2 MUNE and the representativity of the mean MUAP

The remaining single MU templates contributed to the estimate of the mean MUAP. A qualitative comparison of the mean MUAP topographical profile with that of the maximum CMAP allows a crude estimate of the representativity of the mean MUAP for the muscle as a whole (Fig. 6.6, left). Ideally, the two profiles should be identical except for a single scaling factor (the MUNE) for all electrodes in the grid. The top figure (subject 1) presents the best fit that we observed in the eight subjects. Only for electrodes in the rightmost column and lowest rows, there is some deviation between the two signals in the amplitude of the negative peak. By contrast, the profiles of subjects 2 and 8 show clear differences for many electrodes, not only in the amplitude of the peaks but also in the peak latencies and the number of MUAP phases.

The resulting MUNE values per electrode are shown both graphically and as a mean ± standard deviation on the right side of Figure 6.6. Each position in the map shows the MUNE value of the corresponding electrode. Occasionally, the best fit between the mean MUAP and CMAP required a change of sign. In these cases, the mean MUAP is mostly positive while the CMAP's main phase is negative. Most likely, for these electrode positions and MUAP samples, the contributions of distant MUs outweigh the contributions of closer MUAPs. In the maximum CMAP, nearer MUs are dominant, causing the CMAP at these electrodes to be negative. This sign reversal between MUAP and CMAP results in a negative MUNE (e.g., the top left electrodes in Fig. 6.6, subject 8). Although physiologically meaningless, negative MUNE values are useful as an indication of a very poor match between mean MUAP and CMAP. The numerical results as presented in Figure 6.6 for three subjects are presented for all subjects in Table 6.1. This table also shows the MUNE values for a virtual large electrode.

Finally, the mean MUAP of subject 2, which poorly represents the corresponding CMAP (Fig. 6.6), was used to demonstrate the sensitivity of the MUNE to shifts in electrode position (Fig. 6.7). With shifts of only two rows (6 mm) between plots, the resulting MUNE changes dramatically. Please note the temporal similarity between maximum CMAP (gray) and MUNE × mean MUAP (black) in most of these cases. This illustrates again that temporal information alone is insufficient to assess representativity adequately.

6.4 Discussion

The goal of this work was to explore possible advantages of high-density sEMG, in particular for MUNE applications in which motor unit potentials have to be recognized. As explained in Section 6.2, the choice for the combination of multichannel recordings with the F-wave technique was, in a way, arbitrary. In this as well as in other MUNE methods, the addition of topographical information does not fundamentally change the inherent advantages and problems as discussed elsewhere.[35, 127] Adding information by applying multiple electrodes even gives the justified impression of a more complex method in its data collection and analysis. A larger study should elucidate whether this increase in complexity is outweighed by the advantages.

During the recording, the multichannel technique is similar to its conventional counterpart. The major difference is that an electrode grid is applied instead of a single electrode, which does not bring about additional discomfort to the subject. With respect to data analysis, manual editing was required at various stages in this

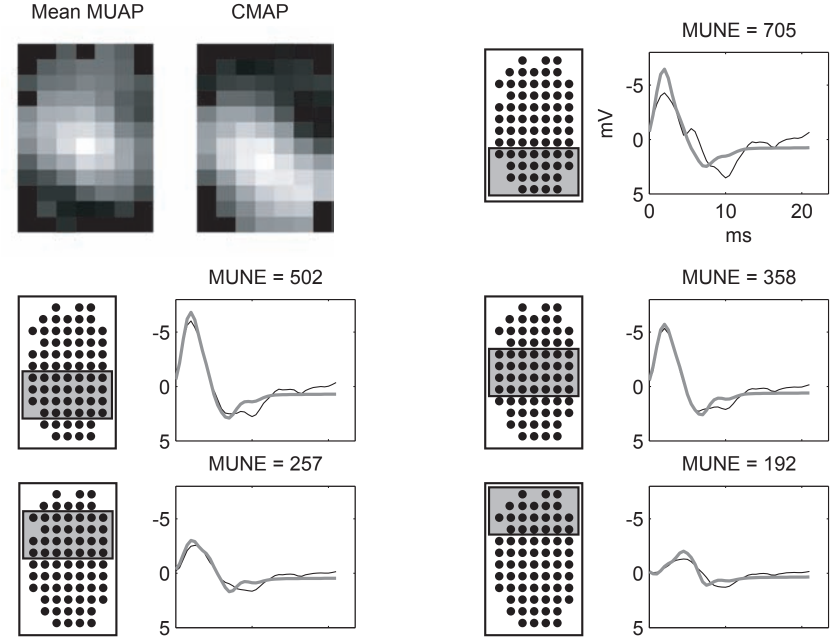

Figure 6.7: Example of the influence of electrode position on the mean MUNE for a situation in which the mean MUAP is not representative for the muscle as a whole (top left; same as middle of Fig. 6.6, subject 2). The gray block in each of the grids covers up to 28 electrodes. The mean MUAP (black, thin; multiplied by the MUNE) and CMAP (gray) signals on the right of each grid are calculated as the average of the signals of these electrodes. Note the fairly good match of the temporal signals in many of the situations.

first set of experiments in order to learn at what point decisions have to be made and on what grounds an algorithm should decide one way or the other. For this study, the duration of the full post-hoc analysis procedure with gained experience lasted approximately 2 - 3 h per recording. Further automation can be – and presently is being – accomplished. The high-density sEMG method is currently used in combination with the adapted MPS technique[146] in a recently started two-center study in which patients with hereditary motor-sensory neuropathy type 1a and amyotrophic lateral sclerosis are included.

Arguably the most important methodological drawback of the F-response technique that cannot be mitigated by its combination with high-density sEMG, is the lack of timing information, which is required for the reconstruction of the mean MUAP out of the individual F-responses.[35, 127] Although multichannel sEMG allows elimination of latency differences between MUAPs that are caused by a varying position of the electrode with respect to their motor endplate zones, latency differences caused by differing nerve conduction times remain unknown. Aligning the signals with respect to their onset therefore introduces inaccuracies that make it impossible to obtain a perfectly representative mean MUAP.

High-density sEMG as such also has a few disadvantages. It requires specialized data-acquisition equipment, and the combination of spatial and temporal aspects of the data necessitates computerized processing. The most important technical drawback is the increased noise level that results from increased electrode impedances (usually between 100 and 300 kΩ). At these impedances, electrode noise is about 5 μV peak-peak, i.e., about half of the total noise level of the sEMG signals (the other half being amplifier noise). This high noise level may make the detection and classification of the smallest MUAPs difficult. However, this effect is remedied to a large extent by the additional information supplied by the multiple electrodes. Furthermore, recent developments in high-density sEMG electrodes have led to significantly lower impedances,[74] thereby minimizing this disadvantage for future work.

The mean of the MUNE values in the subjects in whom more than 10 MUAPs could be detected is 342. This value is at the upper limit of the normal range found in the literature.[127] The most likely explanation for this tendency toward high values is the combination of the following two aspects. First, single-channel electrode recordings over the abductor pollicis brevis will focus on that muscle and pick up only minor contributions from other median-innervated muscles such as the more distant opponens and flexor pollicis muscles. With our recordings, some electrodes may have been over these muscles rather than over the abductor pollicis brevis. This may have generated a signal that is above the detection threshold at those electrodes, but too small to detect on a conventional electrode. A similar argument would hold for low-amplitude MUAPs of small spatial extent in the mAPB. Second, in conventional MUNE methods that largely depend on visual assessment of surface MUAPs, there may be a selection bias toward larger MUAPs since these are most easily recognized. The computer-based objectivity of the multichannel technique ensures that all small MUAPs that it encounters are included. These factors combined may well have resulted in a high MUNE.

Furthermore, the relation that is suggested by Table 6.1 (between sample size, MUNE, and standard deviation of the MUNE) indicates that the highest standard deviations, and, hence, the worst representativity, occur in the smallest samples and result in the “worst” (highest) MUNEs. The MUNE values that are obtained in the presence of a good fit and from larger samples (subjects 1, 3, 5, and 6) are in good accord with previously reported values. These results underline the importance of obtaining a sufficiently large sample. They also confirm the importance of a MUNE reliability measure as supplied by the multichannel technique.

6.4.1 Detecting and classifying MUAPs

Multichannel recordings aid the process of detecting and classifying MUAPs in a number of ways. First, the temporal properties of a MUAP (wave shape as a function of time) are predominantly determined by the characteristics of the MU in the fiber direction, being the position of the motor endplate zone, the conduction velocity over the fibers, and the average fiber length. Often, these properties do not differ much between MUs, explaining the limited resolving power of temporal MUAP wave shapes. By contrast, the MUAPs' spatial properties are determined to a large extent by the position and size of the MUs. Although the spatial information by itself is also insufficient to distinguish all MUAPs reliably, the combination of spatial and temporal information makes our procedure more accurate than one that is based on temporal information alone. This is particularly important for all those studies of muscle electrophysiology that depend on sEMG signals for the detection of single MUAPs, that is, not only for MUNE but, for instance, also for motor unit decomposition on the basis of sEMG data (Chapter 5, Ref. [105]).

Second, for those techniques that use stimulation of the motor nerve to recruit MUs (with the exception of the statistical technique), high-density sEMG can be of significant help in the resolution of combinations of MUAPs (see Fig. 6.5). Naturally, this is especially important when the frequent occurrence of MUAP combinations is inherent in a technique; that is, it is much more important for the increment-counting technique and the adapted MPS technique[146] than for the presented F-response method.

Third, the spatiotemporal profile of each MUAP supports the determination of its origin. MUAPs from MUs that are far away from the recording electrodes generally show a homogeneous amplitude map, whereas nearby MUs result in a MUAP pattern with a clearly localized amplitude peak.[123] The MUAPs with a homogenous MUAP profile sometimes demonstrate an initial positive phase in the EMG, accompanied by a lack of a significant negative phase. These are most likely generated by the median-innervated lumbrical muscles in the hand. As yet, we retain all MUAPs found. If desired, however, these MUAPs can be removed from subsequent analysis steps.

Fourth, especially the spatial distribution of MUAPs may be abnormal in subjects with a denervating/reinnervating disease. Collateral reinnervation may result in MUs with a larger spatial extent. In addition, because after reinnervation MUs are more likely to differ between one another, the discriminating power of the corresponding MUAP topography increases. We therefore expect that wave shape data in the spatial domain will be particularly useful in neurogenic conditions.

6.4.2 Assessing mean MUAP representativity

The accuracy of a MUNE relies primarily on how well the sampled population of motor units represents the muscle as a whole. This representativity can be assessed qualitatively from a comparison of the topographical profiles of the mean MUAP and the maximum CMAP. A quantitative measure is provided by the standard deviation of the MUNE values over the grid (Fig. 6.6, Table 6.1). The results that we have obtained thus far suggest that the representativity of the mean MUAP is acceptable for standard deviations below 100 and good below 50.

We prefer to use absolute rather than relative (% of MUNE) limits, to avoid cases with very high MUNEs being mistakenly thought of as acceptable. This choice may need reconsideration when results from the application of our technique in patients with neurogenic disorders become available. Note that the values of 50 and 100 must not be interpreted as remaining uncertainties in the resulting mean MUNE. For that purpose, the standard deviation is an overly pessimistic measure, because it indicates which (extreme) values can be observed. By calculating a mean MUNE over multiple electrodes, the sampling bias of a particular electrode location has been reduced markedly. To estimate the remaining uncertainty in the mean MUNE, the standard error of the mean (that is, the standard deviation divided by the square root of the number of included MUNE values) would be a more appropriate measure.

In the 2 subjects in whom less than 10 MUAPs could be detected, the match between mean MUAP and CMAP was very poor. On the basis of Table 1, we tentatively conclude for MUNE techniques in general that to ascertain a representative mean MUAP in a healthy subject, at least 15 and preferably more MUAPs should be available. This is more than the minimum sample size of 10 that is sometimes used,[18, 36, 51, 147] and supports the somewhat higher limit of 15-20 MUAPs mentioned elsewhere.[15, 130, 143]

The power of a single channel of sEMG to assess mean MUAP representativity is strikingly low (Fig. 6.7). Often, the mean MUAP and maximum CMAP signals are similar temporally and the resulting MUNE may seem reasonable, but in fact be inaccurate. The MUNE will then be sensitive to changes in electrode size as well as position, with obvious consequences for MUNE reproducibility. Conversely, we believe that with the availability of a means to assess the representativity of the mean MUAP, reproducibility can be improved. Our tool provides quantitative information regarding the representativity problem of a subset of MUAPs for the muscle as a whole. Its results are, perhaps, disconcerting, but is has to be understood that the problems encountered are, although usually inapparent, inherent in all techniques that aim to obtain a representative MU sample. If unnoticed there, they present themselves only through the high variability in MUNE values between subjects or in repeat studies.

7

ESTIMATION OF THE DISTRIBUTION OF MOTOR UNIT SIZES IN THE M. VASTUS LATERALIS USING HIGH-DENSITY SURFACE EMG

Quantitative estimates of motor unit (MU) size are usually made using the macro-EMG recording technique. The present study evaluates the use of high-density surface EMG (sEMG) as a non-invasive alternative for MU size estimation in the m. vastus lateralis. Two experiments were performed. In the first, sEMG recordings were combined with simultaneous intramuscular macro-EMG measurements. This allowed us to compare directly a MU's macro MU action potential (MUAP) and surface MUAP. In the second experiment, the MU size distributions found in the first experiment were compared to sEMG distributions obtained without triggers from the macro-EMG needle. We assumed that if a) the two sEMG distributions are identical, and b) the needle-triggered sEMG distribution correlates well with the macro-EMG distribution, then an appropriate MU size indicator for sEMG is obtained. The results show that to establish a good correlation ($r = 0.92$) between sEMG and macro EMG, a subject-dependent correction for subcutaneous fat layer thickness is required. If this correction factor is taken into account, a reliable estimate of the distribution of MU sizes can be obtained using high-density sEMG.

JH Blok, G Drost, E van Alphen, JP van Dijk, BU Kleine, MJ Zwarts, DF Stegeman

To be submitted

7.1 Introduction

A proper estimation of the distribution of motor unit (MU) sizes in a particular muscle can be important in the diagnosis of neuromuscular disorders. For instance, the process of motor nerve fiber loss (denervation) and subsequent reinnervation of afflicted muscle fibers leads to a prominent MU size increase.[84] Because MUs are the functional units in a muscle, MU size estimation can be based on the bio-electrical (functional) representation of individual MUs in the EMG signal. In routine clinical investigations, such an "electric size" estimation is made qualitatively by judgement of concentric or monopolar needle EMG recordings. In more specialized laboratories, the so-called macro-EMG technique is used for a quantitative assessment.[132]

This study evaluates the use of surface EMG (sEMG) as a non-invasive means of MU size estimation in the vastus lateralis muscle. In general, the problem in obtaining and validating a size distribution of MUs with surface EMG is threefold. First, there is no gold standard for MU size estimation. Macro EMG is the best available approximation[125] and has been used to validate sEMG-based MU size estimation for the biceps brachii.[121] For validation purposes, we therefore chose to compare our sEMG estimates with simultaneously obtained macro-EMG estimates. Second, there is the problem of isolating the contributions of individual MUs from the sEMG interference pattern, and third, the influence on size estimations of the surrounding tissue such as the muscle itself, the skin, and subcutaneous structures, is larger for surface EMG than for needle techniques.

The second problem can be approached by means of high-density recordings, in which a large number of electrodes are used to cover the skin over the muscle (Chapter 4 and Ref. [154]). This multichannel approach may be chosen over the conventional single channel recording for various reasons. Most important in the present context is that it may enable the isolation of individual MU firings from the surface EMG pattern (Chapter 5). Another advantage is the reduced dependency of the results on the exact placement of the surface electrodes, because the grid covers a large part of the muscle. Finally, previously obtained results for the m. biceps brachii suggest that the decline of potential amplitude over the skin surface perpendicular to the fiber direction may be used as an indicator of MU depth, and, hence, as a modifier of estimated MU size.[123]

Unfortunately, we found that it is often impossible to detect reliably the contributions of single MUs in the high-density sEMG recorded from the vastus lateralis. The spatiotemporal MUAP profiles provided by the multichannel approach were not sufficiently distinctive for this purpose. This was true even at low contraction levels, which in the biceps brachii allowed complete interference-pattern decomposition (Chapter 5). Therefore, the current study complements this approach with a computationally simpler alternative, based solely on signal amplitude. This alternative does not yield a MU size estimate for individual MUs, but a mean estimate for a group of MUs with alike surface MU action potentials (MUAPs). As long as all groups studied have a similar number of members, the MU size distributions resulting from the two approaches can also be expected to be similar.

Thus, the main goal of our investigation was to obtain a MU size indicator from the surface EMG signal that can easily be determined, yet results in MU size distributions that correspond well with those obtained with macro EMG. In addition, to address the third problem mentioned above, this study attempts to determine the influence of the conductive properties of the (sub)cutaneous structures on MU size estimation. More specifically, we wanted to answer the question whether practical application of the method requires correction for subcutaneous fat layer thickness and/or MU depth.

7.2 Methods

Two experiments were performed. In the first, surface EMG (sEMG) recordings were combined with simultaneous macro-EMG measurements. This allowed us to compare the macro MU action potential (MUAP) and surface MUAP of a particular MU on a one-to-one basis. Using this comparison, we could select the sEMG signal characteristic that correlated best with our standard for MU size, i.e., the area below the macro-EMG MUAP. In a second experiment, the needle-triggered sEMG size distributions found in the first experiment were compared to distributions found without needle triggers. The purpose of this combination of two experiments was to find a method for the estimation of the size distribution of motor units using only sEMG. We assumed that if (a) the two sEMG distributions are identical, and (b) the needle-triggered sEMG distribution correlates well with the macro-EMG distribution, then an appropriate MU size indicator is obtained.

The measurements were performed on the vastus lateralis muscle during voluntary, low force isometric contraction. The results of a similar study for the biceps brachii muscle have been published previously.[121] Evaluating the validity of those results for the vastus lateralis, a largely different muscle, was one of the driving factors for the present study.

7.2.1 Macro MUAPs versus surface MUAPs

In the first series of experiments, the macro EMG was recorded with a standard macro-EMG electrode.[132] The electrode has a single fiber recording surface (25 μm diameter at the side of the cannula, 7 mm from the needle tip). The lower part of the cannula, a 15 mm region from the tip, is bare; the rest is isolated with Teflon coating. A two-channel recording (A/D rate 20 ksamples/s; 12 bits conversion) was made using a Medelec Mystro MS20 (Oxford Instruments, Oxon, UK). On one channel, the single fiber signal (filter 500 Hz - 5 kHz; recording-dependent sensitivity of 50-500 μV/div) was acquired, using the cannula as reference. On the other channel, the macro-EMG signal (filter 10 Hz - 5 kHz; recording-dependent sensitivity of 0.5-5 mV/div) was recorded as the signal between the cannula and a remote reference: a surface electrode over the patella. For recording the sEMG,

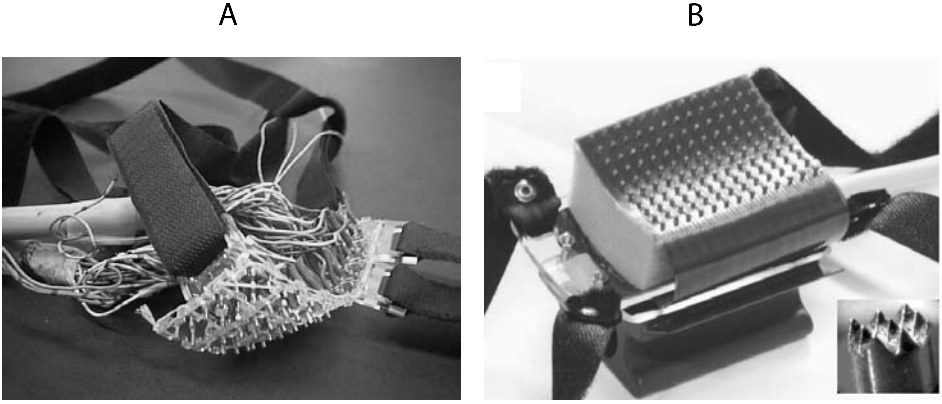

Figure 7.1: (A) The high-density surface EMG electrode grid with 60 channels used in the first series of experiments. (B) The large grid with 130 electrodes used in the second series. The inset shows a close-up of an electrode.

a grid of 60 gold-coated surface electrodes (1.5 mm diameter, interelectrode distance 6 mm) was used (see Fig. 7.1A). The signals were recorded with a Biosemi Mark 6 amplifier system (filter 3 Hz - 400 Hz, A/D rate 2 ksamples/s; 16 bits, 0.5 μV/bit conversion). The electrode grid consists of 4 rows of 15 electrodes and was placed above the m. vastus lateralis with the long side perpendicular to the muscle fiber direction. The sEMG recordings were made using a monopolar montage with a reference surface electrode over the patella.

The subject was sat on a bench, with knee flexion of approximately 90° and the lower leg fixed in a specially designed ergometer (see Fig. 4.3). After placement of the surface electrodes, the needle was inserted in the muscle through a hole in the center of the grid. The subject was then asked to contract the muscle slightly, and the EMG needle was manipulated until a stable signal from a regularly firing single muscle fiber was obtained. This signal was recorded for 30 seconds, as were the corresponding macro-EMG and sEMG signals. After the recording, the depth of the recorded MU was estimated as the distance between the skin surface and the single fiber lead on the needle. This procedure was repeated approximately ten times for each subject. Mostly, the needle was repositioned through the same insertion, but occasionally a second insertion site was used to ascertain selection of different MUs. A total of eight healthy subjects participated: four men and four women between 22 and 40 years of age with no prior history of neuromuscular disorders. To increase the range of MUAP sizes studied, five patients (three men, two women) suffering from the postpolio syndrome were included in this study. Recordings were made from the patient's least affected leg.[38] All subjects and patients gave their informed consent for the experiment, and the protocol was approved by the ethical committee of the Radboud University Nijmegen Medical Center.

The recorded macro-EMG and sEMG signals were averaged off-line with the time-

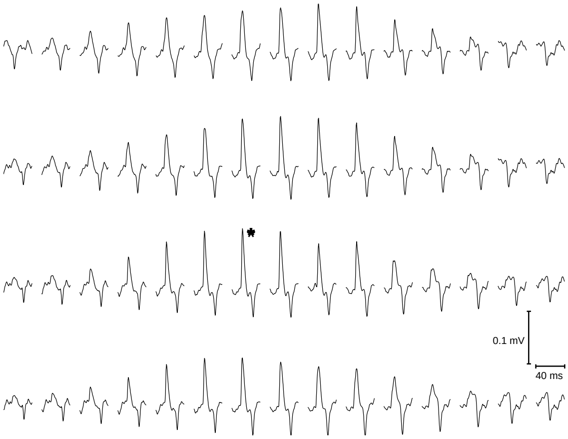

Figure 7.2: Spatiotemporal profile ("fingerprint") of an averaged monopolar surface MUAP. Each signal position in the profile corresponds to the position in the grid of the electrode that was used to record the signal. The asterisk marks the position where the MUAPs peak-peak amplitude is largest.

lock provided by the single fiber signal. For this purpose, the signals from the two sets of EMG equipment were first synchronized using a co-registered time code signal. Next, an 8-s selection of the single fiber data was made on the basis of the following criteria. First, the single fiber signal should show clear peaks of at least one fiber, with an amplitude that remained more or less constant during the recording. Second, if peaks of fibers belonging to different MUs were present, these should be clearly distinguishable, for example, by their amplitude. Third, the corresponding macro and surface EMG should be of good quality. For each 8-s segment, the positions of the maxima of the single fiber peaks were used as trigger points (between 33 and 159 triggers per segment), and the macro-EMG signals were averaged in a window of 40 ms around this trigger (15 ms pre- and 25 ms post-trigger). The monopolar surface signals were digitally high-pass filtered at 20 Hz, and then averaged in a window of 140 ms (40 ms pre- and 100 ms post-trigger). The averaged sEMG MUAPs can be displayed for each electrode separately, resulting in a "fingerprint" of the MU (example in Fig. 7.2). Using the spatiotemporal information available in the fingerprints, together with the corresponding macro-EMG signals, identical MUAPs could be identified and doubles were removed from the analysis. In these cases, different fibers of the same MU apparently generated the single fiber signals in consecutive recordings. We also removed those MUAPs from the analysis that had a poor signal to noise ratio after averaging and, hence, did not show a clear peak in any of the sEMG signals upon visual inspection.

As is common practice in quantifying the macro-EMG signal,[132] the signal area under the 40-ms averaged macro MUAPs was used as an indication for the size of the units. From the sEMG signals, the MUAP with the largest peak-peak amplitude was selected (indicated by the asterisk in Fig. 7.2; the same signal is

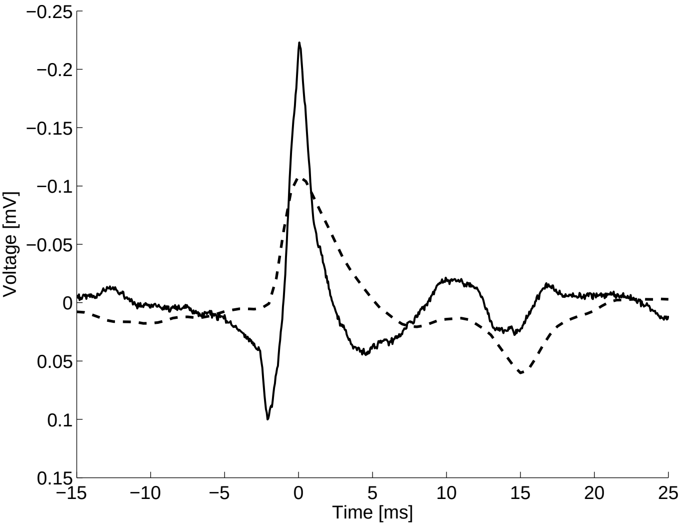

Figure 7.3: Averaged macro MUAP (solid) and surface MUAP (dashed) from the same MU. The latter corresponds to the signal marked with an asterisk in Figure 7.2.

presented as the dashed curve in Fig. 7.3). Generally, this MUAP will be recorded closest to the MU and is least biased by influences of intermediate tissue and MU depth. This MUAP's peak-peak amplitude and signal area were determined and correlated with the macro MUAP size. Because signal onset and offset could not be clearly marked, sEMG MUAP area was calculated below the signal from a fixed 15 ms before to 25 ms after its largest peak.

7.2.2 Needle-triggered versus surface-triggered sEMG

In the second series of experiments, again two MU size distributions were compared. The first of these was obtained in the previous experiment using the single fiber signal as trigger, the second using only sEMG. To obtain the latter distribution, we applied a different grid to the m. vastus lateralis, one that is commonly used in our department for recordings on this muscle.[38] See Figure 7.1B. This second grid has 126 channels (corner electrodes are not connected). The electrode type in this grid (see inset) is the same as in Figure 7.1A, but the interelectrode distance is 5 mm instead of 6 mm. The 10 columns of the grid, each containing 13 electrodes, were placed parallel to the muscle fibers. The same amplifier system was used as in the previous experiment. Both this grid and the recording system have been more extensively described in Chapter 4. In this experiment, delivered force was measured simultaneously with the sEMG using a custom-built ergometer (Fig. 4.3). Visual feedback of this force enabled subjects to maintain a constant contraction level, thus assuring a stable interference pattern for analysis.

First, the maximum voluntary contractile force (MVC) was measured. Next, the subject was asked to produce a certain force level (as a percentage of the MVC) as constantly as possible during 30 seconds. During those 30 seconds, the sEMG and the force were recorded. Up to five repeat measurements were performed at force levels between 1% and 15% MVC. Actual levels were chosen on the basis of the presence of clearly recognizable peaks in bipolar signals, which were calculated by subtraction of the monopolar signals of each pair of adjacent electrodes in column direction. There was a short pause of about one minute between measurements to prevent fatigue from becoming a significant factor. This recording series was conducted for four of the eight healthy subjects that participated in the first experiment.

In the absence of a needle trigger, MUAP extraction from the sEMG requires that the trigger moments be found in the sEMG itself. Two different approaches to MUAP template formation were used. The first has been described in Chapter 5 and was also used by Drost et al.[38] It uses the spatiotemporal information present in the multichannel recording to detect and characterize the contributions of single MUs in the sEMG. Thus, it becomes possible to decompose the sEMG interference pattern, in much the same way as characteristic temporal MU properties can be used to decompose the needle-EMG signal.[24, 76, 136]

Even though the use of the spatial information can offer advantages in the clustering of peaks, this information is not always sufficiently distinctive. For contraction levels over 5% MVC, superimposition of peaks often prohibits signal segmentation and classification. In addition, MUAP fingerprints tend to become more alike for greater MU depth and for increasing thickness of the subcutaneous fat layer. For deep or large muscles, the resulting lack of spatially distinctive characteristics leads to signals that are too complicated for the spatial clustering method. For the m. vastus lateralis, a large muscle that is often covered by a substantial layer of adipose tissue, this means that it is usually impossible to isolate more than a few (1 to 3) MUAPs reliably. This number is too small to base a MU size distribution estimate on. For that reason, the above analysis procedure was complemented with a second approach. This alternative method groups the peaks solely on the basis of their peak amplitudes, assuming that MUAPs of approximately the same peak amplitude have been generated by a single MU – or by a small number of MUs of about the same size. A similar technique based on a combination of muscle fiber conduction velocity (MFCV) and MUAP amplitude was recently proposed by Beck et al.[8]

For this purpose, after digitally high-pass filtering all bipolar channels at 20 Hz, the channel with the largest peak-peak amplitudes was determined and the root-mean-square (rms) value of its data calculated. Next, all peaks in the rectified signal were detected that exceeded a level of two times this rms-value, and the peak with the maximum amplitude was sought. A threshold was set at a level of 80% of the amplitude of that peak, and all peaks above the threshold were grouped together. Subsequently, of the remaining peaks, the one with the largest amplitude was determined, a new threshold was set at 80% of this peak, and the procedure was repeated until there were no more ungrouped peaks left. Note that this procedure gradually decreases the absolute width of the amplitude range (in each step, 80-100% of the largest remaining peak). Thereby, it compensates to some extent for the fact that there are but a few large MUs with large MUAPs, while MU numbers increase with decreasing MU size.

When all peaks had been assigned, clusters containing less than 20 peaks were discarded as unreliable. Peak positions in the remaining clusters were used as triggers for sEMG averaging as before, yielding monopolar multichannel MUAP profiles. Again, the MUAP with the largest peak-peak amplitude was selected, and its signal area determined as estimate of MU size. Finally, the resulting MU size distributions were compared to those obtained with needle triggers in the first experiment.

7.2.3 Motor unit depth and subcutaneous tissue

Using the combined macro and sEMG recordings, the depth dependence of the surface MUAP area was examined for both MU depth below the skin surface and within the muscle tissue (that is, below the subcutaneous layer). For the latter purpose, layer thickness was assumed to be the same as the depth of the most superficial MU recorded with the macro-needle single fiber tip in a particular subject. In these and following analyses, each surface MUAP area was first divided by the corresponding macro MUAP area. This normalization compensates for the effect of the actual MU size differences on the surface MUAP. Subsequently, the effect of skin layer thickness was assessed. To reduce potentially confounding effects of MU depth, it would be optimal to study size-normalized MUAPs obtained at a fixed depth within the muscle tissue between subjects (that is, as a function of subcutaneous fat layer thickness). Such fixed-depth recordings were not available. Instead, we assumed that MUs were sampled fairly homogeneously from the muscle. In that ideal case, the mean position of the MUs will tend to be close to the center of the muscle. As an approximation to true depth normalization, we therefore took the mean of the size-normalized sEMG MU size estimates and studied this mean size as a function of layer thickness.

In addition, simulation studies were performed using the volume conductor model for sEMG described in Chapter 3, to assess the expected effect of MU depth and subcutaneous tissue layer thickness on the surface MUAP area. The cylindrical volume conductor model was first assumed to have a circumference of 38 cm, that is, the smallest of the limb circumferences of our 13 subjects. This circumference corresponds to a limb radius of 6 cm. The thickness of the skin was assumed to be 2 mm, while that of the subcutaneous fat layer was 1 mm. Subsequent simulation runs were performed for subcutaneous fat layer thicknesses of 6, 11, and 21 mm, increasing the limb radius to a final value of 8 cm. In each simulation run, MU depth (the depth of the center of the MU within the muscle tissue and below the subcutaneous layer) was varied from 5 to 20 mm. All other model parameters were given the default values shown in Table 3.1. From the simulated sEMG signals, the one with the largest peak-peak amplitude was used for area determination.

7.2.4 Statistics

To assess the strength of the relationship between the macro-EMG based and needle-triggered sEMG based MU size estimates, the Pearson correlation coefficient r is determined. The regression coefficient obtained by linear regression analysis on the same data is used to rescale the sEMG MU size estimates. This enables quantitative comparison of the two MU size distributions by means of the Kolmogorov-Smirnov (KS) test (if both distributions contain at least 10 samples). Agreement is determined between the distributions obtained in individual subjects as well as between the merged results from all subjects (overall MU size distribution). In addition, agreement is assessed by means of a Bland-Altman plot.[10]

7.3 Results

7.3.1 Macro MUAPs versus surface MUAPs

In Figure 7.4, the signal area A_s (A and B) and peak-peak amplitude PP_s(C and D) of the largest signal of each of the averaged surface MUAP templates are plotted versus the signal area A_m of the corresponding averaged macro MUAP. Figures 7.4A and C show the results for the healthy subjects only; in Figures 7.4B and D, results for patients and controls have been combined. A modest Pearson correlation coefficient r between the macro-EMG size estimate and the sEMG size estimates can be found (Table 7.1). The line that best fits the data in a least-squares sense is drawn in each of the plots; its parameters are also presented in Table 7.1. For these fits, it has been assumed that the relation between macro MUAP and surface MUAP is proportional, that is, the fit is forced through the origin. Note that for the macro MUAP area and the surface MUAP area of healthy subjects only, the resulting scaling factor is 0.77, which is remarkably close to unity given the differences in source-electrode distance involved. Because correlation coefficients were similar for surface MUAP area and peak-peak amplitude, we chose to use only the area A_s for further analysis. This parameter is likely to be more robust than peak-peak amplitude. In addition, it may be expected to correlate better with macro MUAP area, first, because A_m and A_s are of the same nature physically, and second, because signal area is less influenced by the spatial filtering properties of the intermediate tissue than amplitude.

The pairwise comparison of estimates from the same MU, as allowed by the setup of the first experiment, was not possible in the second experiment. We were, therefore, particularly interested in the distributions of MU size estimates. If these do not differ, we may assume that the methods used to obtain them result in equivalent population estimates of the underlying true MU size distribution. In Figure 7.5A, the size estimates of individual MUs from both macro EMG and sEMG in healthy subjects are plotted next to each other (circles and asterisks, respectively). The above scaling factor of 0.77 (Table 7.1) was used to bring the

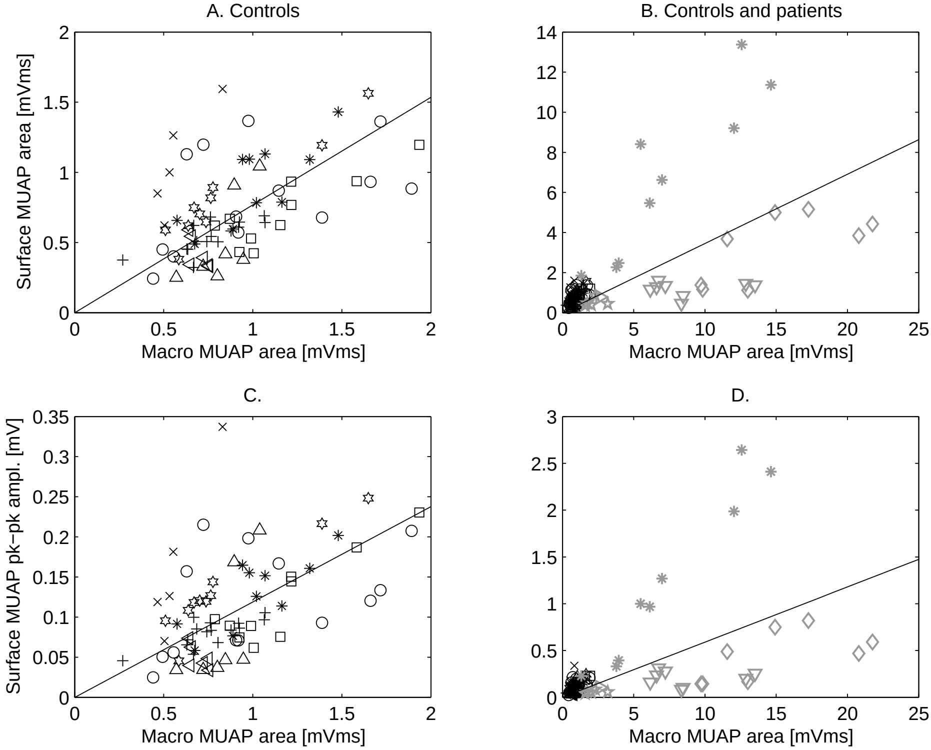

Figure 7.4: (A) Surface MUAP area versus macro MUAP area for healthy subjects. Different symbols represent different subjects. (B) Idem, for patients (grey symbols) and healthy subjects (black) combined. (C) and (D). As (A) and (B), but for surface MUAP peak-peak amplitude versus macro MUAP area.

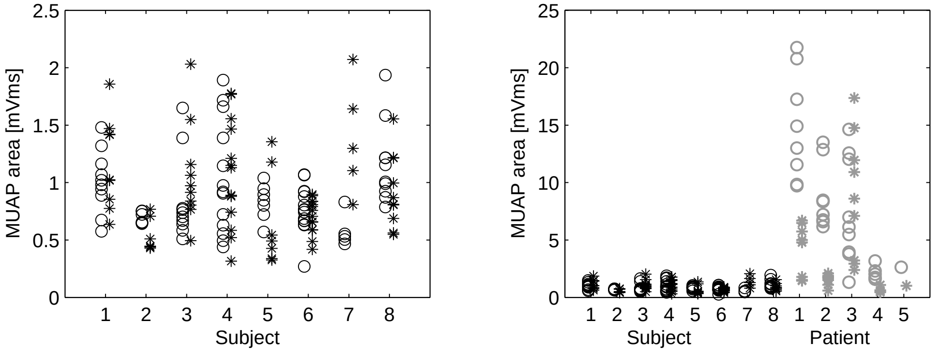

Figure 7.5: (A) Macro MUAP area distributions ("o") versus surface MUAP area distributions ("*") for each subject. (B) Idem, for subjects and patients combined.

Table 7.1: Correlation and fits of macro MUAP area A_m versus surface MUAP size parameters area A_s and peak-peak amplitude PP_s.

Included	Optimal fit	Pearson r
Controls	$A_s = 0.77\ A_m$	0.53
Controls + patients	$A_s = 0.35\ A_m$	0.63
Controls	$PP_s = 0.12\ A_m$	0.54
Controls + patients	$PP_s = 0.06\ A_m$	0.58

Table 7.2: Correlation and fits of macro MUAP area A_m versus surface MUAP size parameter area corrA_s with subcutaneous fat layer thickness correction applied to the latter.

Included	Optimal fit	Pearson r
Controls	$\mathrm{corr}A_s = 0.95\ A_m$	0.56
Controls + patients	$\mathrm{corr}A_s = 0.97\ A_m$	0.92

data together as close as possible. With this fixed scaling factor, the macro and surface distributions showed a fair correspondence for all subjects, except subject 7. Figure 7.5B shows the distributions of MU sizes for both healthy subjects and post-polio patients. For this Figure, the same scaling factor of 0.77 has been used. This choice may seem surprising given the scaling factor of 0.35 presented in Table 7.1 for controls and patients combined. However, because the latter linear regression analysis result is disproportionally determined by the three patients with the largest MUs (see Fig. 7.4), we consider it less reliable a priori than the value of 0.77.

A sufficiently large data set for the Kolmogorov-Smirnov test (> 10 samples) was obtained only for subjects 1, 3, 4, 6, and 8. For the first three of these subjects, the distributions did not differ statistically significantly (all p >0.4), for the last two it did ($p = 0.001$ in subject 6 and $p = 0.007$ in subject 8). If all MU size estimates were merged into a single, large set (with 107 estimates) for both the macro EMG and the surface EMG, these two sets also differed significantly ($p = 0.000$).

In patient 5, only a single surface MUAP template could be extracted. This was primarily due to significant artifacts in the multichannel surface EMG that masked the MUAPs, but also to repeat recordings (and subsequent removal) of this MUAP. Hence, for this patient, no conclusion can be drawn regarding the match of its macro and surface MUAP size distributions. The expected increase in mean MU size was confirmed by macro EMG for three of the remaining four patients. In patients 1 and 3, both the macro EMG and the sEMG MUAP area have increased; in patient 2, the macro EMG area is clearly much larger than in healthy subjects, but this is not reflected in the sEMG. For patient 4,

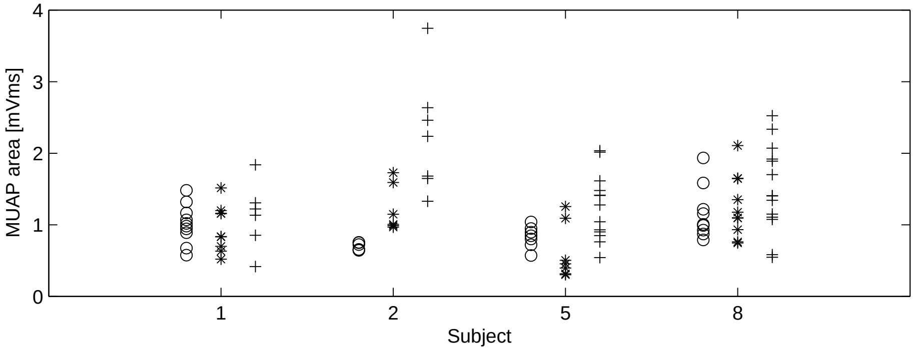

Figure 7.6: Distribution of surface MUAP sizes obtained with needle triggers ("*") and without needle triggers ("+") compared to macro MUAP size distribution ("o"). Surface MUAP areas are corrected for skin layer thickness (including subcutaneous fat) according to the relation in Figure 7.8B.

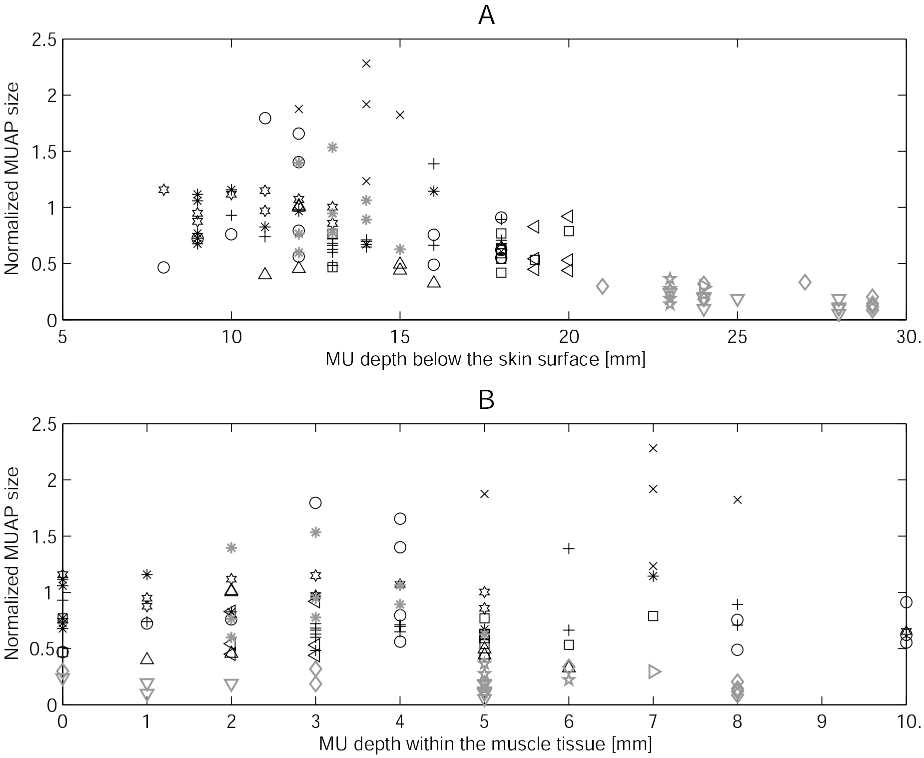

Figure 7.7: Influence of MU depth on sEMG MUAP size (normalized for MU size via the macro-EMG MUAP). MU depth is expressed in mm below the skin surface (A) and within the muscle tissue (B). Black symbols mark results for healthy subjects, grey symbols results for the post-polio syndrome patients.

both the sEMG and the macro EMG suggest that the MU sizes are not or only marginally larger than in healthy subjects. Although the macro EMG and sEMG size distributions both tend to an increase in most patients, the match between their distributions is poor compared to that in the healthy subjects.

7.3.2 Needle-triggered versus surface-triggered sEMG

The second step toward obtaining a proper indicator of MU size from sEMG alone was to compare the needle-triggered with surface-triggered sEMG-based MU size estimates. If allowed by the signal characteristics, a few templates (0-3 per subject) were constructed with the clustering method that uses the spatial information of the MU peaks (see Chapter 5). However, most templates were constructed with the amplitude-clustering method. Of each template, the monopolar MUAP with the largest peak-peak amplitude was selected and its area determined. In Figure 7.6, the distributions obtained from these analyses are plotted next to those found in the previous experiment. Both sEMG distributions have already been corrected for skin layer thickness by means of a scaling factor determined in the next paragraph. With the exception of subject 2, the two sEMG distributions seem to agree reasonably well upon visual inspection. Results from the Kolmogorov-Smirnov test, which in individual subjects could be performed only for subject 8, showed no significant differences between any two of the three distributions (all p >0.08). The same was true for the overall distributions (33 samples for the needle-triggered macro and sEMG distributions versus 40 for the sEMG-triggered distribution; $p > 0.12$ in all three cases).

7.3.3 Motor unit depth and subcutaneous tissue

In a study of Roeleveld et al.,[122] a depth-dependence of the surface signals was observed. By bringing this modifying effect of MU depth on MUAP size into the analysis, correspondence between macro EMG and sEMG could be somewhat improved in that study. In the present study, a depth-dependence of the normalized surface MUAP area seems absent (Fig. 7.7), specifically if MU depth within the muscle tissue is considered (Fig. 7.7B). By contrast, Figure 7.8A shows a clear decline of mean normalized MUAP size with skin (including subcutaneous fat) layer thickness. Because this relation seemed approximately exponential,

$$\text{mean MUAP size} = c_1 \exp(-c_2 L), \tag{7.1}$$

with c_1 and c_2 constants and L the skin layer thickness, a linear relationship between the logarithm of the mean MUAP sizes and L,

$$\log\,(\text{mean MUAP size}) = \log(c_1) - c_2 L \tag{7.2}$$

was expected and, indeed, observed (Fig. 7.8B). Regression analysis on the log-transformed MUAP data yielded values of 1.1 and 0.13 for c_1 and c_2, respectively.

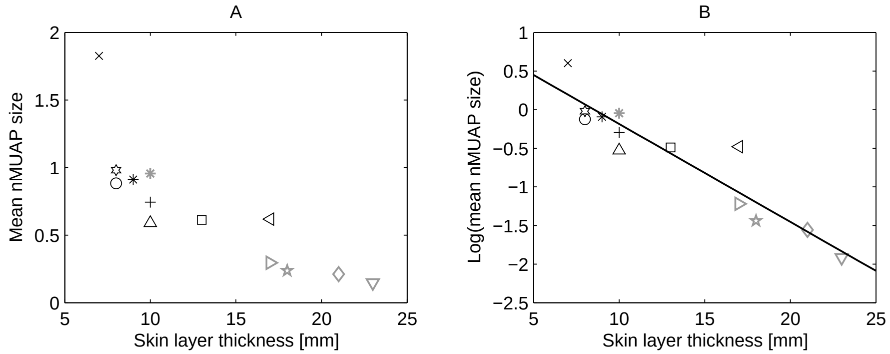

Figure 7.8: Relation between the skin (including subcutaneous fat) layer thickness and mean normalized surface MUAP size [(A) linear, and (B) logarithmic]. Black symbols mark results for healthy subjects, grey symbols results for the post-polio syndrome patients. The linear relationship between the skin layer thickness and the logarithm of the mean normalized surface MUAP area confirms the exponential decline of area with thickness.

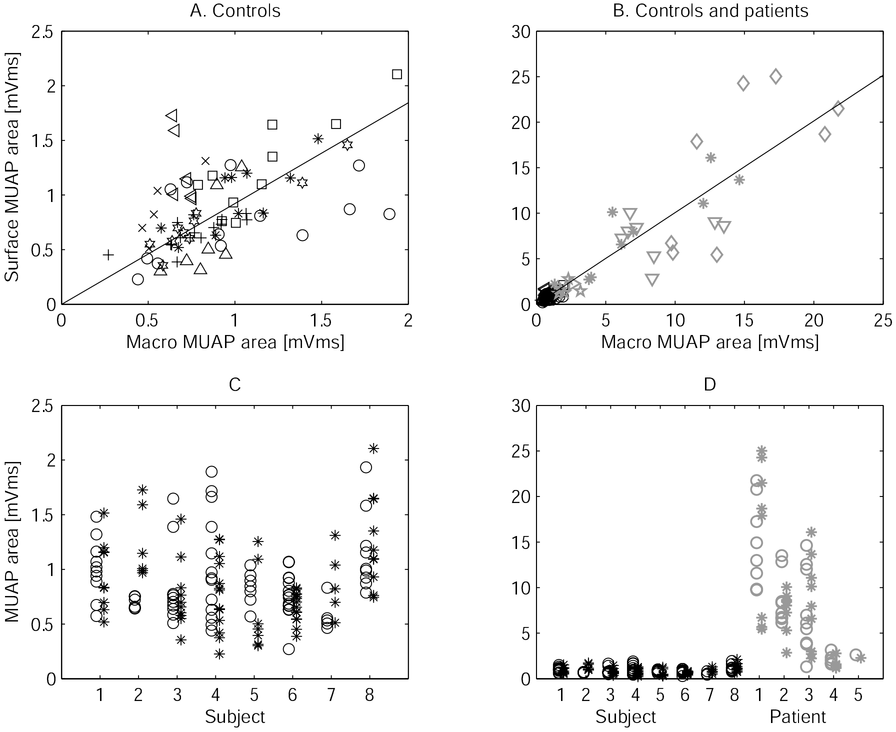

Figure 7.9: (A) and (B) As in Figure 7.4, and (C) and (D) as in Figure 7.5, but with surface MUAP area corrected for skin layer thickness (including subcutaneous fat) according to the relation in Figure 7.8B.

These determined a subject-dependent scaling factor $SF = 1/(1.1 \exp(-0.13L))$, which was next used to correct each of the (not size-normalized) MUAP sizes for the subject's skin layer thickness L. This procedure resulted in Figure 7.9, the skin layer thickness-corrected analogue of Figures 7.4A and B, and 7.5.

The adjustment for skin layer thickness improved the correlation between the macro and surface MUAP size distributions, particularly for the patients (compare Table 7.2 with Table 7.1). Statistical analysis showed that with the correction applied, none of the macro-EMG MU size distributions in subjects 1, 3, 4, 6, or 8 differed significantly anymore from the sEMG-based distributions (KS-test; all $p > 0.13$). In all 5 subjects, the maximum difference between the cumulative distributions remained the same or decreased compared to the situation without correction. Furthermore, the two overall MU size distributions for the total of 107 estimates no longer differed statistically significantly ($p = 0.72$); the maximum difference between the corresponding cummulative distribution functions was reduced by a factor of 3.

Figure 7.10 visualizes the agreement between the macro-EMG and (skin-layer thickness corrected) sEMG MUAP size distributions shown in Figure 7.9 by means of a Brand-Altman plot.[10] From each of the 26 distributions (two for 13 subjects), the mean and 75th and 25th percentiles were determined. Next, the differences between the macro-EMG and sEMG values were calculated per subject and plotted versus the mean of the two estimates. Figure 7.10 shows that for these three parameters, the sEMG size estimate can deviate substantially from the gold standard macro EMG. This may be either an overestimation or an underestimation. However, the changes in pathology are considerably larger (most grey symbols representing patients are well-separated from the black ones), suggesting that increases in MU size will generally be well-reflected in the sEMG. Dashed lines represent limits of agreement ($\pm 2\times$ standard deviation), the solid line the mean of the 13 values (systematic bias).

The results of the simulations in Figure 7.11 illustrate that, for larger subcutaneous fat layer thickness in particular, MUAP size changes but little with increasing MU depth within the muscle tissue. For the healthy subjects that participated in this study, the smallest subcutaneous fat layer thickness was 5 mm (mean, 8 mm; range, 5-15 mm); in patients, this thickness was much larger (mean, 16 mm; range, 8-21 mm). The difference between the deepest and most superficial MU recorded in individual subjects was 1 cm at most. From Figure 7.11, these numbers imply that MU depth may have modified surface MUAP size by only a factor of 2-3 from the deepest to the most superficial MUs studied (dotted arrow at MU depth of 15 mm in Fig. 7.11). This provides theoretical confirmation of our observation that the influence of MU depth is limited for recordings on the m. vastus lateralis. The experimental finding of a fairly rapid decline of mean surface MUAP size with subcutaneous fat layer thickness is not well reflected in the simulation results, however. On the basis of the latter, the largest and smallest mean normalized MUAPs were not expected to differ by more than a factor of 3 at most (compare values of 6 mm and 21 mm simulations at the most superficial

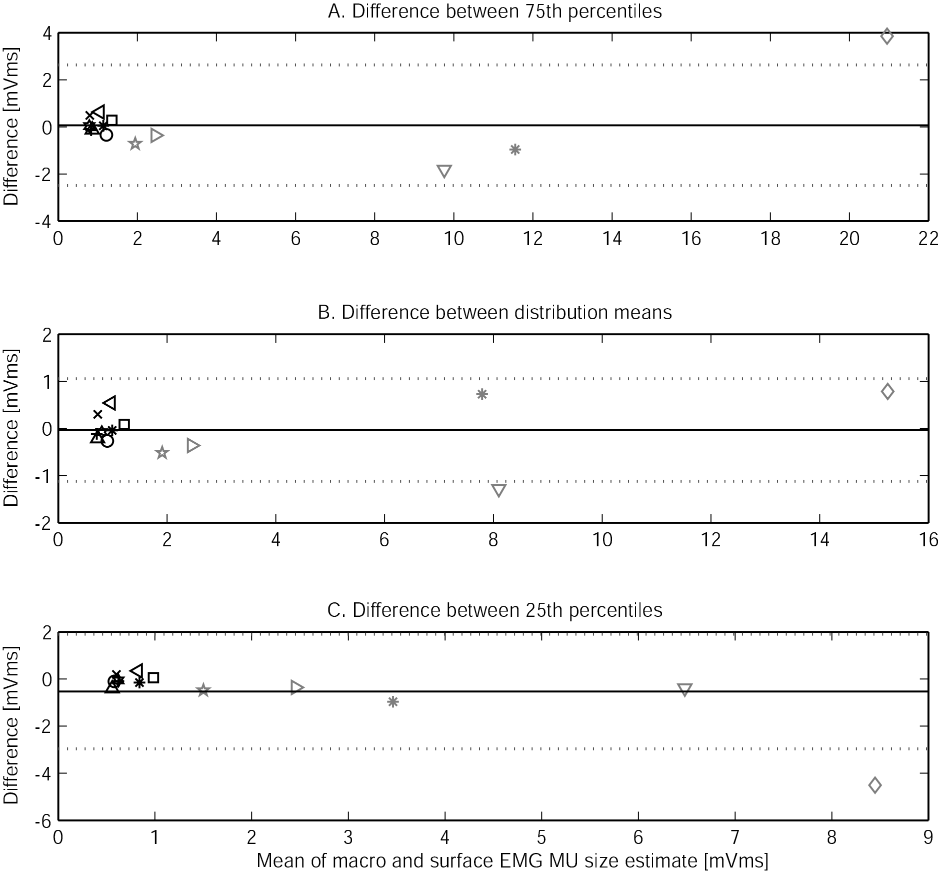

Figure 7.10: Bland-Altman plots of agreement between surface and macro-EMG MU size distribution parameters [(A) 75th percentile; (B) mean; (C) 25th percentile], expressed as difference between the two values versus their mean, for healthy subjects (black) and patients (grey). The dashed lines represent limits of agreement, the solid line (mean of all values) systematic bias.

MU depth of 5 mm; left, solid arrow in Fig. 7.11). In reality, however, this factor is approximately 8 (from Fig. 7.8).

7.4 Discussion

7.4.1 Motor unit size distribution estimation

The results of the present study suggest that it is possible to obtain a clinically useful estimate of the distribution of motor unit sizes using sEMG in the vastus lateralis muscle. This conclusion is primarily based on the agreement between the MU size distributions obtained using single fiber-triggered high-density sEMG

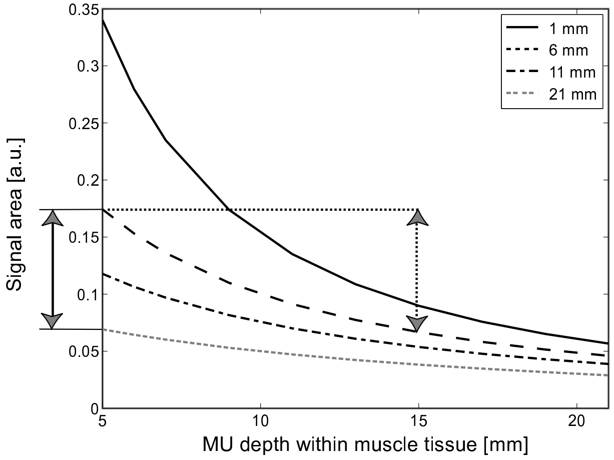

Figure 7.11: Simulation results. Effect of increasing MU depth on the area of the MUAP recorded at the skin surface, for varying thickness of the subcutaneous fat tissue layer (different lines). For arrows see text.

and macro EMG (Figs. 7.9 and 7.10). To establish a good correlation, we found that a correction for skin layer thickness including subcutaneous fat is required. Using this single, subject-dependent scaling factor, a correlation coefficient of 0.92 between the two distributions was obtained if results for patients and controls were combined. Patients were included to increase the range in MU sizes studied. For the healthy controls alone, correlation was only moderate (0.54), reflecting a fairly small range in MU size for that group: the majority of macro-EMG area values fell within a range of 0.5-1.0 mVms (see Fig. 7.9A).

Figure 7.10 shows that the sEMG estimate of the size distribution's mean and 75th and 25th percentiles may deviate from the gold standard macro-EMG estimate by a maximum of approximately 50% in individual (particularly healthy) subjects. This is a large discrepency. However, it should be considered in the light of the 2 (patients 4 and 5) to 18-fold (patient 1), that is, 100-1700%, increase in mean MU size observed in patients compared to controls. This implies that even in the case of the largest discrepancy, the difference in MU size between patients and controls will generally be retained in the sEMG, as may also be deduced from the separation of the black (healthy subjects) and grey (patients) symbols in each of the Blant-Altman plots.

The second experiment aimed to compare needle-triggered with surface-triggered sEMG distributions. In its analysis, some MUAPs could be obtained by means of the spatial decomposition procedure that was described in Chapter 5 and that was also used by Drost et al. for recordings on the m. vastus lateralis[38] – with, for unknown reasons, more success than in the present study. We complemented this decomposition approach by amplitude clustering. The latter method is significantly faster, because it requires far less computing time and user interaction.

With amplitude clustering, an "average" MUAP is found for all peaks in a range of amplitudes. In principle, the procedure can be applied to any recording, but its implicit assumption that peaks represent single MU firings is only valid at low force levels. At these low levels, the chance of superimpositions of MUAPs occurring is still fairly low. However, as soon as sufficient (i.e., more than 20) superimpositions of similar size are present to form a cluster, they will result in an overestimate of the sizes of the MUs that contribute to the interference pattern, and, hence, in an upward broadening of the MU size distribution. To minimize this problem, registrations were made at contraction levels below 15% MVC.

Although sEMG interference pattern decomposition on the basis of spatiotemporal information is more accurate and provides additional information regarding MUs (Chapters 4 and 5), our results indicate that amplitude clustering suffices for the purpose of MU size distribution estimation. On the basis of the limited data presented in this study no firm conclusions can be drawn, yet the distributions that can be obtained through amplitude clustering seem in reasonable accord with needle-triggered sEMG distributions (Fig. 7.6). Probably the major reason for the acceptable performance of the amplitude-clustering method is the same as that which explains why spatial decomposition often fails in the m. vastus lateralis: the spatiotemporal similarity between (bipolar) MUAPs.

For the vastus lateralis, superficial motor units are larger than deeper motor units.[70] Because superficial and large MUs tend to generate large MUAPs in the bipolar sEMG, this strongly favors the detection of these MUs over smaller and deeper ones. In the distributions obtained without needle-triggers, they may, therefore, be overrepresented. In turn, this might have affected the agreement between the needle-triggered and sEMG-triggered surface distributions (Fig. 7.6). This effect is counteracted, however, by the fact that a disproportionally large number of macro-EMG recordings will probably also have been made from large MUs, because the chance of obtaining a single fiber recording from a MU increases with the number of fibers in this unit (that is, with its size).

7.4.2 Motor unit depth and skin layer thickness

A remarkable finding in the present study was the small difference in area between the macro MUAPs and the surface MUAPs, with the area of the latter about three-quarters of that of the macro MUAP. As can be seen in Figure 7.3, the amplitude of the surface MUAP is substantially smaller than that of the macro MUAP, but the surface MUAP is considerably broader, which accounts for the approximating area values. Apparently, the volume conductor properties of the vastus and overlying layers have only a marginal influence on this parameter. The same phenomenon probably explains the basically absent modifying effect of MU depth within the muscle tissue on MUAP size (Fig. 7.7). The trend towards a decline with depth below the surface that – despite the large scatter in the data – seems to be present in Figure 7.7A, is primarily due to the effect of varying skin layer thickness. Previous findings of a clear MU depth-dependency of the size variables in the m. biceps brachii[122] could, therefore, not be confirmed for the m. vastus lateralis.

It should be acknowledged that depth estimation in the present study was not very accurate. In the earlier study,[122] the depth of the MU was determined with scanning EMG, which gives a very precise location of the electrophysiological center of the unit. In the present study, MU depth was determined as the distance between the single fiber lead and the skin. It was assumed that the single fiber lead-off surface was placed in the center of the unit, but this is only true on average. Therefore, an additional uncertainty of about 5 mm (the approximate radius of a MU cross-section) arises. It is not clear to what extent a reduction of this uncertainty (hence, better MU depth estimates) would contribute to more accurate MU size estimates. Its effect may well be small, given that a) our data do not even show a trend toward a MUAP size decline with MU depth (Fig. 7.7B), and b) the use of the accurately known MU depth in the previous m. biceps brachii studies hardly improved the correlation between the size distributions of macro MUAPs and surface MUAPs.[121] Indeed, for 7 of the 8 subjects in this study and for all of the patients, it would have been possible to give a sufficiently accurate estimate of the size distribution of their MUs, similar to the macro-EMG results, by using sEMG and a single, subject-dependent scaling factor. In our opinion, these findings justify the use of the MU size variable without any correction for the depth of the MU within the muscle.

Our data suggest a fairly strong dependence of the sEMG MU size estimate on the thickness of the skin layer (Fig. 7.8). Correcting for this dependency significantly improved the correlation between the macro-EMG and sEMG size estimates, as can be seen from a comparison of Figures 7.4 and 7.5 with Figure 7.9, and Table 7.1 with Table 7.2. Predominantly, this improvement results from the rescaling of MU size estimates in the most obese subjects. In our experiment, these tended to be the patients. For one subject (subject 2), this corrective approach failed. An acceptable explanation for this exception has not been found.

As said, patients were included to increase the range in MU sizes studied. Unknowingly at the time of recruitment, we thereby also increased the range of subcutaneous fat layer thickness. From Figures 7.7 and 7.8, it is clear that the patients in our study differed significantly from the control population in this volume conductor property of the lower limb. Consequently, MU depth below the skin surface tended to be larger in patients (Fig. 7.7A). The fact that the two groups differ so obviously in two relevant respects is somewhat unfortunate, because it makes it potentially more troublesome to merge them together for an overall analysis, such as the one used to derived the correction factor for skin layer thickness.

The correction factor for skin layer thickness was determined after compensating for the influence of the two variables that we expected to be the most important co-determinants of MUAP size: anatomical MU size (number of fibers) and MU depth. However, if patients and controls differ in an unforeseen aspect that significantly influences MUAP area, the scaling factor and the results obtained with it may not be correct. In principle, such an aspect might concern a pathophysiological change leading to increased temporal dispersion (such as differences in muscle fiber conduction velocity or MFCV), and, hence, differences in phase cancellation effects. In this study, such effects were minimized in two ways. First, only the area of the monopolar MUAP with the largest peak-peak amplitude is used. This signal can usually be recorded from the electrode that is closest to the motor endplate zone. Therefore, it is least influenced by temporal dispersion due to differences in MFCV between muscle fibers. Second, whatever the cause, the effects of dispersion increase with the duration of action potential propagation over the muscle fibers. For that reason, it probably has its most pronounced influence on the MUAPs (final) positive peak, which results from the termination of the action potential at the tendon. Increased dispersion will reduce this peaks amplitude and increase its duration. Compared to these two measures, positive peak area will remain relatively unaffected. Hence, our use of MUAP area rather than amplitude also provided a means to minimize effects of dispersion.

Any other factor differentiating patients from controls is not so easily thought of. Furthermore, its existence is contradicted to some extent by the good fit in Figure 7.8 of the data of patient 3 (marked by the grey asterisk) amongst the control values, even though his macro MUAP size data clearly indicate this to be one of the most severely affected patients (Fig. 7.9). We are therefore of the opinion that the relation between mean normalized surface MUAP size and skin layer thickness as presented in Figure 7.8 is not confounded by as yet unidentified differences between patients and controls. Consequently, their data may be combined and the resulting subject-dependent scaling factor is valid independent of whether it is applied to patients or controls.

Part V

Discussion and Summary

8

GENERAL DISCUSSION

8.1 Achievements

A (partial) replacement of invasive needle EMG with a non-invasive alternative, yielding similar diagnostic information, would have significant advantages. This thesis presents several tools that serve this purpose. They suggest interesting new perspectives for surface EMG (sEMG) techniques in clinical neurophysiology.

In modern medicine, the progress from invasive to minimally invasive or non-invasive techniques often relies heavily on the possibilities offered by medical technology. In general terms, diagnostic or therapeutic procedures tend to be easiest when the target organ or tissue is within visual or manual reach, or, as in the case of electrodiagnostic medicine, when the distance between a diagnostic sensor and the tissue of interest is small (as a rule, a signal that is picked up by the sensor rapidly decays with distance). Performing the same procedure, or obtaining the same information, through an (almost) intact skin and over larger distances requires technology to overcome the problems of invisibility or inaccessibility of the target tissue, or the loss of signal intensity. The development of new sEMG instrumentation and applications fits into this trend, both in its aim of providing a non-invasive diagnostic tool and in the role played by biophysics and engineering.

Part II of this thesis illustrates how mathematics and simulation studies can be used in this development process. They may help solve methodological problems of techniques, by systematic evaluation of their theoretical framework and underlying assumptions. In addition, simulation studies allow getting variables under control which cannot easily be controlled in reality. Amongst other advantages, this implies that they can provide a gold standard with which the results of analysis methods can be compared (Chapter 2). Finally, simulation studies can provide insight in the factors that influence the results of a particular recording as well as in the interactions between these factors (Chapter 3).

Part III focuses on the design of new sEMG instrumentation. Chapter 4 provides an overview of the data-acquisition system realized, a multichannel sEMG recording system with a high electrode density. This system enabled exploration of the clinical and scientific possibilities of topographical sEMG. A second necessary step toward this goal involved extension of the data acquisition system with an analysis algorithm that can decompose the sEMG interference pattern (Chapter 5). This combined hardware and software engineering approach resulted in spatiotemporal potential profiles of motor units, which in turn allowed for extensive motor unit characterization.

Part IV shows how a biophysical approach can aid the translation of recorded data to clinically meaningful information. More specifically, it can guide the design and help validate the (software) tools that are required to perform this translation (Chapters 6 and 7).

Together, the results presented illustrate that with high-density sEMG, physiological and topographical information becomes available that is beyond the reach of needle EMG, even at the level of single motor units. This topographical perspective is able to provide new insight into pathophysiological mechanisms, such as conduction block in myotonia congenita.[37, 39] For these reasons, multichannel surface EMG may be considered an important new research tool as well as an additional clinical diagnostic instrument.

8.2 Motor unit number estimation

In principle, motor unit number estimation (MUNE) might involve direct, anatomical counts of motor nerve fibers, but as yet there is no such technique that can be readily and repeatedly applied in the clinical diagnostic setting. Generally, (electro)physiological methods are used, two of which are presented in more detail in this thesis (Chapters 2 and 6). The large variety of existing MUNE methods has previously triggered the question of which method to use.[127] This question becomes all the more relevant with the modifications described in this thesis. Presently, the following seems the optimal strategy (given sufficient time and the availability of high-density sEMG equipment):

- If the muscle of interest is a proximal muscle, (multichannel) spike triggered averaging should be performed.[14]
- If the muscle of interest is a distal muscle, the multichannel variant of the adapted multiple point stimulation technique is the method of choice.[28, 66, 146]

Although recently a motor unit number index has been proposed that is calculated from voluntary sEMG,[106] needle EMG spike-triggered averaging (STA) is the only "true" MUNE technique that is based on voluntary contraction of the muscle of interest.[14] For that reason, it should be used whenever electrically eliciting motor unit action potentials (MUAPs) is difficult or impossible. Despite its invasive nature, this makes it a particularly valuable technique for proximal muscles such as the biceps brachii. High-density sEMG will likely have some additional value for STA, mostly with regard to assessing mean MUAP representativity, but also in recognizing whether a specific MUAP has been recorded previously. In theory, sEMG-triggered averaging as described in Chapter 5 (and, in a more basic form, by Shahani et al.[126]) might eliminate some of the disadvantages of the current needle-based STA method. However, this approach is unlikely to yield a sufficiently large and unbiased sample of MUAPs unless decomposition algorithms are devised that can handle the interference pattern at higher contraction levels. Recent steps in this direction are promising.[8, 54]

In Chapter 6, multichannel modifications to MUNE are primarily evaluated for the F-response method (FRM). This choice - rather then a choice for the multiple point stimulation (MPS) technique - was motivated by the smaller operator-dependency of and manual dexterity required by the FRM. However, the FRM may not work well in patients, because in many cases, and particularly in ALS, the persistency of F-waves is increased.[16] When the occurrence of an F-wave of a particular motor unit (MU) is no longer relatively rare compared to that of its M-wave, then the main advantage of the FRM for data analysis is lost. For that reason, the method of (adapted) MPS seems preferable.

The (Poisson) statistical technique is the only method that is implemented using dedicated MUNE software on commercially available equipment and that is - partly for that reason - fairly widely used. Although based on an elegant concept, it remains the least intuitive of MUNE techniques and questionable methodologically: irrespective of the distribution that is assumed to underly the observed CMAP variability (Poisson or binomial), the statistical method relies on a fairly large number of assumptions with limited validity (Chapter 2). At best, the outcome of the Poisson method in particular should be regarded as an indication of the general condition of the muscle rather than a MUNE. The binomial variant of the statistical MUNE method has not yet been sufficiently refined and validated to warrant recommendation. However, if future research proves it to be an accurate and reproducible method in (neurogenic) pathology, its ease of application and objectivity may make it preferable over (adapted) multiple point stimulation, especially for routine clinical diagnostics. Presently, it is also unclear to what extent the statistical method could profit from additional topographical information. Spatiotemporal information may serve the purpose of improved repositioning of the electrode in consecutive recording sessions, and, hence, improve reproducibility. Alternatively, simultaneous recordings with multiple electrodes may reduce some of the variability in the resulting MUNE, thereby eliminating the need for the two or more consecutive recording sessions suggested by Olney et al.[111]

8.3 Simulation studies

In this thesis, two models are described: the model of alternation in Chapter 2 and the Anvolcon volume conductor model in Chapter 3. Both of these models have thus far been applied only in the so-called forward direction. In this forward direction, mathematical descriptions of the underlying physiological processes are used to generate a model output that should resemble recorded data. Forward models are often used in the testing of new hypotheses, because any model result that is based on these new assumptions has to agree with measured data. By contrast, in the inverse direction, simulated or measured potentials are used to derive information regarding the underlying physiology (e.g., for source characterization or localization). Numerical parameter estimation procedures are applied to yield model parameter values (e.g., describing source characteristics) that result in the best approximation of the original signal given the model used.

The possibility of performing an inverse procedure depends on the number of parameters involved (the less parameters, the more reliable and goal-directed the parameter estimation). A good (sEMG) model takes the structure of the real system into account in a reductional way, and represents only the important elements of the system. Because there are many factors that significantly influence the sEMG potential profile and, hence, required incorporation in Anvolvon, the Anvolcon model is too complex for inverse use. By contrast, the few parameters of the alternation model imply that it probably will allow application in an inverse sense. Starting from measured CMAP variability, perhaps in combination with information provided by the “scan” made in statistical MUNE, this model can provide a means to estimate the (average) recruitment range of MUs, the distribution of their recruitment thresholds and, hence, the number of MUs that are simultaneously probabilistically active. This direction is now being explored and opens possibilities for further improvements in the statistical MUNE method.

The fact that models and model parameter settings are often valid only in a specific situation is well-illustrated in Chapter 7. The Anvolcon model and its parameters were originally designed for the biceps brachii, and served to improve our understanding of the relations between surface EMG topography, MU size, and MU depth.[119] Chapter 7 shows that some of the experimentally obtained results for the vastus medialis, a muscle very different from the biceps, cannot be readily reproduced by Anvolcon, at least not without drastically altering the settings of the tissue conductivities. This suggests that one or more of the physiological properties that are of significant importance for the sEMG topography are not yet included in the model. Possibly, these concern deviations from assumptions of cylinder symmetry of the volume conductor, or of tissue homogeneity. Use of more recently developed analytical models, such as that of Farina et al.,[47] or of numerical instead of analytical models[83, 131] might be able to circumvent these problems.

8.4 Recommendations for further developments in multichannel surface EMG data acquisition

8.4.1 Electrodes and grid design

The topographical differences between individual MUAPs are larger than anticipated when the first grids were designed (Fig. 6.4). For the small grid in particular (Fig. 4.2B), many MUAPs fall at least partly outside the area covered by the grid. For that reason, the grid area should be increased. This can be achieved in (a combination of) two ways: by increasing the number of electrodes, or by increasing the interelectrode distance (IED). Depending on the intended application, a choice for either option may be made, based on the relative importance of the following advantages and disadvantages.

A further increase in the number of surface electrodes is technically feasible, and advantages seem fairly obvious. Disadvantages of such a choice mainly lie in a concomitant increase in equipment costs, complexity, and manageability, as well as in a larger quantity of data to be analyzed. At present, it is not clear if and when an increase in electrode number would yield sufficient new, independent information to merit such an approach.

With respect to the IED, it should be noted that an increase may occasionally result in spatial undersampling of the MUAPs (in other words, the Nyquist sampling criterium may not be met; see Chapter 4). In these cases, the characterization of the detected MUAPs becomes less accurate, for example, in the determination of the position of the motor endplate zone. In addition, an increase in IED will reduce the effect of higher-order spatial filters. Bipolar or Laplacian filters (see Fig. 4.6) limit the uptake area – that is, the maximum depth from which MUAPs can be recorded – of surface electrodes to a degree that depends on the distance between the electrodes. Shorter IEDs result in stronger (high-pass) filtering. To be able to look selectively at contributions from very superficial MUs, short IEDs may be required.

An increase of the IED of the small grid seems feasible without affecting the accuracy of the decomposition procedures of voluntary surface EMG (Chapter 5) or of the classification of electrically elicited MUAPs (Chapter 6): differences between MUAPs are so large that the electrodes do not need to be as densely spaced as they presently are. Hence, for applications such as MUNE that do not have a very accurate characterization of individual MUAPs as their primary aim, the IED in both the fiber direction and the direction perpendicular to the fibers may be increased to 5 or 6 mm instead of 3 mm. The approximate doubling of the IED in both directions will increase the area covered by the electrodes by a factor of 4. Present grid dimensions are 22 mm × 46 mm, of which only 19 mm × 37 mm are effectively used. A doubling of the effective area to 30 mm × 50 mm will probably suffice to cover all MUAPs adequately. The remaining factor of 2 suggests that the number of electrodes and amplifiers required can be halved without affecting the accuracy of the decomposition and classification procedures that are described in Chapter 6, but this remains to be shown. For the biceps brachii and the vastus lateralis muscles (as studied in Chapters 5 and 7), this redundancy factor will be much smaller, because present (large) grid dimensions already result from an IED of 5 mm.

Further improvements in grid design can result from increasing its flexibility. At present, lack of flexibility results in poor electrode to skin contact for, in particular, the outermost rows and columns of the grids. Consequently, only 70-80 of the 128 electrodes could be used effectively (Section 6.2.4). A solution to this problem has recently been provided by Lapatki et al.,[74] who introduced a self-adhesive type of highly flexible grid, which is manufactured using flexprint techniques. Furthermore, combination of such a grid with a wearable multichannel acquisition system for long-term sEMG recordings (such as recently proposed by Pozzo et al.[114]) might be particularly useful for applications in dynamic conditions, such as kinesiology or sports science. Parenthetically, for this type of applications, an even larger IED than the 5 mm mentioned above can be allowed to preserve full muscle covering.[141]

8.4.2 Temporal sample frequency

The high-density sEMG recordings described in this thesis were temporally sampled with a frequency of 2 kHz. A higher sample frequency (4 or, preferably, 10 kHz) is recommended for a number of reasons. First, a higher sample frequency allows a more accurate determination of signal onset. The corresponding latency can be used for a number of purposes, including nerve fiber conduction velocity estimation. Second, the part of the signal that carries most of the characteristic temporal MUAP information (its negative peak) is presently described with only 5-8 samples. Because of the fairly high impedance of the electrodes, the noise level in these samples is substantial. An increase in the number of available samples can probably be used to make the detection and template-matching of the smaller MUAPs in particular more reliable.

8.4.3 Voluntary activity and relaxation

One of the most important factors that contribute to the ease and reliability of the data analysis of electrically elicited series of CMAPs or MUAPs is the absence of voluntary activity in the recorded responses. Because the two kinds of activity are of the same nature and share their signal morphology, the distinction between unwanted voluntary and electrically elicited activity is very difficult to make and to implement in software. Although not impossible, realisation of such algorithms requires significant additional research and effort. At present, automated MUNE (both single-channel and multichannel) is feasible only when voluntary activity is absent. Therefore, much attention should be given to factors that help improve muscle relaxation, such as increasing subject comfort during the recording and providing auditive and/or visual feedback.

8.5 Outlook

8.5.1 The future of surface EMG in electrodiagnostic medicine

Motor units are the basic building blocks of the neuromuscular system. The electrical activity of a MU contains information regarding central motor control mechanisms (MU recruitment and firing patterns; see Chapter 5). At the same time, MU activity is determined by various properties of the peripheral nervous system, including those of the nerve supply to the muscle, the muscle fibers, and the neuromuscular junction. Because of this wealth of information that can in principle be accessed by studying a MU's electrical activity, it may be expected that the MU will remain central to the EMG investigation. Furthermore, because of the functional rather than anatomical nature of a motor unit, EMG itself will probably maintain an irreplaceable role within the diagnostic process and follow-up of neuromuscular disorders.

Future developments in electromyography in general will probably be (and presently are; see Ref. [97]) directed towards:

- Ongoing reduction of patient discomfort, e.g., by using sEMG rather than needle EMG, minimizing stimulus intensity or number of stimuli, or reducing the duration of the investigation. In turn, such improvements may lead to increased use of EMG, either in study frequency (follow-up studies in the same patient) or by extension of the scope of its application. For example, EMG may be used more often in children than is the case presently.
- Further development and validation of quantitative EMG techniques as well as optimization of the use of available data.
- Assessment of the cost-effectiveness of electrodiagnostic techniques for the many purposes for which they are used.

The last item implies that the as yet rather time-consuming data analysis of high-density sEMG needs to be automated further before the technique can gain wide acceptance for diagnostic purposes. The first two points suggest that quantitative applications of sEMG are likely to receive rising attention, albeit on the condition that these applications are able to address the level of single MUs. Because meeting this condition is not possible with conventional single-channel techniques, it may be expected that the role of multichannel sEMG in future developments will increase. A further boost of the use of high-density recordings will probably come from the intrinsic value of the topographical information that it provides: high-density sEMG can bring to light – sometimes even without extensive data processing – clinically relevant information that otherwise would remain invisible.[37]

For some purposes, such as assessments of nerve fiber involvement (denervation and reinnervation) in suspected pathology, needle EMG and sEMG can yield more or less equivalent diagnostic information. In those cases, a particular investigator's choice for either technique may be motivated by the concomitant differences in patient (dis)comfort, required degree of objectivity and reliability of the outcome, the complexity of data acquisition and analysis, as well as the time required for the complete investigation. In other cases, however, the electromyographer has less of a choice. Only when a needle is used can the investigator observe the spontaneous activity of single muscle fibers and the reaction of these fibers to the disturbing presence of a needle, both of which may be of interest for other reasons than assessments of axonal involvement. Similarly, sEMG recordings are required to assess the integrated activity of a whole muscle.

For sEMG to become a generally accepted diagnostic alternative for (some) needle EMG investigations, it must first be able to distinguish neurogenic from myopathic disorders. Chapters 2, 6, and 7 show that, in principle, this goal can be met. Using the alternative methods presented in these chapters, it is possible to obtain information regarding two important MU characteristics (size and number) in a fully non-invasive way. In addition, these sEMG techniques have the advantage of providing quantitative information instead of the semi-quantitative assessment that is often made from needle EMG. A second important step would be taken if sEMG recordings enabled distinction between disorders within each of these two major classes of disorders. In needle EMG, such an assesment is often made by careful selection of the investigated muscles. This strategy can, in principle, also be followed in sEMG. Further research should show whether this is not only a theoretical but also a realistic option, given the limited available time in a clinical setting. Finally, in the ideal scenario, sEMG should be able to make distinctions at an even lower level, between disorders that are genetically different but which cannot be classified by needle EMG (such as the difference between Becker's and Thomsen's type of myotonia congenita). As yet, it is too early to predict whether sEMG will ever be able to reach this goal. However, if it does, that will probably be due – at least in part – to the availability of topographical information.

In general, quantitative analysis of single MU activity from voluntary contractions requires EMG signal decomposition. That is, individual MUAPs should be identified in the interference pattern and classified, so that the constituent MUAPs and firing trains that make up the signal can be determined. For needle EMG signals, this decomposition process is difficult but very well feasible.[24, 138] When surface electrodes are used, it is considerably more complex. The filtering properties of the volume conductor reduce the shape differences between MUAPs and increase their duration, thereby increasing the likelihood of superimposition of MUAPs and the difficulty of MUAP classification. Nevertheless, Chapter 5 shows that the recognition of MUs using surface EMG is possible using the MUAPs' characteristics distributions over the skin. This spatial distribution can be recorded only when registrations are made at multiple sites over the muscle, that is, by multichannel surface EMG. The characteristics of the multichannel signals can be used to unravel MU firing patterns, including superimpositions. In this way, it is presently possible to detect up to six simultaneously active MUs. The actual number achievable depends on the subject and muscle investigated (tending to higher values in neurogenic diseases[69]). With current analysis techniques, it may often prove too low to obtain a representative MU sample, for example for MUNE purposes. Ongoing research, possibly along the lines of that performed by Gazzoni et al.,[54] should therefore address methods for increasing this number in a wide variety of recording conditions.

8.5.2 The future of multichannel surface EMG in research

The topographical information that can be obtained through multichannel sEMG opens a range of possibilities for research.[93, 154] Many of these are currently being explored, even more are not.

First, the topographical perspective offers a new view on (patho)physiological conditions, and, hence, is likely to generate novel insights. This is true both at the level of the entire muscle and that of single MUs. For example, the tools described in Chapters 5 and 6 allow the collection of sets of spatiotemporal MUAPs,[73] which possess an information content that still lies mostly unexplored. Changes in MU (or MUAP) characteristics with progressing disease or increasing age, the effects of training or fatigue: for each of these topics a topographical view may provide important new physiological information at the single MU level. This is well-illustrated by several recent studies of neuromuscular fatigue,[8, 63, 98] which are based on assessments of the muscle fiber conduction velocity (MFCV).

Second, high-density recordings can be used to guide the design of grids and software for sEMG applications that by themselves do not require many densely spaced electrodes. For example, in a recent study Beck et al.[9] used 4 columns of 8 electrodes with an interelectrode distance (IED) of 6 mm to evaluate the influence of a) the IED used to derive each bipolar signal and b) the distance between the two bipolar signals (ISD), on estimates of the MFCV. Their conclusions can be used to configure a 4-electrode grid with optimal IED and ISD. A similar design study searching for "lower limits" was also performed for the use of multichannel sEMG in muscle force estimation,[141] and is conceivable for other applications such as MUNE, MU size estimation, and MUAP characterization. Such an approach may bridge the gap between a 128-channel recording system and "conventional" equipment. Nowadays, the latter often allows 10- or even 32-channel recordings, and, hence, the incorporation of some topographical information. Similarly, topographical studies can address diagnostically relevant problems regarding, for example, the influence of electrode dimensions or recording site over a muscle on the amplitude and reproducibility of the CMAP.[26, 27] This type of information may be used in devising conventional, single-channel sEMG recording protocols for nerve conduction studies.

Third, a multichannel version of applications that conventionally employ one or only a few electrodes may serve as gold standard for the latter. For example, a true gold standard method for motor unit number estimation is still lacking. Thus far, methods have been evaluated only by means of converging evidence: if multiple methods used by multiple investigators on multiple healthy subjects yielded similar MUNEs, this value would be taken as normal value for a particular muscle. However, this approach can be applied only to (healthy) populations and not to individual subjects. Recent improvements in the multichannel MUNE method[28] allow collection of larger sets of MUAPs (up to 30) than conventional methods. Particularly when used in conjunction with the mean MUAP representativity assessment as described in Chapter 6, these improvements will result in a MUNE that is more reliable than that of conventional methods. Therefore, even though the multichannel technique may not yet be ready for routine clinical application, it may be used as (near-)gold standard to evaluate existing and new techniques.

SUMMARY

This thesis shows that a biophysical approach can bring new perspectives to the surface electromyography (sEMG) technique, which thus far has played only a minor role in the diagnostics of neuromuscular disorders. Such a contribution may be the development of a new instrument, for example, the sEMG recording system with 128 electrodes that is presented in Chapter 4. Alternatively, it may come from providing or revising the theoretical framework for an (already existing) application. Chapter 2 illustrates the latter for a method of motor unit number estimation or MUNE (a motor unit is a functional unit in a muscle). This so-called statistical MUNE technique estimates the number of motor units (MUs) that is responsible for the observed variation in the muscle's reaction (the compound muscle action potential or CMAP) to a series of electrical stimuli with equal strength. In its existing form, this method was appealing for a number of reasons, but it suffered from methodological problems that limited its usefulness and accuracy. Chapter 2 provides an alternative, based on a different mathematical perspective on the observed CMAP variation.

The main goal of the developments laid down in the present thesis was the realisation of a system that would allow exploration of the clinical and scientific possibilities of topographical surface electromyography (sEMG). The term "topographical sEMG" is used to indicate that the method uses not only temporal but also spatial information. To enable the comparison of this new, multichannel technique with conventional needle EMG, the design focus was on its possibilities in MU analysis. At the same time, the method should be able to make optimal use of the additional information that multichannel sEMG may yield on the whole muscle.

Some of the design specifications of the new instrument followed directly from the sEMG signal characteristics themselves. To provide a better understanding of these signal characteristics and, hence, to guide the design process, a biophysical model was developed (Chapter 3). This model is based on a mathematical description of the conductive behavior of muscle, subcutaneous fat, and skin tissue. Its results determined, amongst other things, the distance between the electrodes in the electrode grids. Other design specifications followed from technical and operational demands. Together, these led to the multichannel sEMG recording system with a high electrode density described in Chapter 4. This chapter provides an overview of the data-acquisition system realized and concludes with an illustration of the use of some of the available data-analysis tools in the characterization of single MUs.

In voluntary contractions of a muscle, each MU has its own pattern of activation,

with firing moments that are only weakly related to those of other MUs. Because in the sEMG the contributions of many MUs are present, this independent firing results in a so-called interference pattern. From this sEMG interference pattern, the contributions of individual MUs cannot be as easily recognized as from needle EMG recordings, because the details of the MU signals are less pronounced in sEMG than in needle EMG. Nevertheless, Chapter 5 shows that, at least for low contraction levels, multichannel sEMG allows for accurate determination of the firing moments of individual MUs. Using the topographical differences between the MUs that contribute to the sEMG, a peak detection and classification algorithm can decompose the sEMG interference pattern. First, this provides non-invasive access to central MU firing characteristics during voluntary contractions. If combined with subthreshold transcranial magnetic stimulation, which modifies the firing sequences of single MUs, such an approach presents a method by which neuronal firing events can both be influenced and quantified non-invasively (Chapter 5). Second, averaging the sEMG over the detected firing instances for all electrodes yields a low-noise template of the MU's spatiotemporal potential profile, which allows extensive MU characterization (Paragraph 4.5)

The EMG has diagnostic value in both myogenic and neurogenic disorders. Because the latter tend to result in an increased EMG amplitude and less interference in the surface EMG, the signals in neurogenic disorders can be more easily handled and analyzed. In turn, this makes them most apt for initial application and validation of new sEMG applications. For that reason, both of the two major characteristics of these disorders, increased MU size and decreased MU number, are addressed rather extensively in this thesis. Chapter 7 compares the results of a multichannel method to estimate the MU size distribution with those of macro-EMG, a needle EMG technique whose results may be taken as gold standard for size estimation. Both techniques were applied in healthy subjects and in patients with post-poliomyelitis syndrome, a neurogenic condition. The results of this study not only show that a reliable estimate of the distribution of MU sizes can indeed be obtained using high-density sEMG, but also that this requires a subject-dependent correction for subcutaneous fat layer thickness.

Chapters 2 (see above) and 6 concern two different methods to estimate the number of functioning motor units in a muscle (MUNE). Both of these methods involve the recording of the surface EMG in response to electrical stimulation of the motor nerve. Using stimulation, the control function of the brain can temporarily be taken over by the experimenter, so that a larger or smaller (depending on the stimulus strength) number of MUs can be recruited simultaneously. In this way, the moment of activation is known, with obvious advantages for data analysis. Chapter 6 illustrates the additional value that high-density recordings can have for a number of already existing MUNE techniques. Hitherto, this type of technique has been performed with just a single recording surface electrode. The multichannel study shows that topographical information can support MUNE techniques in two ways: by providing extra information in the data-analysis stage that simplifies the analysis (without changing the analysis methods themselves) and by providing a means of assessing the reliability of the outcome of the procedure.

SAMENVATTING

Dit proefschrift laat zien dat een biofysische benadering nieuwe perspectieven biedt aan de oppervlakte EMG (sEMG) techniek, die tot nu toe slechts een geringe rol speelt bij de diagnostiek van neuromusculaire aandoeningen. Deze bijdrage vanuit de biofysica kan bestaan uit de ontwikkeling van een nieuw meetinstrument, zoals bijvoorbeeld het sEMG-registratiesysteem met 128 elektroden uit hoofdstuk 4. Een andere bijdrage kan komen in de vorm van het bieden of herzien van het theoretisch kader van een (eventueel reeds bestaande) toepassing. Hoofdstuk 2 illustreert deze laatste mogelijkheid aan de hand van een methode om het aantal motorische eenheden (de functionele eenheden van een spier; in het Engels "motor units", afgekort als MU) te schatten. Deze zogenaamde statistische motor unit number estimation of MUNE methode schat het aantal motor units dat verantwoordelijk is voor de waargenomen variatie in de reactie van de spier op een serie elektrische stimuli met constante sterkte. In zijn bestaande vorm had deze methode een aantal aantrekkelijke kanten, maar tevens last van methodologische problemen die de bruikbaarheid en nauwkeurigheid ervan beperkten. Hoofdstuk 2 biedt een alternatief dat gebaseerd is op een ander wiskundig perspectief op de waargenomen variatie in spierrespons.

Het belangrijkste doel van het onderzoek dat in dit proefschrift wordt beschreven was de realisatie van een systeem dat een verkenning van de klinische en wetenschappelijke mogelijkheden van topografisch sEMG mogelijk maakt. "Topografisch sEMG" wil zeggen dat de methode naast temporele ook spatiële (ruimtelijke) informatie gebruikt. Om deze nieuwe, multikanaals techniek te kunnen vergelijken met conventioneel naald-EMG onderzoek is het accent bij het ontwerp van dit systeem gelegd op de mogelijkheden om informatie over individuele motor units (MUs) te kunnen verkrijgen. Daarnaast moest de nieuwe methode optimaal gebruik kunnen maken van de extra informatie die multikanaals sEMG biedt met betrekking tot de spier als geheel.

Een aantal van de ontwerpspecificaties voor het nieuwe instrument volgden direct uit de eigenschappen van de sEMG signalen zelf. Om deze signaalkarakteristieken beter te begrijpen en daarmee richting te geven aan het ontwerpproces is een biofysisch model ontwikkeld (hoofdstuk 3). Dit model is gebaseerd op een wiskundige beschrijving van de geleidende eigenschappen van spier-, onderhuids vet- en huidweefsel. De modelresultaten hebben onder andere bepaald wat de afstand tussen de elektroden moest worden in de uiteindelijke "elektrodenmatjes". Andere ontwerpspecificaties volgden uit technische en operationele vereisten. Samen leidden ze tot het multikanaals sEMG-registratiesysteem dat beschreven wordt in hoofdstuk 4. Dit hoofdstuk geeft een overzicht van het gerealiseerde data-acquisitie systeem en eindigt met een illustratie van het gebruik van een aantal van de beschikbare data-analyse methoden bij de karakterisering van individuele motor units.

Bij vrijwillige aanspanning van een spier heeft elke MU zijn eigen activeringspatroon, met vuurmomenten die slechts zwak gerelateerd zijn aan die van andere MUs. Omdat in het sEMG de bijdragen van veel MUs aanwezig zijn, leidt dit onafhankelijke vuurgedrag tot een zogenaamd interferentiepatroon. Het is veel moeilijker om de bijdragen van afzonderlijke MUs te herkennen in een oppervlakte EMG interferentiepatroon dan in het naald-EMG. De voornaamste reden hiervoor is dat de details van MU signalen in het oppervlakte EMG veel minder uitgesproken – en daarmee karakteristiek – zijn. Hoofdstuk 5 laat echter zien dat het (in ieder geval voor lage aanspanningsniveaus) mogelijk is om middels multikanaals sEMG de vuurmomenten van MUs nauwkeurig te bepalen. Door gebruik te maken van de topografische verschillen tussen de MUs die bijdragen aan het sEMG blijkt een piekdetectie en -classificatie algoritme in staat om het sEMG interferentie patroon uit elkaar te rafelen. Dit levert in de eerste plaats een niet-invasieve manier op waarmee zicht kan worden verkregen op centrale aspecten van MU vuurkarakteristieken gedurende vrijwillige aanspanning. Als deze methode gecombineerd wordt met transcraniële magnetische stimulatie met een lage intensiteit (een techniek die de vuurpatronen van individuele MUs kan beinvloeden), kunnen neuronale vuringen gemodificeerd én gekwantificeerd worden (hoofdstuk 5). In de tweede plaats kan door voor alle elektroden het sEMG te middelen over de gedetecteerde vuurmomenten een ruisarm spatiotemporeel profiel ("vingerafdruk") van een MU verkregen worden. Zo'n profiel leent zich bij uitstek voor een uitgebreide, al dan niet kwantitatieve MU karakterisering (paragraaf 4.5).

Het EMG heeft diagnostisch belang voor zowel myogene als neurogene aandoeningen. Omdat de laatsten in het algemeen leiden tot een toename van de EMG amplitude en een afname van de interferentie in het sEMG aanspanningspatroon, kunnen de signalen die kenmerkend zijn voor neurogene aandoeningen eenvoudiger geanalyseerd worden. Dit leidt er vervolgens weer toe dat zij vaak het meest geschikt zijn voor initiële toepassingen en validatie van nieuwe (s)EMG technieken. De beide voornaamste kenmerken van deze aandoeningen, een toename in de MU grootte en een afname van het aantal MUs, komen in dit proefschrift dan ook relatief uitgebreid aan de orde. Hoofdstuk 7 vergelijkt de resultaten van een multikanaals methode om de MU grootte distributie te schatten met die van macro-EMG, een naald-EMG techniek die als gouden standaard methode geldt voor MU grootte bepalingen. Beide methoden zijn toegepast bij gezonde proefpersonen en patiënten met het post-polio syndroom, een neurogene aandoening. De resultaten van deze studie laten zien dat het mogelijk is om een betrouwbare schatting van de distributie van MU groottes te verkrijgen middels multikanaals sEMG, maar ook dat hiervoor een persoonsafhankelijke correctiefactor nodig is die bepaald wordt door de dikte van de onderhuidse vetlaag.

De hoofdstukken 2 (zie hierboven) en 6 betreffen twee verschillende methoden om het aantal functionele motor units in een spier te bepalen (MUNE). Deze methoden maken beide gebruik van registratie van sEMG activiteit die het gevolg is van elektrische stimulatie van de motorische zenuw. Door gebruik te maken van stimulatie kan de sturende functie van de hersenen tijdelijk overgenomen worden door de onderzoeker, zodat een kleiner of groter deel (afhankelijk van de sterkte van de stimuli) van de MUs tegelijkertijd geactiveerd wordt. Het tijdstip van activatie is daarmee bekend, met duidelijke voordelen voor de data-analyse. Hoofdstuk 6 laat de toegevoegde waarde zien van multikanaals registraties voor een aantal reeds bestaande MUNE technieken. Tot nu toe hebben deze gebruik gemaakt van een enkele elektrode. De multikanaalsstudie laat zien dat topografische informatie MUNE methoden op twee manieren kan ondersteunen: doordat de extra informatie in het data-analyse stadium de analyse vergemakkelijkt (zonder de methode in essentie te veranderen) en doordat ze een maat biedt waarmee de betrouwbaarheid van een meting kan worden beoordeeld.

REFERENCES

[1] Abramowitz M, Stegun IA. Handbook of mathematical functions. New York: Dover, 1970.

[2] Andreassen S, Rosenfalck A. Relationship of intracellular and extracellular action potentials of skeletal muscle fibers. CRC Crit Rev Bioeng 1981; 6:267–306.

[3] Awiszus F. Quantification and statistical verification of neuronal stimulus responses from noisy spike train data. Biol Cybern 1993;68:267–274.

[4] Awiszus F. Spike train analysis. J Neurosci Methods 1997;74:155–166.

[5] Awiszus F, Feistner H. Abnormal EPSPs evoked by magnetic brain stimulation in hand muscle motoneurons of patients with amyotrophic lateral sclerosis. Electroencephalogr Clin Neurophysiol 1993;89:408–414.

[6] Awiszus F, Feistner H. Comparison of single motor unit responses to transcranial magnetic and peroneal nerve stimulation in the tibialis anterior muscle of patients with amyotrophic lateral sclerosis. Electroencephalogr Clin Neurophysiol 1995;97:90–95.

[7] Baker JR, Davey NJ, Ellaway PH, Friedland CL. Short-term synchrony of motor unit discharge during weak isometric contraction in Parkinson's disease. Brain 1992;115:137–154.

[8] Beck RB, Houtman CJ, O'Malley MJ, Lowery MM, Stegeman DF. A technique to track individual motor unit action potentials in surface EMG by monitoring their conduction velocities and amplitudes. IEEE Trans Biomed Eng 2005;52:622–629.

[9] Beck RB, O'Malley M, van Dijk JP, Nolan P, Stegeman DF. The effects of bipolar electrode montage on conduction velocity estimation from the surface electromyogram. J Electromyogr Kinesiol 2004;14:505–514.

[10] Bland JM, Altman DG. Statistical methods for assessing agreement between two methods of clinical measurement. Lancet 1986;8476:307–310.

[11] Blok JH, Stegeman DF, Drost G. The use of spatiotemporal information in motor unit classification. In: The state of the art on signal processing methods for surface electromyography, deliverable 7 of the SENIAM project, Hermens H, Merletti R, Rix H, Freriks B, editors. Enschede: Roessingh Research and Development, 1999; pp. 185–193.

[12] Blok JH, van Asselt S, van Dijk JP, Stegeman DF. On an optimal pasteless electrode to skin interface in surface EMG. In: The state of the art on sensors and sensor placement procedures for surface electromyography, deliverable 5 of the SENIAM project, Hermens HJ, Freriks B, editors. Enschede: Roessingh Research and Development, 1997; pp. 71–76.

[13] Boniface SJ, Mills KR, Schubert M. Response of single spinal motoneurons to magnetic brain stimulation in healthy subjects and patients with multiple sclerosis. Brain 1991;114:643–662.

[14] Bromberg MB. Motor unit estimation: reproducibility of the spike-triggered averaging technique in normal and ALS subjects. Muscle Nerve 1993;16:466–471.

[15] Bromberg MB, Abrams JL. Sources of error in the spike-triggered averaging method of motor unit number estimation (MUNE). Muscle Nerve 1995; 18:1139–1146.

[16] Brown WF, Doherty TJ, Chan M, Andres A, Provost SM. Human motor units in health and disease. Muscle Nerve 2000;Supplement 9:S7–S18.

[17] Brown WF, Milner-Brown HS. Some electrical properties of motor units and their effects on the methods of estimating motor unit numbers. J Neurol Neurosurg Psychiatry 1976;39:249–257.

[18] Brown WF, Strong MJ, Snow R. Methods for estimating numbers of motor units in biceps-brachialis muscles and losses of motor units with aging. Muscle Nerve 1988;11:423–432.

[19] Buchthal F. The general concept of motor unit. Neuromusc Disorders 1961; 38:3–30.

[20] Buchthal F, Guld C, Rosenfalck P. Multielectrode study of the territory of motor unit. Acta Physiol Scand 1957;39:83–104.

[21] Christodoulou CI, Pattichis CS. Unsupervised pattern recognition for the classification of EMG signals. IEEE Trans Biomed Eng 1999;46:169–178.

[22] Classen J, Benecke R. Inhibitory phenomena in individual motor units induced by transcranial magnetic stimulation. Electroencephalogr Clin Neurophysiol 1995;97:264–274.

[23] Daube JR. Estimating the number of motor units in a muscle. J Clin Neurophysiol 1995;12:585–594.

[24] De Luca CJ. Precision decomposition of EMG signals. Meth Clin Neurophysiol 1993;4:1–28.

[25] Dengler R, Gillespie J, Argenta M, Elek J, Wolf W, Struppler A. The impact of paired motor unit discharges on tremor. Electromyogr Clin Neurophysiol 1989;29:113–117.

[26] Dijk van JG, van Benten I, Kramer CG, Stegeman DF. CMAP amplitude cartography of muscles innervated by the median, ulnar, peroneal, and tibial nerves. Muscle Nerve 1999;22:378–389.

[27] Dijk van JG, van der Kamp W, van Hilten BJ, van Someren P. Influence of recording site on CMAP amplitude on its variation over a length of nerve. Muscle Nerve 1994;17:1286–1292.

[28] Dijk van JP, Lapatki BG, van Schaik IN, Bour LJ, Zwarts MJ, Stegeman DF. High-density sEMG recognizes alternation in adapted multiple point stimulation MUNE. Clin Neurophysiol 2005;116:484.

[29] Dimitrov GV, Dimitrova NA. Precise and fast calculation of the motor unit potentials detected by a point and rectangular plate electrode. Med Eng Phys 1998;20:374–381.

[30] Dimitrov GV, Lateva ZC, Dimitrova NA. Model of the slow components of skeletal muscle potentials. Med Biol Eng Comput 1994;32:432–436.

[31] Dimitrova NA, Dimitrov GV. Precise and fast MUP calculation as a prerequisite for inverse EMG modelling. In: The state of the art on modelling methods for surface electromyography, delivarable 6 of the SENIAM project, Hermens HJ, Stegeman DF, Blok JH, Freriks B, editors. Enschede: Roessingh Research and Development, 1998; pp. 45–60.

[32] Disselhorst-Klug C, Rau G, Schmeer A, Silny J. Non-invasive detection of the single motor unit action potential by averaging the spatial potential distribution triggered on a spatially filtered motor unit action potential. J Electromyogr Kinesiol 1999;9:67–72.

[33] Disselhorst-Klug C, Silny J, Rau G. Improvement of spatial resolution in surface-EMG: a theoretical and experimental comparison of different spatial filters. IEEE Trans Biomed Eng 1997;44:567–574.

[34] Disselhorst-Klug C, Silny J, Rau G. Estimation of the relationship between the noninvasively detected activity of single motor units and their characteristic pathological changes by modelling. J Electromyogr Kinesiol 1998; 8:323–335.

[35] Doherty T, Simmons Z, O'Connell B, Felice KJ, Conwit R, Chan KM, Komori T, Brown T, Stashuk DW, Brown WF. Methods for estimating the numbers of motor units in human muscles. J Clin Neurophysiol 1995;12:565–584.

[36] Doherty TJ, Brown WF. The estimated numbers and relative sizes of thenar motor units as selected by multiple point stimulation in young and older adults. Muscle Nerve 1993;16:355–366.

[37] Drost G, Blok JH, Stegeman DF, van Dijk JP, van Engelen BGM, Zwarts MJ. Propagation disturbance of motor unit action potentials during transient paresis in generalized myotonia: a high-density surface EMG study. Brain 2001;124:352–360.

[38] Drost G, Stegeman DF, Schillings ML, Horemans HL, Janssen HM, Massa M, Nollet F, Zwarts MJ. Motor unit characteristics in healthy subjects and those with postpoliomyelitis syndrome: a high-density surface EMG study. Muscle Nerve 2004;30:269–276.

[39] Drost G, van Dijk JP, Stegeman DF, van Engelen BG, Zwarts MJ. Maintaining constant voluntary force in generalized myotonia despite muscle membrane disturbances: insights from a high-density surface EMG study. J Clin Neurophysiol 2004;21:114–123.

[40] Duchene J, Hogrel JY. A model of EMG generation. IEEE Trans Biomed Eng 2000;47:192–201.

[41] Dumitru D, Amato AM, Zwarts MJ, editors. Electrodiagnostic medicine. 2nd edition. Philadelphia: Hanley and Belfus, 2001.

[42] Dumitru D, King JC, Rogers WE. Motor unit action potential components and physiologic duration. Muscle Nerve 1999;22:733–741.

[43] Ellaway PH. Cumulative sum technique and its application to the analysis of peristimulus time histograms. Electroencephalogr Clin Neurophysiol 1978; 45:302–304.

[44] Everitt BS. Cluster analysis. New York: Halsted Press, 1993.

[45] Fang J, Agarwal GC, Shahani BT. Decomposition of multiunit electromyographic signals. IEEE Trans Biomed Eng 1999;46:685–697.

[46] Farina D, Merletti R. A novel approach for precise simulation of the EMG signal detected by surface electrodes. IEEE Trans Biomed Eng 2001;48:637–646.

[47] Farina D, Mesin L, Martina S, Merletti R. A surface EMG generation model with multilayer cylindrical description of the volume conductor. IEEE Trans Biomed Eng 2004;51:415–426.

[48] Farmer SF, Halliday DM, Conway BA, Stephens JA, Rosenberg JR. A review of recent applications of cross-correlation methodologies to human motor unit recording. J Neurosci Methods 1997;74:175–187.

[49] Feasby TE, Brown WF. Variation of motor unit size in the human extensor digitorum brevis and thenar muscles. J Neurol Neurosurg Psychiatry 1974; 37:916–926.

[50] Feinstein B, Lindegard B, Nyman E, Wohlfart G. Morphological studies of motor units in normal human muscles. Acta Anat 1955;23:127–142.

[51] Felice KJ. A longitudinal study comparing thenar motor unit number estimates to other quantitative tests in patients with amyotrophic lateral sclerosis. Muscle Nerve 1997;20:179–185.

[52] Galea V, de Bruin H, Cavasin R, McComas AJ. The numbers and relative sizes of motor units estimated by computer. Muscle Nerve 1991;14:1123–1130.

[53] Garland SJ, Miles TS. Responses of human single motor units to transcranial magnetic stimulation. Electroencephalogr Clin Neurophysiol 1997; 105:94–101.

[54] Gazzoni M, Farina D, Merletti R. A new method for the extraction and classification of single motor unit action potentials from surface EMG signals. J Neurosci Methods 2004;136:165–177.

[55] Geddes LA, Baker LE. The specific resistance of biological material - a compendium of data for the biomedical engineer and physiologist. Med Biol Eng 1967;5:271–293.

[56] Gielen FL, Cruts HE, Albers BA, Boon KL, Wallinga de Jonge W, Boom HB. Model of electrical conductivity of skeletal muscle based on tissue structure. Med Biol Eng Comput 1986;24:34–40.

[57] Gootzen THJM, Stegeman DF, Heringa A. On numerical problems in analytical calculations of extracellular fields in bounded cylindrical volume conductors. J Appl Physics 1989;66:4504–4508.

[58] Haig AJ, Gelblum JB, Rechtien JJ, Gitter AJ. Technology assessment: the use of surface EMG in the diagnosis and treatment of nerve and muscle disorders. Muscle Nerve 1996;19:392–395.

[59] Hanajima R, Ugawa Y, Terao Y, Sakai K, Furubayashi T, Machii K, Kanazawa I. Paired-pulse magnetic stimulation of the human motor cortex: differences among I waves. J Physiol (Lond) 1998;509:607–618.

[60] Henderson RD, McClelland R, Daube JR. Effect of changing data collection parameters on statistical motor unit number estimates. Muscle Nerve 2003; 27:320–331.

[61] Heringa A, Stegeman DF. Comments on “Potentials produced by arbitrary current sources in an infinite- and finite-length circular conducting cylinder”. IEEE Trans Biomed Eng 1987;34:73–74.

[62] Heringa A, Stegeman DF, de Weerd JP. Calculated potential and electric field distributions around an active nerve fiber. J Appl Phys 1989;66:2724–2731.

[63] Houtman CJ, Stegeman DF, van Dijk JP, Zwarts MJ. Changes in muscle fiber conduction velocity indicate recruitment of distinct motor unit populations. J Appl Physiol 2003;95:1045–1054.

[64] Huppertz HJ, Disselhorst-Klug C, Silny J, Rau G, Heimann G. Diagnostic yield of noninvasive high spatial resolution electromyography in neuromuscular diseases. Muscle Nerve 1997;20:1360–1370.

[65] Jackson JD. Classical electrodynamics. 2nd edition. New York: John Wiley & Sons, 1975.

[66] Kadrie HA, Yates SK, Milner Brown HS, Brown WF. Multiple point electrical stimulation of ulnar and median nerves. J Neurol Neurosurg Psychiatry 1976;39:973–985.

[67] Kimura J. Electrodiagnosis in diseases of nerve and muscle: Principles and practice. 3rd edition. Oxford University Press, 2001.

[68] Kleine BU, Praamstra P, Stegeman DF, Zwarts MJ. Impaired motor cortical inhibition in Parkinson's disease: motor unit responses to transcranial magnetic stimulation. Exp Brain Res 2001;138:477–483.

[69] Kleine BU, Schelhaas HJ, Stegeman DF, Zwarts MJ. Fasciculations in ALS: firing pattern analysis discriminates between spinal or peripheral origin. In: Abstractbook of the XIIth European Congress of Clinical Neurophysiology. Stockholm: Intellecta Tryckindustri, 2005; p. 72.

[70] Knight CA, Kamen G. Superficial motor units are larger than deeper motor units in human vastus lateralis muscle. Muscle Nerve 2005;31:475–480.

[71] Koning de P, Wieneke GH, van der Most van Spijk D, van Huffelen AC, Gispen WH, Jennekens FG. Estimation of number of motor units based on macro-EMG. J Neurol Neurosurg Psychiatry 1988;51:403–411.

[72] Kumagai K, Yamada M. The clinical use of multichannel surface electromyography. Acta Paediatr Jpn 1991;33:228–237.

[73] Lapatki BG, Oostenveld R, van Dijk JP, Jonas IE, Zwarts MJ, Stegeman DF. Topographical characteristics of motor units of the lower facial musculature revealed by means of high-density surface EMG. J Neurophysiol 2005; doi:10.1152/jn.00265.2005. In print.

[74] Lapatki BG, van Dijk JP, Jonas IE, Zwarts MJ, Stegeman DF. A thin, flexible multielectrode grid for high-density surface EMG. J Appl Physiol 2004;96:327–336.

[75] Lateva ZC, McGill KC. The physiological origin of the slow afterwave in muscle action potentials. Electroencephalogr Clin Neurophysiol 1998; 109:462–469.

[76] LeFever RS, De Luca CJ. A procedure for decomposing the myoelectric signal into its constituent action potentials - Part I: technique, theory, and implementation. IEEE Trans Biomed Eng 1982;29:149–157.

[77] LeFever RS, Xenakis AP, De Luca CJ. A procedure for decomposing the myoelectric signal into its constituent action potentials - Part II: execution and test for accuracy. IEEE Trans Biomed Eng 1982;29:158–164.

[78] Liguori R, Dahl K, Fuglsang-Frederiksen A. Turns-amplitude analysis of the electromyographic recruitment pattern disregarding force measurement. I. Method and reference values in healthy subjects. Muscle Nerve 1992; 15:1314–1318.

[79] Lomen-Hoerth C, Olney RK. Comparison of multiple point and statistical motor unit number estimation. Muscle Nerve 2000;23:1525–1533.

[80] Lomen-Hoerth C, Olney RK. Effect of recording window and stimulation variables on the statistical technique of motor unit number estimation. Muscle Nerve 2001;24:1659–1664.

[81] Lomen-Hoerth C, Slawnych MP. Statistical motor unit number estimation: From theory to practice. Muscle Nerve 2003;28:263–272.

[82] Loudon GH, Jones NB, Sehmi AS. New signal processing techniques for the decomposition of EMG signals. Med Biol Eng Comput 1992;30:591–599.

[83] Lowery MM, Stoykov NS, Dewald JP, Kuiken TA. Volume conduction in an anatomically based surface EMG model. IEEE Trans Biomed Eng 2004; 51:2138–2147.

[84] Luciano CA, Sivakumar K, Spector SA, Dalakas MC. Electrophysiologic and histologic studies in clinically unaffected muscles of patients with prior paralytic poliomyelitis. Muscle Nerve 1996;19:1413–1420.

[85] Lynn PA. Direct on-line estimation of muscle fiber conduction velocity by surface electromyography. IEEE Trans Biomed Eng 1979;26:564–571.

[86] Masuda T, Miyano H, Sadoyama T. The distribution of myoneural junctions in the biceps brachii investigated by surface electromyography. Electroencephalogr Clin Neurophysiol 1983;56:597–603.

[87] Masuda T, Miyano H, Sadoyama T. The propagation of motor unit action potential and the location of neuromuscular junction investigated by surface electrode arrays. Electroencephalogr Clin Neurophysiol 1983;55:594–600.

[88] Masuda T, Sadoyama T. Skeletal muscles from which the propagation of motor unit action potentials is detectable with a surface electrode array. Electroencephalogr Clin Neurophysiol 1987;67:421–427.

[89] Masuda T, Sadoyama T. Distribution of innervation zones in the human biceps brachii. J Electromyogr Kinesiol 1991;1:107–115.

[90] McComas AJ, Fawcett PRW, Campbell MJ, Sica REP. Electrophysiological estimation of the number of motor units within a human muscle. J Neurol Neurosurg Psychiatry 1971;34:121–131.

[91] McGill KC, Cummins KL, Dorfman LJ. Automatic decomposition of the clinical electromyogram. IEEE Trans Biomed Eng 1985;32:470–477.

[92] McGill KC, Dorfman LJ. Automatic decomposition electromyography (ADEMG): validation and normative data in brachial biceps. Electroencephalogr Clin Neurophysiol 1985;61:453–461.

[93] Merletti R, Farina D, Gazzoni M. The linear electrode array: a useful tool with many applications. J Electromyogr Kinesiol 2003;13:37–47.

[94] Merletti R, Farina D, Gazzoni M, Merlo A, Ossola P, Rainoldi R. Surface electromyography. A window on the muscle, a glimpse on the central nervous system. Eur Med Phys 2001;37:57–68.

[95] Merletti R, Knaflitz M, De Luca CJ. Myoelectric manifestations of fatigue in voluntary and electrically elicited contractions. J Appl Physiol 1990; 69:1810–1820.

[96] Merletti R, Lo Conte L, Avignone E, Guglielminotti P. Modeling of Surface Myoelectric Signals - Part I: Model implementation. IEEE Trans Biomed Eng 1999;46:810–820.

[97] Merletti R, Parker PA. Electromyography. Physiology, engineering, and noninvasive applications. 1st edition. Hoboken: John Wiley & Sons, 2004.

[98] Merletti R, Rainoldi A, Farina D. Surface electromyography for noninvasive characterization of muscle. Exerc Sport Sci Rev 2001;29:20–25.

[99] Metting van Rijn AC, Peper A, Grimbergen CA. High quality recording of bioelectric events. I: interference reduction, theory and practice. Med Biol Eng Comput 1990;28:389–397.

[100] Metting van Rijn AC, Peper A, Grimbergen CA. Amplifiers for bioelectric events: a design with a minimal number of parts. Med Biol Eng Comput 1994;32:305–310.

[101] Miller TM, Kogelnik AM, Olney RK. Proposed modification to data analysis for statistical motor unit number estimate. Muscle Nerve 2004;29:700–706.

[102] Mills KR, Schubert M. Short term synchronization of human motor units and their responses to transcranial magnetic stimulation. J Physiol (Lond) 1995;483:511–523.

[103] Monster AW, Chan H. Surface electromyogram potentials of motor units; relationship between potential size and unit location in a large human skeletal muscle. Exp Neurol 1980;67:280–297.

[104] Naeije M, Zorn H. Estimation of the action potential conduction velocity in human skeletal muscle using the surface EMG cross-correlation technique. Electromyogr Clin Neurophysiol 1983;23:73–80.

[105] Nakamura H, Yoshida M, Kotani M, Akazawa K, Moritani T. The application of independent component analysis to the multi-channel surface electromyographic signals for separation of motor unit action potential trains: part I - measuring techniques. J Electromyogr Kinesiol 2004;14:423–432.

[106] Nandedkar SD, Nandedkar DS, Barkhaus PE, Stålberg EV. Motor unit number index (MUNIX). IEEE Trans Biomed Eng 2004;51:2209–2211.

[107] Nishizono H, Saito Y, Miyashita M. The estimation of conduction velocity in human skeletal muscle in situ with surface electrodes. Electroencephalogr Clin Neurophysiol 1979;46:659–664.

[108] Nunez PL. Toward a quantitative description of large-scale neocortical dynamic function and EEG. Behav Brain Sci 2000;23:371–437.

[109] Okada RH. Potential produced by an eccentric current dipole in a finite-length circular conducting cylinder. IRE Trans Med Electron 1956;7:14–19.

[110] Olivier E, Bawa P, Lemon RN. Excitability of human upper limb motoneurones during rhythmic discharge tested with transcranial magnetic stimulation. J Physiol (Lond) 1995;485:257–269.

[111] Olney RK, Yuen EC, Engstrom JW. Statistical motor unit number estimation: reproducibility and sources of error in patients with amyotrophic lateral sclerosis. Muscle Nerve 2000;23:193–197.

[112] Papoulis A. Probability, random variables and stochastic processes. Singapore: McGraw-Hill, 1991.

[113] Persson A. The negative after-potential of frog skeletal muscle fibers. Acta Physiol Scand 1963;58:suppl. 205.

[114] Pozzo M, Bottin A, Ferrabone R, Merletti R. Sixty-four channel wearable acquisition system for long-term surface electromyogram recording with electrode arrays. Med Biol Eng Comput 2004;42:455–466.

[115] Prutchi D. A high-resolution large array (HRLA) surface EMG system. Med Eng Phys 1995;17:442–454.

[116] Pullman SL, Goodin DS, Marquinez AI, Tabbal S, Rubin M. Clinical utility of surface EMG: report of the therapeutics and technology assessment subcommittee of the American Academy of Neurology. Neurology 2000; 55:171–177.

[117] Rau G, Disselhorst-Klug C. Principles of high-spatial-resolution surface EMG (HSR-EMG): single motor unit detection and application in the diagnosis of neuromuscular disorders. J Electromyogr Kinesiol 1997;7:233–239.

[118] Reucher H, Rau G, Silny J. Spatial filtering of noninvasive multielectrode EMG: Part I – Introduction to measuring technique and applications. IEEE Trans Biomed Eng 1987;34:98–105.

[119] Roeleveld K, Blok JH, Stegeman DF, van Oosterom A. Volume conduction models for surface EMG: confrontation with measurements. J Electromyogr Kinesiol 1997;7:221–232.

[120] Roeleveld K, Sandberg A, Stålberg EV, Stegeman DF. Motor unit size estimation of enlarged motor units with surface electromyography. Muscle Nerve 1998;21:878–866.

[121] Roeleveld K, Stegeman DF, Falck B, Stålberg EV. Motor unit size estimation: confrontation of surface EMG with macro EMG. Electroencephalogr Clin Neurophysiol 1997;105:181–188.

[122] Roeleveld K, Stegeman DF, Vingerhoets HM, van Oosterom A. Motor unit potential contribution to surface electromyography. Acta Physiol Scand 1997;160:175–183.

[123] Roeleveld K, Stegeman DF, Vingerhoets HM, van Oosterom A. The motor unit potential distribution over the skin surface and its use in estimating the motor unit location. Acta Physiol Scand 1997;161:465–472.

[124] Rosenfalck P. Intra- and extracellular potential fields of active nerve and muscle fibres. Ph.D. thesis, Michaelsen Institute, University of Copenhagen, 1969.

[125] Sandberg A, Hansson B, Stålberg E. Comparison between concentric needle EMG and macro EMG in patients with a history of polio. Clin Neurophysiol 1999;110:1900–1908.

[126] Shahani BT, Fang J, Dhand UK. A new approach to motor unit estimation with surface EMG triggered averaging technique. Muscle Nerve 1995; 18:1088–1092.

[127] Shefner JM. Motor unit number estimation in human neurological diseases and animal models. Clin Neurophysiol 2001;112:955–964.

[128] Sherrington CS. Ferrier Lecture: Some functional problems attaching to convergence. Proc R Soc Lond 1929;105:332–362.

[129] Simmons Z, Epstein DK, Borg B, Mauger DT, Kothari MJ, Shefner JM. Reproducibility of motor unit number estimation in individual subjects. Muscle Nerve 2001;24:467–473.

[130] Slawnych M, Laszlo C, Hershler C. Motor unit number estimation: sample size considerations. Muscle Nerve 1997;20:22–28.

[131] Spaan E, Blok JH, Arends T, Stegeman DF. Finite element modelling of volume conduction in muscle based structures. In: Biona report 13 Motion systems; Proceedings of the Ist International conference on motion systems, Blickhan R, Wisser A, Nachtigall W, editors. Jena: Innovationskolleg Bewegungssysteme, 1998.

[132] Stålberg E. Macro EMG, a new recording technique. J Neurol Neurosurg Psych 1980;43:475–482.

[133] Stålberg E. Single fiber EMG, macro EMG and scanning EMG. New ways of looking at the motor unit. CRC Crit Rev Clin Neurobiol 1986;2:125–167.

[134] Stålberg E, Falck B, Sonoo M, Stålberg S, Astrom M. Multi-MUP EMG analysis - a two year experience in daily clinical work. Electroencephalogr Clin Neurophysiol 1995;97:145–154.

[135] Stålberg E, Nandedkar SD, Sanders DB, Falck B. Quantitative motor unit potential analysis. J Clin Neurophysiol 1996;13:401–422.

[136] Stashuk D. EMG signal decomposition: how can it be accomplished and used? J Electromyogr Kinesiol 2001;11:151–173.

[137] Stashuk D, Brown WF. Decomposition enhanced spike triggered averaging: an improved method for estimating motor unit numbers in proximal muscles. Muscle Nerve 1994;17:1120.

[138] Stashuk D, Paoli GM. Robust supervised classification of motor unit action potentials. Med Biol Eng Comput 1998;36:75–82.

[139] Stashuk D, Qu Y. Robust method for estimating motor unit firing-pattern statistics. Med Biol Eng Comput 1996;34:50–57.

[140] Stashuk DW, Doherty TJ, Kassam A, Brown WF. Motor unit number estimates based on the automated analyis of F-responses. Muscle Nerve 1994;17:881–890.

[141] Staudenmann D, Kingma I, Stegeman DF, van Dieën JH. Towards optimal multi-channel EMG electrode configurations in muscle force estimation: a high density EMG study. J Electromyogr Kinesiol 2005;15:1–11.

[142] Stegeman DF, Blok JH, Hermens HJ, Roeleveld K. Surface EMG models: properties and applications. J Electromyogr Kinesiol 2000;10:313–326.

[143] Stein RB, Yang JF. Methods for estimating the number of motor units in human muscles. Ann Neurol 1990;28:487–495.

[144] Vander AJ, Sherman JH, Luciano DS. Human physiology. 5th edition. New York: McGraw-Hill Publishing Company, 1990.

[145] Vugts C, van der Velden L, Hingstman L. Behoefteraming neurologen 2004-2015. Utrecht: NIVEL, 2004.

[146] Wang FC, Delwaide PJ. Number and relative size of thenar motor units estimated by an adapted multiple point stimulation method. Muscle Nerve 1995;18:969–979.

[147] Wang FC, Pasqua VD, Delwaide PJ. Age-related changes in fastest and slowest conducting axons of thenar motor units. Muscle Nerve 1999;22:1022–1029.

[148] Weber M, Eisen A. Assessment of upper and lower motor neurons in Kennedy's disease: implications for corticomotoneuronal PSTH studies. Muscle Nerve 1999;22:299–306.

[149] Wood SM, Jarratt JA, Barker AT, Brown BH. Surface electromyography using electrode arrays: a study of motor neuron disease. Muscle Nerve 2001; 24:223–230.

[150] Yamada M, Kumagai K, Uchiyama A. The distribution and propagation pattern of motor unit action potentials studied by multi-channel surface EMG. Electroencephalogr Clin Neurophysiol 1987;67:395–401.

[151] Yamada M, Kumagai K, Uchiyama A. Muscle fiber conduction velocity studied by the multi-channel surface EMG. Electromyogr Clin Neurophysiol 1991;31:251–256.

[152] Yamamoto T, Yamamoto Y. Electrical properties of the epidermal stratum corneum. Med Biol Eng 1976;14:151–158.

[153] Yao W, Fuglevand RJ, Enoka RM. Motor unit synchronization increases EMG amplitude and decreases force. J Neurophysiol 2000;83:441–452.

[154] Zwarts MJ, Stegeman DF. Multichannel surface EMG: basic aspects and clinical utility. Muscle Nerve 2003;28:1–17.

[155] Zwarts MJ, van Weerden TW. Transient paresis in myotonic syndromes. A surface EMG study. Brain 1989;112:665–680.

[156] Zwarts MJ, van Weerden TW, Links TP, Haenen HTM, Oosterhuis HJG. The muscle fiber conduction velocity and power spectra in familial hypokalemic periodic paralysis. Muscle Nerve 1988;11:166–173.

LIST OF PUBLICATIONS

Papers in international peer-reviewed journals

Smit X, De Kool BS, Blok JH, Visser GH, Hovius SER, van Neck JW. Recovery of electrophysiological signals with time after rat sciatic nerve repair: a magnetoneurographic study. J Peripher Nerv Syst, accepted.

Garssen MPJ, Blok JH, van Doorn PA, Visser GH. Conduction velocity distribution in neurologically well-recovered but fatigued Guillain-Barré syndrome patients. Muscle Nerve, in print.

Cherian PJ, Swarte RMC, Blok JH, Bröker-Schenk PMM, Visser GH. Ictal nystagmus in a newborn baby after birth asphyxia. Clin EEG Neurosci, in print.

Kool de BS, van Neck JW, Blok JH, Walbeehm ET, Hekking I, Visser GH. Ultrasound imaging of the rabbit peroneal nerve. J Peripher Nerv Syst 2005;10:369-374.

Blok JH, van Dijk JP, Zwarts MJ, Stegeman DF. Motor unit action potential topography and its use in motor unit number estimation. Muscle Nerve 2005;32:280-291.

Blok JH, Visser GH, de Graaf S, Zwarts MJ, Stegeman DF. Statistical motor number estimation assuming a binomial distribution. Muscle Nerve 2005;31:182-191.

Drenthen J, van Hulst RA, Blok JH, van Heel MD, Haitsma JJ, Lachmann B, Visser GH. Quantitative EEG monitoring during cerebral air embolism and hyperbaric oxygen treatment in a pig model. J Clin Neurophysiol 2003;20:264-272.

Blok JH, Stegeman DF, van Oosterom A. A three-layer volume conductor model and software package for applications in surface electromyography. Ann Biomed Eng 2002;30:566-577.

Blok JH, van Dijk JP, Drost G, Zwarts MJ, Stegeman DF. A high-density multichannel surface electromyography system for the characterization of single motor units. Rev Sci Instr 2002;73:1887-1897.

Drost G, Blok JH, Stegeman DF, van Dijk JP, van Engelen BGM, Zwarts MJ. Propagation disturbance of motor unit action potentials during transient paresis in generalized myotonia. A high-density surface EMG study. Brain 2001;124:352-360.

Stegeman DF, Blok JH, Hermens HJ, Roeleveld K. Surface EMG models: properties and applications. J Electromyogr Kinesiol 2000;10:313-326.

Kleine BU, Blok JH, Oostenveld R, Praamstra P, Stegeman DF. Magnetic stimulation induced modulations of motor unit firings extracted from multi-channel surface EMG. Muscle Nerve 2000;23:1005-1015.

Roeleveld K, Blok JH, Stegeman DF, van Oosterom A. Volume conduction models for surface EMG; confrontation with measurements. J Electromyogr Kinesiol 1997;7:221-232.

Co-editorships

Hermens HJ, Freriks B, Merletti R, Stegeman DF, Blok JH, Rau G, Disselhorst-Klug C, Hägg G. European recommendations for surface electromyography. Results of the SENIAM project, deliverable 8 of the SENIAM project. Enschede: Roessingh Research and Development, 1999.

Hermens HJ, Stegeman DF, Blok JH, Freriks B. The state of the art on modelling methods for surface electromyography, deliverable 6 of the SENIAM project. Enschede: Roessingh Research and Development, 1998.

Book chapters

Walbeehm ET, Blok JH, de Kool BS, van Neck JW, Hovius SER. Magnetoneurographic evaluation of the proximal segment after different types of repair. Chapter 4 (pp. 63-74) of The role of the proximal segment in peripheral nerve regeneration (PhD thesis E.T. Walbeehm). Rotterdam: Optima Grafische Communicatie, 2004.

Walbeehm ET, de Kool BS, Blok JH, van Neck JW, Hovius SER. The distal/proximal peak-to-peak amplitude ratio as a measure of regeneration across a nerve repair. Chapter 5 (pp. 75-88) of above PhD thesis.

Walbeehm ET, Blok JH, Kuypers PDL, van Neck JW, Hovius SER. Primary-versus delayed-primary nerve repair evaluated by magnetoneurography. Chapter 6 (pp. 89-101) of above PhD thesis.

Drost G, Blok JH, van Dijk JP, van Engelen BGM, Zwarts MJ, Stegeman, DF. High density SEMG during transient paresis in Beckers's myotonia. In: Future applications of surface electromyography, deliverable 4 of the SENIAM project, Hermens HJ, Freriks B, editors. Enschede: Roessingh Research and Development, 1999.

Kleine B-U, Praamstra P, Blok JH, Stegeman DF. Single motor unit discharge patterns recorded with multi-channel SEMG. In: Future applications of surface electromyography, deliverable 4 of the SENIAM project, Hermens HJ, Freriks B, editors. Enschede: Roessingh Research and Development, 1999.

Blok JH, Stegeman DF, Freriks B, Hermens HJ. The SENIAM models for surface electromyography. In: European recommendations for surface electromyography.

Results of the SENIAM project, deliverable 8 of the SENIAM project, Hermens HJ, Freriks B, Merletti R, Stegeman DF, Blok JH, Rau G, Disselhorst-Klug C, Hägg G, editors. Enschede: Roessingh Research and Development, 1999.

Blok JH, Stegeman DF, Drost G. The use of spatiotemporal information in motor unit classification. In: The state of the art on signal processing methods for surface electromyography, deliverable 7 of the SENIAM project, Hermens HJ, Merletti R, Rix H, Freriks B, editors. Enschede: Roessingh Research and Development, 1999.

Blok JH, Stegeman DF. Simulated bipolar SEMG characteristics. In: The state of the art on sensors and sensor placement procedures for surface electromyography, deliverable 5 of the SENIAM project, Hermens HJ, Freriks B, editors. Enschede: Roessingh Research and Development, 1997.

Blok JH, van Asselt S, van Dijk JP, Stegeman DF. On an optimal pasteless electrode to skin interface in surface EMG. In: The state of the art on sensors and sensor placement procedures for surface electromyography, deliverable 5 of the SENIAM project, Hermens HJ, Freriks B, editors. Enschede: Roessingh Research and Development, 1997.

Stegeman DF, Blok JH, Hermens HJ, Roeleveld K. Surface EMG models: properties and applications. In: The state of the art on modelling methods for surface electromyography, deliverable 6 of the SENIAM project, Hermens HJ, Stegeman DF, Blok JH, Freriks B, editors. Enschede: Roessingh Research and Development, 1998.

Roeleveld K, Drost G, Stegeman DF, Blok JH, Scholle HCh. Estimation of motor unit position from surface EMG topographical maps. In: The state of the art on modelling methods for surface electromyography, deliverable 6 of the SENIAM project, Hermens HJ, Stegeman DF, Blok JH, Freriks B, editors. Enschede: Roessingh Research and Development, 1998.

Blok JH, Stegeman DF. Modelling surface EMG signals. In: European activities on surface electromyography, deliverable 1 of the SENIAM project, Hermens HJ, Merletti R, Freriks B, editors. Enschede: Roessingh Research and Development, 1996.

Stegeman DF, Roeleveld K, Blok JH. EMG topography as an instrument in clinical neurophysiology: a unipolar recording approach. In: European activities on surface electromyography, deliverable 1 of the SENIAM project, Hermens HJ, Merletti R, Freriks B, editors. Enschede: Roessingh Research and Development, 1996.

Other papers and abstracts (as first author only; approximately 25 as co-author)

Blok JH, Maathuis EM, Visser GH. The extent of alternation as a function of stimulus intensity. XIIth European congress of clinical neurophysiology, Stockholm (Sweden), 2005.

Blok JH, Visser GH, Zwarts MJ, Stegeman DF. Statistical motor unit number estimation assuming a binomial distribution. VIIIth Quantitative EMG congress, Nijmegen (The Netherlands). Clin Neurophysiol 2005;116:485-486.

Blok J, Drost G, van Dijk H, Zwarts M, Stegeman D. Multikanaals oppervlakte-elektromyografie: een niet-invasief alternatief voor naald-EMG? Klinische Fysica 2000.

Blok JH, Stegeman DF. Anvolcon: a three-layer volume conductor model for applications in surface electromyography. World congress on medical physics and biomedical engineering, Chicago (USA), 2000.

Blok JH, Stegeman DF, van Dijk JP, Zwarts MJ. Multi-channel surface EMG improves motor unit number estimation. Clin Neurophysiol 1999;110 (suppl. 1):90.

Blok JH, Stegeman DF, van Dijk JP. Single motor unit analysis from surface EMG topography. Electroenceph Clin Neurophysiol 1997;103:220.

Blok JH, Stegeman DF, Roeleveld K. Motor unit contribution to surface EMG: II. Theoretical basis. XVIIIth Annual international conference of the IEEE/EMBS, Amsterdam (The Netherlands), 1996.

Blok JH, Stegeman DF, Houtman CJ. An estimation procedure to determine motor unit structure from surface EMG data. Xth International congress of EMG and clinical neurophysiology, Kyoto (Japan), 1995.

Blok JH, Stegeman DF, Houtman CJ, Roeleveld K. Determination of motor unit structure and volume conductor properties from surface EMG data: the inverse problem in electromyography. Xth International conference for physics students, Kopenhagen (Denmark), 1995.

DANKWOORD

Aan het begin van dit proefschrift heb ik een citaat opgenomen dat weergeeft hoe fysici en technici een bijdrage kunnen leveren aan het wetenschappelijk bedrijf. Maar de oorspronkelijke tekst ging verder: “Nothing tends so much to the advancement of knowledge as the application of a new instrument. The native intellectual powers of men in different times are not so much the causes of the different success of their labours as the peculiar nature of the means and artificial resources in their possession.” Met andere woorden, het feit dat dit proefschrift er nu ligt, is maar ten dele het resultaat van mijn inbreng en vooral ook te danken aan de bijzonder gunstige omstandigheden die de realisatie ervan mogelijk hebben gemaakt. Zeker als ik tot die “omstandigheden” ook al diegenen reken die in de loop van de afgelopen tien jaar hun bijdrage aan mijn onderzoek hebben geleverd. Hier, aan het einde van het traject en van het boekje, wil ik al deze mensen hartelijk danken, met name de volgende personen.

Dick, twaalf jaar geleden liep ik als natuurkundestudent voor het eerst bij je binnen en nu ben ik je collega-klinisch fysicus bij de KNF in Rotterdam. Een traject dat je als afstudeerbegeleider, opleider klinische fysica en promotor van dichtbij hebt meegemaakt en voor een groot deel mee hebt vormgegeven. Ik heb daardoor zoveel aan je te danken dat ik niet eens aan een opsomming durf te beginnen uit vrees van alles te vergeten. Ik hoop in Rotterdam op termijn een tweede FTG te kunnen realiseren, met een vergelijkbare sfeer. Misschien zegt dat genoeg.

Machiel, met jouw komst heeft de klinische kant van het KNF-onderzoek in Nijmegen een enorme impuls gekregen. De klinisch fysicus in mij was blij met deze aandacht voor toepassingen en de praktijk (en met de randvoorwaarden die jij mede geschapen hebt voor mijn opleiding). De wetenschapper in me heeft altijd dankbaar kunnen putten uit je grote kennis van de literatuur en gebruik kunnen maken van vele waardevolle suggesties, onder andere met betrekking tot de opbouw en rode draad van dit proefschrift.

Hans, je was kamergenoot, sparring partner, programmeur, technische vraagbaak en vriend ineen. Dick noemde ons wel gekscherend “het team”, waarin doorklonk dat voor buitenstaanders regelmatig niet meer duidelijk was wie van ons beiden nou precies wat gedaan had. Vaak wisten we dat zelf ook niet meer en dat kenmerkt onze samenwerking. Leuk dat juist jij het multikanaals MUNE-onderzoek voortzet voor je eigen promotie! We zijn zo’n beetje samen opgegroeid in wetenschapsland. Ik vind het daarom erg fijn dat je mijn paranimf wilt zijn, zodat we ook deze laatste stap van mijn promotietraject samen kunnen zetten. Bedankt voor alles.

De medewerkers van de Instrumentele Dienst Oost hebben waarschijnlijk de meest tastbare bijdrage geleverd aan mijn onderzoek. De elektrodenmatjes, de stimulator en allerlei kleinere projecten: jullie wisten er elke keer weer iets moois van te maken. Hartelijk dank voor jullie inzet en betrokkenheid.

It was a great pleasure and a privilege for me to be able to participate in a European “concerted action” of a group of acclaimed scientists very early in my scientific career. I would like to thank all SENIAM partners for allowing me to join them, as well as for their very helpful comments and suggestions at the meetings. In addition, I would like to express my sincere gratitude to Roberto and Hermie for their willingness to be present at my thesis’ defence.

De leden van de STW-gebruikerscommissie dank ik voor hun belangstelling voor en betrokkenheid bij het multikanaals-sEMG project en de waardevolle discussies en tips tijdens de gebruikerscommissievergaderingen.

Karin en Caroline, Robert, Mireille en Maartje, Gea, Paul, Bert en Bernd, en alle andere onderzoekers en stagiair(e)s die in de afgelopen jaren kortere of langere tijd deel hebben uit gemaakt van de FTG, het was ontzettend leuk en leerzaam om met mensen uit zoveel verschillende disciplines te werken aan parallelle projecten op één terrein. Dat heeft regelmatig een frisse kijk opgeleverd. Ook al nam ik die in mijn eigenwijsheid vaak niet meteen over, ik ben er wel door aan het denken gezet en veel heeft uiteindelijk toch zijn plekje gevonden in dit proefschrift. Bedankt voor al die keren dat jullie met me hebben meegedacht, tips hebben gegeven of me op een nieuw spoor hebben gezet, of – niet te vergeten – proefpersoon wilden zijn. Bedankt ook voor alle gezelligheid bij tussenwerkse (wandelingen) en buitenwerkse activiteiten. Bert ben ik daarbij dank verschuldigd voor het “afstaan” van zijn artikel, dat in dit proefschrift is opgenomen als hoofdstuk 5. Gea, als eerste gebruiker ben je tegen alle mogelijke kinderziektes van de nieuwe hardware en software aangelopen; bedankt voor alle waardevolle feedback. Meer in het algemeen wil ik alle KNF-medewerkers bedanken voor het scheppen van een fijne sfeer op de afdeling, die er voor gezorgd heeft dat ik jarenlang met veel plezier naar mijn werk gegaan ben en met een hele verzameling goede herinneringen uit Nijmegen kon vertrekken.

Gerhard, de eerste maanden in Rotterdam had ik nog wel eens wat heimwee naar Nijmegen. Dat ik me er inmiddels zo goed op mijn plek voel, is voor een groot deel aan jou te danken. Bedankt voor de ruimte die je me gegeven hebt, onder andere om dit proefschrift af te ronden. Ik vind het erg leuk dat iets van de bijzonder goede samenwerking die we hebben al concreet in dit boekje zichtbaar is.

De KNF-medewerkers in Rotterdam ben ik dankbaar voor de prettige werkomgeving die ze me nu bieden. Vooral dankzij jullie heb ik inmiddels geleerd dat de KNF meer is dan EMG, waardoor mijn enthousiasme voor het vakgebied nog steeds groeit. Dat enthousiasme heeft me met name de laatste paar erg drukke jaren keer op keer gemotiveerd om achter de PC te kruipen en verder te schrijven aan dit manuscript.

Esther, het kan zo raar lopen, soms. Van stagiaire tot collega-klinisch fysicus en vriendin, van Nijmegen/Nijmegen via Rotterdam/Sittard naar Den Haag/Den Haag. Ik vind het erg leuk dat we zowel qua vakgebied als qua leefgebied nu veel delen en dat dat op de promotie ook zichtbaar is doordat je mijn paranimf wilt zijn. Dankjewel daarvoor.

Verder wil ik mijn vrienden bedanken voor de onmisbare afleiding en steun. We zitten in deze periode bijna allemaal in het spitsuur van ons leven, hebben veeleisend werk en/of kleine kinderen. Hopelijk lukt het ons, nu deze klus geklaard is en ik weer wat meer “weekendtijd” heb, een klein beetje beter om toch zo nu en dan wat af te spreken.

Tot slot mijn familie. Peter & Judith, Renske en mijn schoonouders, ook jullie bedankt voor jullie oprechte interesse. Mijn ouders ben ik dankbaar voor het meegeven en tot ontplooiing brengen van de eigenschappen die nodig zijn om een promotie tot een goed einde te brengen. Bedankt ook voor het vertrouwen en de praktische & morele steun die jullie me altijd gegeven hebben, en voor de vrijheid om mijn eigen weg te gaan – al leidde die soms letterlijk door oorlogsgebied. Lieve René, bedankt voor alle back-up thuis. Onze Nijmeegse periode is echt afgesloten nu we twee boekjes en twee kinderen rijker zijn. De laatste jaren is er veel voor ons veranderd; de komende tijd kunnen we van het resultaat van al die veranderingen hopelijk ook echt gaan genieten.

CURRICULUM VITAE

Joleen Blok is op 22 januari 1972 geboren in Veldhoven. Na het behalen van haar gymnasium-β diploma aan het Eindhovens Protestants Lyceum (nu Christiaan Huygens Lyceum) in 1990 heeft ze een jaar als "Occasional Student" gestudeerd aan de Queen's University of Belfast, Noord-Ierland. Na dit jaar is ze in Nijmegen begonnen aan de studie Natuurkunde. Deze studie heeft ze in 1995 cum laude afgesloten. Haar afstudeerwerk heeft ze gedaan op de afdeling Klinische Neurofysiologie van het Universitair Medisch Centrum St Radboud. Bij deze afdeling heeft ze in 1996 een gecombineerde aanstelling gekregen als onderzoeker in opleiding/klinisch fysicus in opleiding. Dit proefschrift vormt de afsluiting van haar promotieonderzoek. Een gedeelte van de opleiding Klinische Fysica werd gevormd door de ontwerpersopleiding Fysische Instrumentatie van de Technische Universiteit Eindhoven. Deze tweejarige ontwerpersopleiding heeft Joleen in april 2001 afgerond. Haar registratie als algemeen klinisch fysicus, die het einde vormde van de opleiding klinische fysica, heeft plaatsgevonden in april 2002. Sinds augustus 2002 werkt Joleen als klinisch fysicus op de afdeling Klinische Neurofysiologie van het Erasmus MC te Rotterdam. Ze is getrouwd met René Tolboom en moeder van Ymke en Simon.

Joleen Blok was born on January 22, 1972, in Veldhoven, The Netherlands. After graduating from the Eindhovens Protestants Lyceum in 1990, she enrolled at the Queen's University of Belfast, Northern Ireland (UK), for a one-year course as "Occasional Student". In 1991, Joleen moved to Nijmegen to study physics, and graduated with honours in 1995. The research for her master's thesis, entitled "Volume conduction and EMG. Simulation studies and experiments", was performed at the Department of Clinical Neurophysiology of the Radboud University Nijmegen Medical Centre. This department subsequently employed her as junior scientist / clinical physics trainee. The present PhD thesis is the result of Joleen's work as junior scientist. Part of the clinical physics traineeship was formed by the two-year course "Design and Technology of Instrumentation" of the Technische Universiteit Eindhoven. Joleen completed this designer course in April 2001. She was formally registered as clinical physicist in April 2002. Since August 2002, Joleen has been employed as clinical physicist by the Department of Clinical Neurophysiology of the Erasmus MC in Rotterdam. She is married to René Tolboom and mother of Ymke and Simon.